In vivo genome-wide analysis reveals that eIF2D coordinates motor neuronal synaptic function and locomotion behavior by regulating translation of specific mRNAs

Aida Cardona Alberich

Fakultät für Mathematik, Informatik und Naturwissenschaften der Universität Hamburg

Faculty of Biology

Dissertation submitted to the University of Hamburg

2018

Examiners of the dissertation:

Dr. Kent Duncan
Prof. Dr. Christian Lohr

Date of the disputation:

28th September 2018

1 Abstract

Regulation of protein synthesis is fundamental for all aspects of eukaryotic biology. Historically, research has focused on transcription to explain cell-specific regulation of protein abundance and cell specialization. Now, we know that translation plays a key role in controlling protein levels and enables temporal- and spatially-restricted regulation of gene expression. Although the functions of canonical translation factors are quite well understood, little is known about how translation control of specific mRNAs is achieved, especially *in vivo*. The non-canonical translation factors differ from the canonical factors for their biochemical properties and regulation of specific mRNAs.

eIF2D has been described as non-canonical translation factor for *in vitro* promoting GTP-independent initiator tRNA delivery and post-termination ribosome recycling. However, eIF2D showed no impact on yeast growth or general translation. Studies from hippocampal cultured neurons suggest activity regulation of *eIF2D* mRNA, but the physiological functions and specific mRNA targets of eIF2D in a whole animal have not previously been identified.

This thesis explores the *in vivo* roles of the non-canonical translation factor eIF2D in *Drosophila melanogaster*. Flies lacking eIF2D have specific behavioral defects affecting locomotion speed that can be rescued by expressing eIF2D from either side of the larval Neuromuscular Junction (NMJ). To determine how this related to translational control, mRNAs regulated by eIF2D *in vivo* were identified using an optimized method that combines polysome profiling with RNA-seq (Poly-seq). Prominent among the eIF2D targets were mRNAs coding for proteins implicated in synaptic processes and locomotion, consistent with the observed phenotypes. Moreover, Poly-seq data lead to find protein composition changes at the NMJ in *eIF2D^{KO}* larvae that could explain the phenotypes. Other eIF2D targets also include several mRNAs encoding mitochondrial proteins or gene expression regulation. Some of these eIF2D targets have common mRNA characteristics (e.g. 5' UTR cis-elements) that could explain coordinated regulation of these mRNAs by this factor.

Collectively, these results reveal a new role for eIF2D within the motor system to promote synaptic function via coordinating translation of specific mRNAs through their 5'UTRs.

2 Zusammenfassung

Die Regulation der Proteinbiosynthese ist grundlegend für alle biologischen Prozesse von Eukaryoten. Vergangene Studien fokussierten sich dabei auf die Transkription, um die zellspezifische Regulation von Proteinmengen und Zelldifferenzierung zu beschreiben. Gegenwärtig ist bekannt, dass die Translation eine Schlüsselrolle bei der Kontrolle der Proteinmengen einnimmt und eine zeitlich sowie räumlich beschränkte Regulation der Genexpression ermöglicht. Obwohl die Funktionen von kanonischen Translationsfaktoren weitgehend verstanden werden, bestehen noch große Unklarheiten bezüglich der Translationskontrolle spezifischer mRNAs, insbeondere *in vivo*. Die nichtkanonischen unterscheiden sich von den kanonischen Translationsfaktoren hinsichtlich ihrer biochemischen Eigenschaften und Regulation spezifischer mRNAs.

eIF2D wurde als nichtkanonischer Translationsfaktor für *in vitro* begünstigte GTP-unabhängige Start-tRNA Anlieferung und Postterminations-Ribosomrecycling beschrieben. Jedoch zeigte eIF2D keine Auswirkungen auf Hefewachstum oder allgemeine Translation. Studien mit hippocampal kultivierten Neuronen empfehlen eine Regulation der Aktivität von eIF2D mRNA. Die physiologischen Funktionen und spezifischen mRNA-Targetmoleküle eines ganzen Tieres wurden bisher noch nicht identifiziert.

Diese Thesis untersucht die in vivo Funktionen des nichtkanonischen Translationsfaktors eIF2D in *Drosophila melanogaster*. Fliegen mit eIF2D-Mangel zeigen Verhaltensdefekte, welche die Fortbewegungsgechwindigkeit beeinflussen. Dieser Defekt kann mit der Expression von eIF2D auf beiden Seiten der larvalen neuromuskulären Synapse (Neuromuscular Junction - NMJ) behoben werden. Um die Beziehung zur Translationskontrolle zu ergründen, wurden mRNAs, welche von eIF2D *in vivo* reguliert werden, mit einer optimierten Methode, welche Polysome-profiling mit RNA-seq (Poly-seq) kombiniert, identifiziert. Besonders herausragend unter den eIF2D-Targetmolekülen waren mRNAs, welche an synaptischen Prozessen und Fortbewegung beteiligte Proteine kodieren. Dieses Ergebnis stimmt mit den beobachteten Phänotypen überein. Des Weiteren ermöglichten Poly-seq Daten das Auffinden von Veränderungen in der Proteinkomposition an den NMJ von eIF2D^{KO}-Larven, welche den Phänotypen erklären könnten. Andere eIF2D Target-Moleküle enthalten verschiedene mRNAs, welche mitochondrielle Proteine oder die

Regulation der Genexpression kodieren. Manche dieser eIF2D Target-Moleküle besitzen gemeinsame mRNA Merkmale (z.B. 5' UTR cis-Elemente) welche eine koordinierte Regulation von diesen mRNAs mittels dieses Faktors beschreiben könnten.

Zusammenfassend offenbaren diese Ergebnisse eine neue Rolle für eIF2D innerhalb des Motorsystems, um synaptische Funktionen mittels koordinierter Translation von spezifischen mRNAs durch ihre 5'UTRs zu begünstigen.

3   Contents

7

4 Introduction

4.1 Translation control

4.1.1 Canonical factors and canonical translation control

Control of gene expression for protein encoded genes in eukaryotic cells includes many different processes that are connected: transcription from DNA to RNA and translation of mRNA into protein. However, the transition from DNA to protein is not a simple linear process. The levels of different mRNAs (transcripts) have different correlation to levels of its protein, and this correlation might change under different conditions and biological situations such as stress or during different stages of the development (Liu et al. 2016). To achieve such regulation, translation needs to be highly controlled, and this is done by a group of proteins called translation factors.

Because initiation is typically the rate-limiting step in translation, it is assumed to be the phase with a higher regulation (although not the only one) and thus the most studied one. Canonical translation control is defined by the way most of the mRNAs' translation is regulated, in opposition to non-canonical translation control happening in a set of specific mRNAs without affecting the global transcriptome, or under very specific conditions.

4.1.1.1 Translation initiation

The first step of translation is the joining of the 40S (small) subunit of the ribosome with some of the translation initiation factors. On one hand, charged initiator tRNA with Methionine (Met-tRNA$^{Met}_i$) forms a ternary complex together with eIF2 bound to GTP. eIF3, eIF1, eIF1A and eIF2-GTP- Met-tRNA$^{Met}_i$ attach to the 40S subunit and together form the 43S preinitiation complex (PIC) (Fig. 1A). The 43S complex will bind to the mRNA and start "scanning" at the 5' end of the mRNA in a 3' direction (Fig. 1B) (Hershey 1991; Pestova et al. 2001; Preiss and M 2003). The 5' end of many mRNAs has secondary structure which requires unwinding prior to 43S PIC recruitment. This is achieved by the complex eIF4F (cap-binding protein eIF4E, DEAD-box helicase eIF4A, and scaffold protein eIF4G), together with eIF4B and the poly(A) binding protein (PABP) that binds the 3' poly(A) tail. Physical interaction

between PABP and eIF4G leads to circularization of the mRNA and stimulates translation initiation (Tarun and Sachs 1997; Tarun et al. 1997; Wells et al. 1998). eIF4H or eIF4B can stimulate eIF4A helicase activity by preventing mRNA re-annealing and promoting unidirectional forward unwinding and scanning by the 43S PIC.

The 43S PIC scans the 5'UTR until it reaches a start codon in an optimal context (Kozak sequence) (Fig. 1C) (Kozak 2002). Typically AUG codons have been described as the start codon, in the context GCC(A/G)CCAUGG, with a purine at -3 and G at +4. Nowadays we know that AUG start codons represent a big part of start codons but not only, and others like CUG are able to serve as start codons. The relative abundance for every start codon is still under debate and depends of the specie.

Movement of 43S complexes requires the scanning competent conformation of the ribosome induced by eIF1 and eIF1A (40S subunit conformation changes upon eIF1 and eIF1A binding). eIF1 binds to the interface between the platform and Met-tRNA. The role of eIF1 in initiation is optimal start codon recognition (Pestova et al. 1998; Pestova and Kolupaeva 2002; Mitchell and Lorsch 2008); it establishes correct codon-anticodon discriminating between AUG codons in optimal context from non-AUG codons or AUG codons in poor context, then dissociating the ribosomal complexes. Start codon-anticodon recognition produces a conformational change that makes the interaction of eIF1A and 40S closer and leads to displacement of eIF1, which produces a closed conformation of the 40S on the mRNA. Examples of mutations in eIF1 in yeast show that having a weaker interaction to the 40S promotes more initiation at non-AUG codons (Cheung et al. 2007). Also reduction of eIF1 changes translation of transcripts containing uORFs (Fijalkowska et al. 2017).

After start codon recognition, eIF5 induces eIF2-GTP hydrolyses to eIF2-GDP (Fig. 1D) (Paulin et al. 2001; Jackson et al. 2010). eIF1 also prevents premature hydrolysis of eIF2-GTP, specially at the wrong codon-anticodon pair, thus avoiding starting at the wrong codon (Unbehaun et al. 2004; Algire et al. 2005). At this point, the 80S complex can form with the joining of the 60S ribosomal subunit, catalyzed by

eIF5B (Pestova et al. 2000; Unbehaun et al. 2004), at the same time than the dissociation of some of the initiation factors, especially those ones sitting on the interface of the 40S (Fig 1E). Finally, the 80S ribosome can start elongation (Fig. 1F).
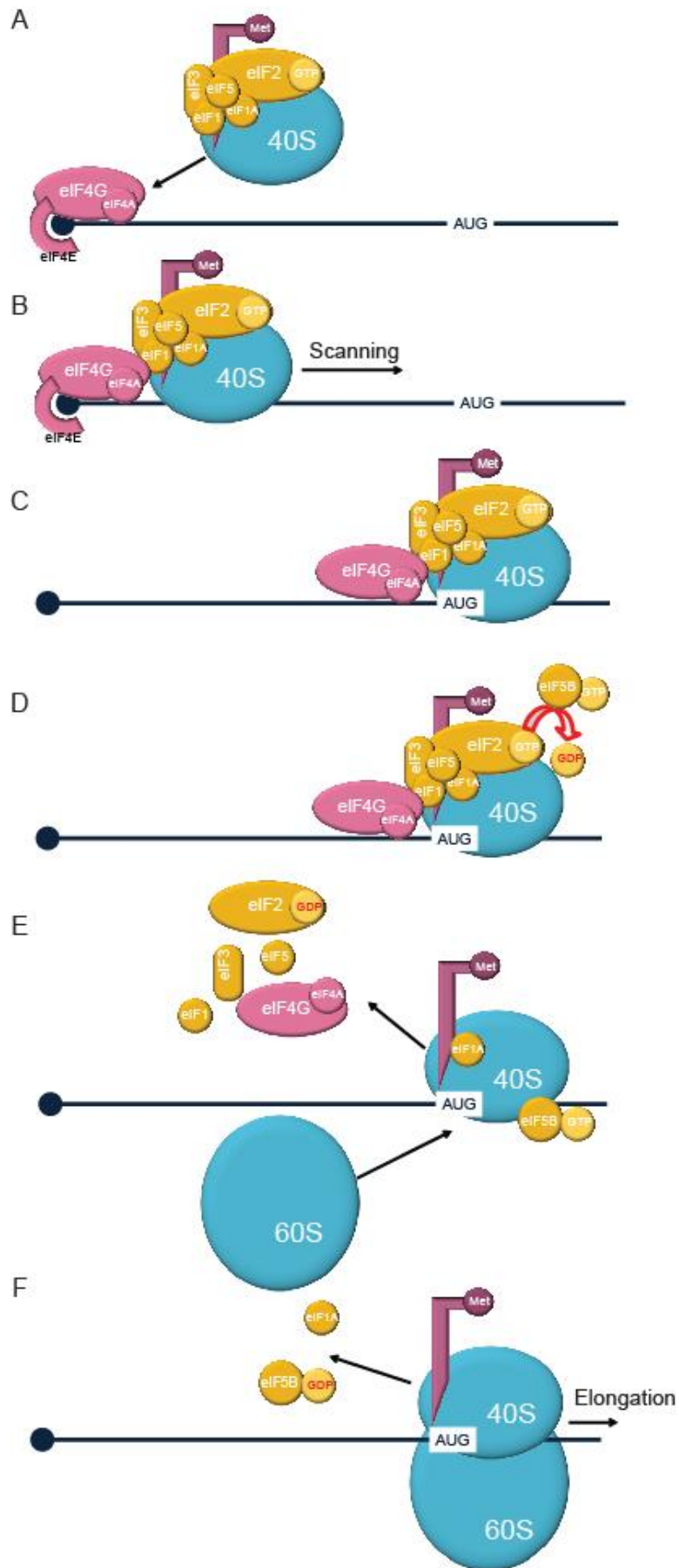
Figure 1. Scheme of Canonical Translation Initiation and the factors involved.

4.1.1.2   Example of regulation of translation initiation

Translation initiation rates can be altered, for example under stress, by controlling levels or activation of the different factors. This is in many cases achieved through regulation of eIF2-alpha, a subunit of eIF2, phosphorylation of which prevents release of eIF2 lowering the available levels for ternary complex formation. There are four mammalian kinases that can phosphorylate eIF2 and each one is activated by different stress stimuli. GCN2 (General control non-depressible 2) is activated by starvation of some amino acids, PKR (RNA-dependent protein kinase) is activated by virus infection of double-stranded RNA, PERK (PKR-like ER kinase) is activated by ER stress due to accumulation of misfolded proteins and HRI (Haem-regulated inhibitor) promotes survival of erythroid precursors at low iron levels (Jackson et al. 2010). GCN2 and PERK have homologous proteins in *Drosophila*, whereas PKR and HRI seem to be restricted to mammals.

Another way to control translation is by different trans-elements that can bind the mRNA. Paradoxically, the 3'UTR can also affect translation initiation through several RNA-binding proteins or microRNAs. Those mechanisms will not be further discussed in this thesis.

Important to remember, is that regulation of translation is crucial for correct gene expression, therefore there are multiple points of regulation and sometimes overlapping pathways.

4.1.1.3   Translation termination and recycling

As in initiation, several factors control and regulate translation termination and disassemble of the ribosome, the newly synthesized peptide, tRNA and mRNA (recycling). The different components appear to be dissociated one by one in a controlled manner to be involved in the next round of translation. First, the stop codon has to be recognized by eRF1 which will be further activated by eRF3 to release the new peptide (Alkalaeva et al. 2006). The second step is to release the 60S subunit from the 40S-mRNA-tRNA complex, which is achieved by ABCE-1 (ATP-binding cassette protein). Finally, tRNA will be dissociated by eIF3, eIF1 and eIF1A (Pisarev et al. 2010), or alternatively by eIF2D or MCTS1/DENR (Skabkin et al. 2010). The

last step is recycling of the 40S subunit from the mRNA. In some cases, the 40S do not dissociate from the mRNA and resume scanning to downstream ORFs instead (Jackson et al. 2010).

4.1.2   Non-Canonical translation and non-canonical factors

Besides the canonical factors and the classic translation pathway, other proteins have been implicated in alternative mechanisms of translation regulation. Those non-canonical factors could work as completely parallel mechanisms, independent of the canonical factors, or partially overlapping, being especially needed in certain times during development or under specific physiological conditions, such as stress. For that, they might use specific elements on the mRNA sequence from secondary structure loops to specific nucleotide sequence.

4.1.2.1   uORFs and Re-initiation

Many transcripts contain upstream ORFs (uORFs) from the protein coding sequence or main ORF (mORF). The number of mRNAs with uORFs depends on the species. In mammals, they are found in about 50% of the mRNAs (Calvo et al. 2009) whereas uORFs seem to be less common in yeast (Ingolia et al. 2009; Lawless et al. 2009; Brar et al. 2012). According to the scanning model, translation will start at the uORF and only a small percentage of ribosomes will reinitiate at the downstream ORF (Ingolia et al. 2011). Post-termination events at a uORF stop codon follow conventional mechanisms with a first step of 60S release. After peptide release, the 40S subunit remains attached to the mRNA and can reinitiate scanning, this time without the associated eIF2-TC, which presumable needs to be acquired during this scanning, before new start codon recognition can occur.

Several studies addressed the question of how uORFs affect translation at the mORF and the mechanisms of re-initiation. The efficiency of re-initiation after uORF translation is inversely correlated with the length of the uORF (Luukkonen et al. 1995) but other studies suggest that the time needed to be translated (elongation duration), more than its length, is what determines the re-initiation probability (Kozak 2001). This fact is consistent with some eIFs staying associated with the ribosome during

elongation and after termination or being involved in termination itself. Re-initiation probability also increases with an increase in intercistronic distance (Kozak 1987). Together, these studies suggest that (1) some of the initiation factors stay attached to the 40S during elongation for a short time, and are needed for re-initiation, and (2) some factors like the eIF2-GTP-Met-tRNA$^{Met}_i$ need to be acquired during the new scanning and this can only happen when there is enough scanning time (Gunisova et al. 2018).

uORFs usually negatively impair translation and act as regulators, but not always, and its impact on the mORF depends also on other cis elements up- and downstream of the uORF, such as hairpins, AU- rich regions or other secondary structures(Grant and Hinnebusch 1994). Under stress conditions when eIF2 is phosphorylated, translation of some uORF-containing mRNAs increases. One well studied example is the translation regulation of the transcription factor activator of amino acid biosynthesis genes in yeast GCN4 (Jia et al. 2000; Natarajan et al. 2001; Harbison et al. 2004; Patil et al. 2004; MacIsaac et al. 2006). Four uORFs in the 5'UTR of GCN4 respond to eIF2 phosphorylation to regulate translation of GCN4 CDS. The 4 uORFs repress translation of the mORF in normal conditions but promote translation in stress condition under starvation (Mueller and Hinnebusch 1986). Moreover, the first and the fourth uORFs impair translation differently: the first uORF alone reduces of translation of the mORF to 50% whereas the fourth reduces translation to 1% (Hinnebusch 2005). Under starvation conditions, half of the ribosomes that translate the first uORF, will bypass the forth uORF and re-initiate directly at the GCN4 CDS, thus increasing translation (Abastado et al. 1991a; Abastado et al. 1991b).

A similar example is the *ATF4,* another transcription factor activated under stress and eIF2 phosphorylation. *ATF4* mRNA contains 2 uORFs, one of those being an uORF that overlaps the main coding sequence but in a different reading frame (o-uORF) in a different reading frame. In normal conditions, after the first short uORF is translated, the 40S subunit continues scanning and reinitiates translation at the o-uORF, therefore translating ATF4 ORF very inefficiently. Under stress conditions, when eIF2 is phosphorylated, the 40S subunit will bypass the o-uORF start codon

and reinitiate at the mORF, probably due to the fact that low concentration of available eIF2 makes it difficult for the 40S to incorporate a new eIF2-TC in time to start at the o-uORF. Then, ATF4 protein levels increase (Vattem and Wek 2004).

4.1.2.2   The role of DENR-MCTS1 in re-initiation and disease

The non-canonical factor DENR (density regulated protein) was shown to regulate translation in ribosome recycling and initiation by recruiting Met-tRNA$^{Met}_{i}$ in some specific viral mRNAs (Dmitriev et al. 2010; Skabkin et al. 2010) and, re-initiation after short stuORFs (upstream ORFs with strong Kozak sequences) together with MCTS1 (Schleich et al. 2014) (Fig. 2). Previous studies focused on finding those canonical initiation factors involved in re-initiation, assuming that re-initiation is just a second round of canonical initiation. In contrast, DENR-MCTS1 was described as the first factor to be selectively involved in re-initiation in a subset of specific mRNAs, without implications in cap-dependent translation, thus uncoupling re-initiation from initiation (Schleich et al. 2014). This re-initiation promotion is independent of the length between the two ORFs, suggesting that this factor is not present in the first round of translation, contrary to what was observed for eIF2. The preference of DENR-MCTS1 for regulation of short stuORFs is even more evident in humans, where only stuORFs coding one amino acid are dependent on them (Schleich et al. 2017).
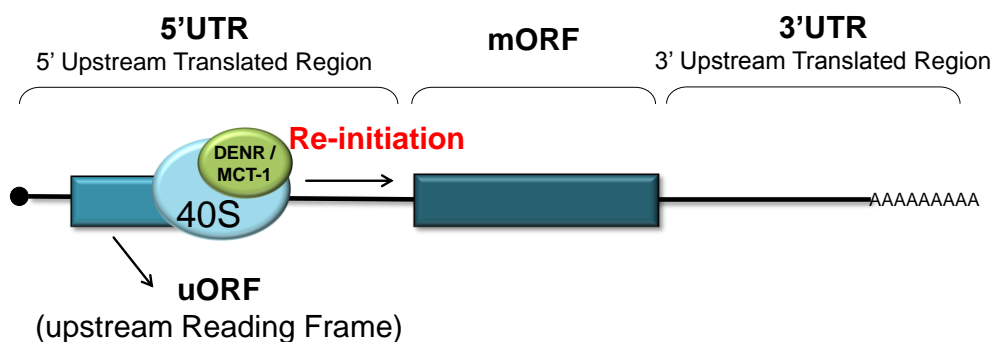
Figure 2. DENR-MCTS1 promote re-initiation after stuORFs.

Some groups have previously reported the importance of canonical translation in neuronal development in humans since mutations in the translation factors eIF2gamma and eIF2B cause X-linked intellectual disability and leukoencephalopathy with vanishing white matter (VWM), respectively (Li et al. 2004; Bugiani et al. 2010). The Heng group (Haas et al. 2016) showed the implication of DENR-MCTS1 in development of cerebral cortical neurons by impairing migration of embryonic cerebral cortical neurons in mouse (Fig. 3), and affecting dendrite spine density and morphology of mushroom-shaped spines. Moreover, human substitution mutations in *DENR* found in autism spectrum disorder human patients, disrupt mRNA translation initiation of stuORF-containing mRNAs and cause defects in development and synaptic connectivity of mouse cerebral cortical neurons. Of the two mutations, only one could rescue the reduction in stuORF reporter activity of DENR-KD cells (Haas et al. 2016), suggesting that DENR might control translation of other mRNAs besides stuORF-containing mRNAs.
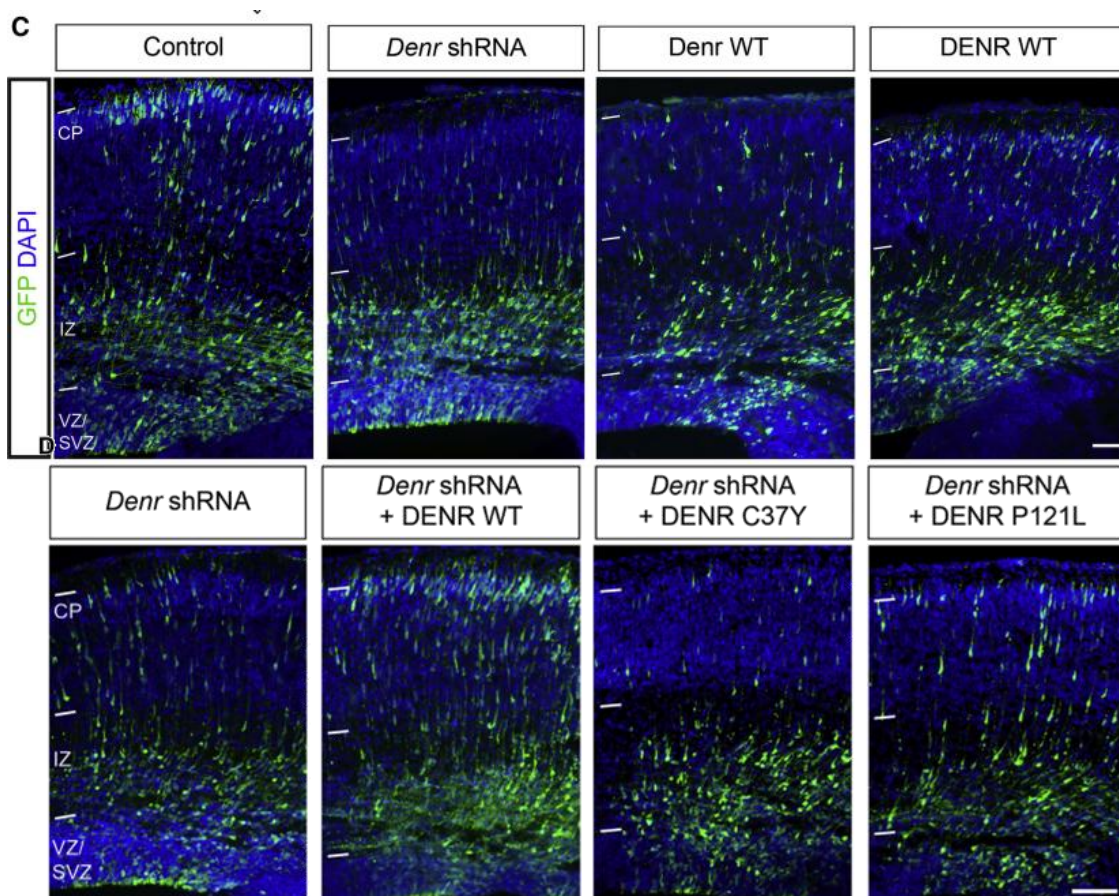
Figure 3. Implications of DENR and DENR mutations in migration of embryonic cerebral cortical neurons (Modified from(Haas et al. 2016))

4.2   Eukaryotic Initiation Factor 2D (eIF2D)

Another example of a non-canonical translation factor, and the focus of this study, is the eukaryotic Initiation Factor 2D (eIF2D).

4.2.1   The structure of eIF2D

eIF2D protein contains two important domains: a PUA domain at the N-terminal and a SUI1 domain at the C-terminal (Fig. 4). It shares those sequences with some other translation factors. PUA domain is an RNA-binding domain also found in MCTS1. The SUI1 domain is a ribosome binding domain also found in DENR and eIF1, the initiation factor implicated in start codon recognition (Fig. 4) (Mitchell and Lorsch 2008).

The structure of eIF2D protein in complex with the 40S subunit of the ribosome in re-initiation configuration has been revealed using cryoelectron microscopy (cryo-EM) (Weisser et al. 2017). This study showed three distinct density areas corresponding to different domains of eIF2D. The first one is located at the top of the ribosomal RNA helix 44, close to the mRNA channel, which suggests interactions with the mRNA, the second is below the platform, and finally the third is directly interacting with the helix h44. These three regions seem to be connected by very flexible domains. The first domain contacts the tRNA acceptor arm and the anticodon stem loop in the proximity of the mRNA channel.

The structure also reveals that eIF2D binds to the 40S subunit in similar places as other translation factors. For example, the SUI1 domain of eIF2D adopts the same structure as eIF1 and shares its position on the 40S. This provides a structural explanation for why previous biochemical studies showed an inhibition of eIF2D-mediated translation by eIF1 (Skabkin et al. 2010): eIF2D and eIF1 compete for the same binding site on the 40S. This also leads to the hypothesis of eIF2D having a biochemical function similar to or partially overlapping with eIF1. As mentioned before, eIF1 is essential for correct start codon recognition, due to the interaction with codon-anticodon, contact also observed in eIF2D. Conformational changes of h44 induced by binding of eIF1 control the subunit-joining step of initiation and mutations in h44 reduce start codon selection in vivo (Qin et al. 2012).

In the same study, the structure of DENR-MCTS1 complex was revealed and compared to eIF2D. In general, the structure and the binding sites were very similar, with one major difference: eIF2D has a domain inexistent in the DENR-MCTS1 complex (the winged helix) which interacts with the central part of helix 44 (h44). Moreover, there are more subtle changes, for example the SWIB domain of eIF2D is slightly shorter than in DENR, which would be enough to cause a different conformation change in the 40S. Other factors like ABCE-1 or eIF3 would not interfere with eIF2D binding to the 40S, but with DENR (Weisser et al. 2017). Together, this suggests different functions of eIF2D and the DENR-MCTS1 complex.

Finally, the WH domain of eIF2D on the h44 would obstruct 60S joining to form the 80S, suggesting that eIF2D must dissociate from the 40S for translation initiation, probably preventing premature 80S formation on poor context start codon.
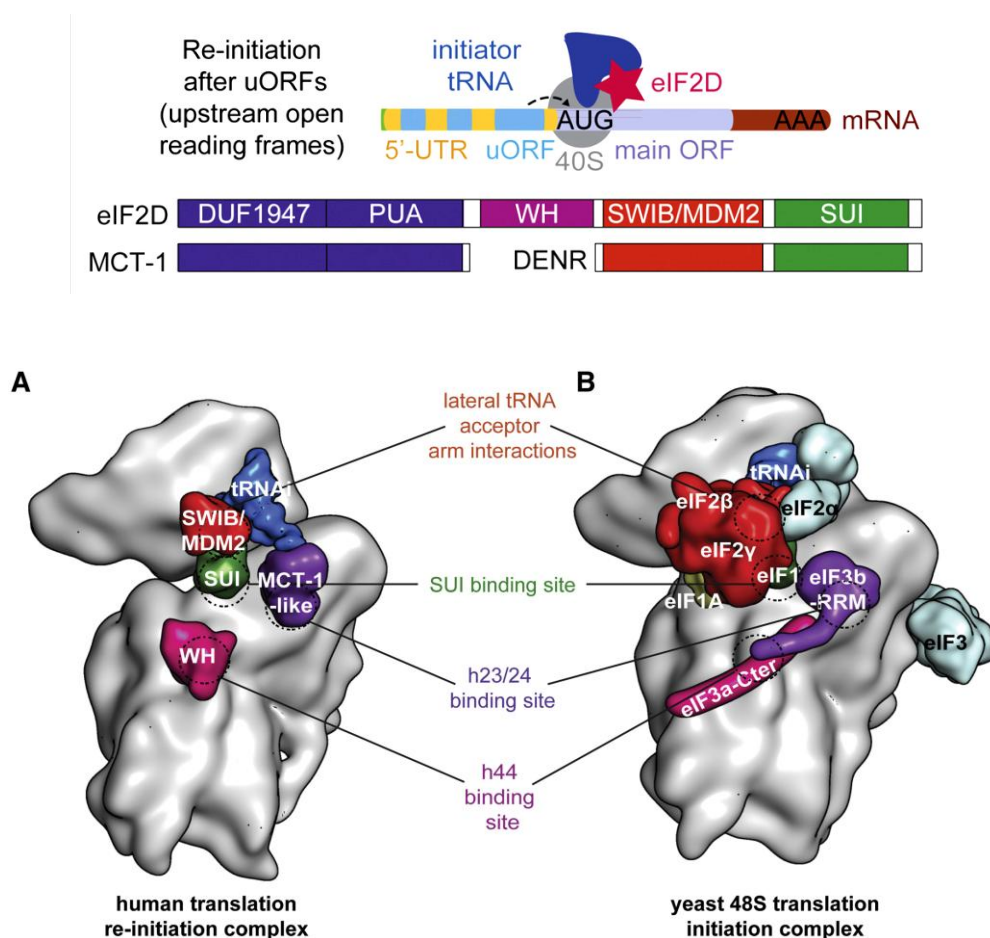
Figure 4. Structure of eIF2D in Re-initiation complex (Weisser et al. 2017)

4.2.2   Biochemical functions of eIF2D in translation

Previous groups have studied the biochemical properties of eIF2D and demonstrated that it has non-canonical translation initiation activity, by GTP-independent delivery of Met-tRNA$^{Met}_i$ to the ribosome on a start codon (Dmitriev et al. 2010). This unusual activity is completely different from the canonical initiator tRNA delivery pathway mediated by eIF2-GTP-Met-tRNA$^{Met}_i$ ternary complex, which is strictly GTP-dependent. Interestingly, GTP-independent tRNA delivery by eIF2D only occurred if ribosomal attachment to the mRNA placed the initiation codon directly in the P site (Dmitriev et al. 2010). However, eIF2D does not promote attachment of Met-tRNA$^{Met}_i$ to 40S subunits (Skabkin et al. 2010). It has been hypothesized that eIF2D might promote translation of leaderless or short 5'UTR mRNAs, where start codon recognition by canonical scanning could not occur (Dmitriev et al. 2010). Moreover, eIF2D strongly promotes initiation complexes formation on model mRNAs with A-rich 5'UTRs. eIF1 seems to destabilize the formation of initiation complexes by eIF2D, probably due to competition for the ribosome binding site, as revealed by the structural studies described above. In contrast to eIF2, eIF2D also promoted delivery of some elongator tRNAs, like tRNA-Phe, if the P site was occupied by a cognate codon (Dmitriev et al. 2010).

Besides non-canonical translation initiation, eIF2D has also been reported to work in post-termination ribosome recycling. In biochemical experiments, terminating ribosomes where incubated with eRF1/eRF3, ABCE1, and eIF6 obtaining an mRNA, tRNA and 40S still bound. Further adding eIF2D before the canonical initiation factors completely released all the components (Pisarev et al. 2010; Skabkin et al. 2010), explaining why pre-incubation of 40S subunits with eIF2D moderately inhibits eIF2-mediated recruitment of Met-tRNA$^{Met}_i$. Moreover, eIF2D and the DENR-MCTS1 complex promote tRNA/mRNA/40S release also in the absence of ABCE-1 (Skabkin et al. 2010). Therefore, eIF2D impaired the ability of these 40S subunits to participate in the next round of initiation. Taken together, it is not clear the function of eIF2D in translation control, since it seems to promote initiation on certain conditions and recycling in others, thus also suppressing re-initiation.

4.2.3 Previous (unpublished) work about eIF2D from the Duncan lab:

4.2.3.1 Characterization of the larval locomotion phenotype and NMJ morphology

The biochemical properties of eIF2D have been addressed in reconstituted in vitro assays, but nothing was known about its biological roles *in vivo* in a multicellular organism. To address eIF2D's role *in vivo*, the Duncan lab generated *eIF2D^{KO}* flies using an imprecise P-element excision approach, which takes out the entire *eIF2D* ORF (Fig. 5A). These flies were characterized and showed no mRNA or protein expression for eIF2D (Fig. 5B, 5C). In parallel, a revertant line with a precise excision of the P-element was obtained. These animals have essentially the same genetic background as the knockout, and are therefore used as a wild type control line.

eIF2D^{KO} flies showed no gross morphological defects (Fig. 5D, 5E), were viable and fertile, but both larvae and flies have impaired locomotion (Fig. 5F) while other behaviors were not affected.
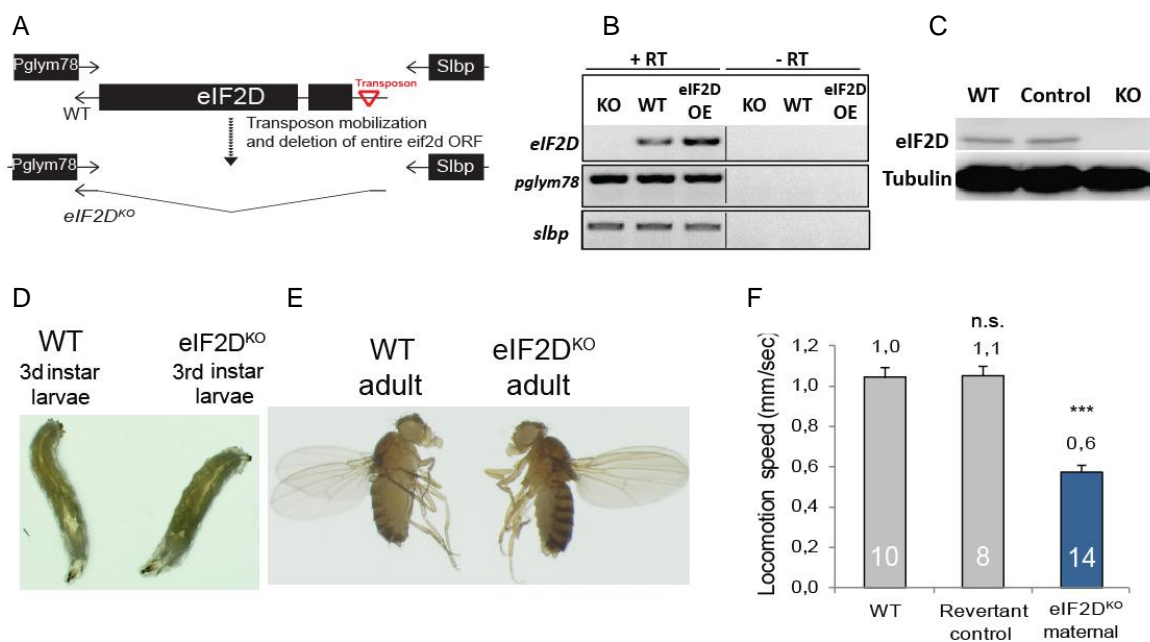
Figure 5. Generation and characterization of *eIF2D^{KO}* flies

*This unpublished data was obtained by Dr. Tatyana Koledachkina in the Duncan lab

4.2.3.2 *Synaptic function and homeostasis are impaired in eIF2D^{KO} larvae*

Drosophila larvae move by firing of motor neurons that project and signal to the muscles through well studied synapses, named Neuromuscular Junctions (NMJ). The *Drosophila* NMJ has been extensively characterized and there are many resources available to study it.

In order to characterize any possible abnormalities in *eIF2D^{KO}* NMJs, morphology and function were examined. First, morphology of the NMJ of *eIF2D^{KO}* larvae was compared to controls and showed no differences either in average bouton number or size (Fig. 6). Muscle size and morphology in *eIF2D^{KO}* larvae of the muscle were also not changed (Fig. 6).
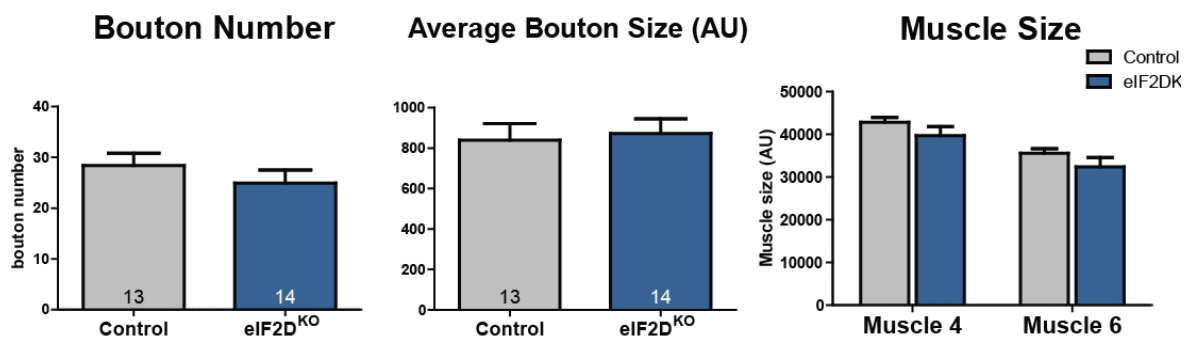
Figure 6. Characterization of eIF2D^{KO} NMJs and muscles

*This unpublished data was obtained by Dr. Tatyana Koledachkina in the Duncan lab

Next, electrophysiological experiments performed in collaboration with Dr. Martin Müller's lab revealed that synaptic function was compromised. *eIF2D^{KO}* larval NMJs show a decrease in synaptic transmission and problems in homeostatic plasticity compensation. Amplitude of evoked excitatory postsynaptic potentials (EPSPs) and miniature excitatory postsynaptic potentials (mEPSPs) were reduced, as was muscle input resistance (Fig. 7). In mutants with impaired synaptic transmission due to reduction of glutamate receptors or upon persistent pharmacological blocking of those receptors, homeostatic compensatory mechanisms would act to increase the release of synaptic vesicles, resulting in an increase in quantal content (Paradis et al. 2001; Davis and Muller 2015). An alternative way to activate this compensation is by

having an overexpression of potassium channels, which results in a hyperpolarized muscle with a decreased input resistance (Paradis et al. 2001). In the case of *eIF2D^{KO}* NMJs, this increase in quantal content to compensate decreased muscle input resistance is not observed (Fig. 7), suggesting a defect in homeostatic plasticity compensation.
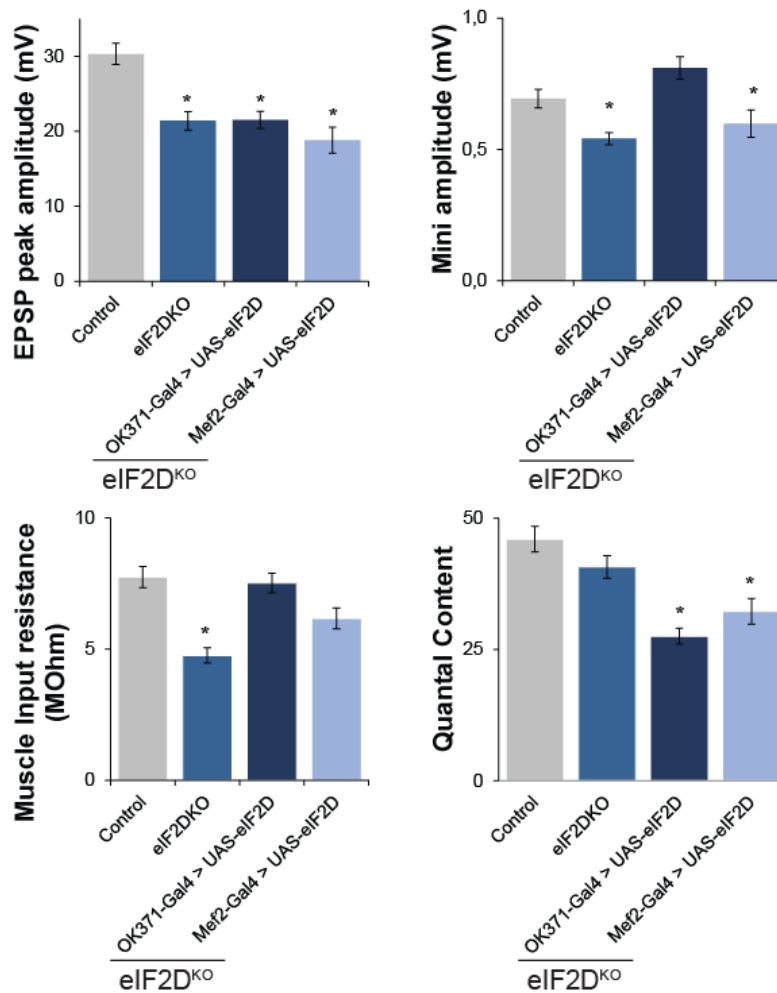
Figure 7. Electrophysiological properties of *eIF2D^{KO}* NMJs.

*This unpublished data was obtained by Dr. Martin Müller and Jennifer Keim, in the Müller lab

4.3 Neurons and Locomotor system

Neurons are a particular cell type with highly polarized morphology and very specialized functions. Motor neurons are a specific type of neuron that project their axons from the ventral nerve cord (VNC) to the muscles, to excite the muscles and produce movement. The motor neurons are mostly glutamatergic in the *Drosophila*

NMJ, but a small fraction of them co-express other neurotransmitters, such as dopamine, leukokinin-1 or insulin (Cantera and Nassel 1992; Gorczyca et al. 1993; Monastirioti et al. 1995). The *Drosophila* larva NMJ has been extensively studied by many groups to understand how the neuron and the muscle communicate with each other to ultimately produce locomotion.

4.3.1   The Drosophila Neuromuscular Junction

The body of the *Drosophila* larva is organized in segments from the anterior to the posterior part of the animal, and hemisegments on each side. Every segment presents a stereotyped arrangement of the muscles which consists of 30 muscles in each hemisegment from the second to seventh abdominal segment (A2 to A7). Every muscle can be recognized by its position in the body, size and shape. Each muscle receives axonal projection of motor neurons axons and each motor neuron projects to one or more specific muscle cells. These connections are highly stereotyped and, as for the muscles, every motor neuron is well characterized. The most studied muscles and their NMJs are muscle 4, because it is big and easily recognizable, and muscle 6 and 7, which are often studied together because they share a common axon terminal.

The motor neurons have their cell bodies located in very specific position in the CNS and project the axons to the muscles. They travel together along the middle axis of the larvae and exit in the segment where they will innervate the muscles. The growth cone is independent of the presence of the target muscle since muscle ablation showed that motor neurons still extend their projections to the sites where their target should be, and might make connections with neighboring muscles instead (Cash et al. 1992).

The development of the NMJ is also well studied. At 13h AEL (after egg laying), the muscles are completely assembled and the terminals of the motor neurons start to search the correct sites to form a functional NMJ. Several synaptic molecules are already present in the motor neuron and muscle before their contact. For example, both glutamate neurotransmitter and glutamate receptors can be detected in the neurons or muscles respectively, prior to synapse formation (Broadie and Bate

1993c; Currie et al. 1995), but are randomly distributed along the muscle membrane. Muscles cells express glutamate receptors even without the innervation of a motor neuron (Broadie and Bate 1993c) but maturation of postsynaptic compartment with correct receptor position requires innervation from a functional motor neuron (Broadie and Bate 1993a; Broadie and Bate 1993b; Broadie and Bate 1993d) although this might not be glutamatergic (Featherstone et al. 2002). Proper synapse formation requires coordinated protein expression and localization from both sides, but the regulation is not yet fully understood. When the innervation of the muscle is delayed or absent, the receptors remain diffused at the muscle surface instead of clustered at the NMJ (Broadie and Bate 1993b).
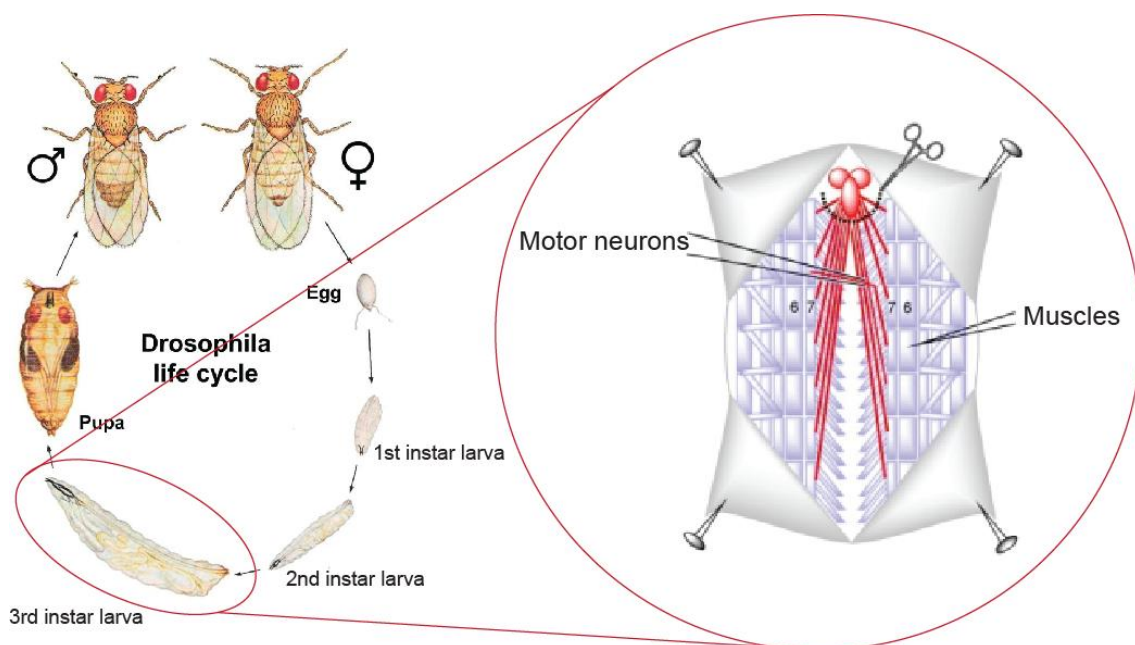
Figure 8. Scheme of the *Drosophila* life cycle and dissection to observe muscles (blue) and CNS and motor neurons (red).

Even after motor neurons and muscles have formed functional synapses, these synapses need to continue developing. During the larval stages of the *Drosophila*, from embryo to pupae, the body and thus the muscles will grow and the axon terminals will need to adjust by increasing varicosity 5 to 10 times more. Many studies of the *Drosophila* NMJ focus on the 3rd instar larvae because the terminals

and the muscles have reached their biggest size making them easier to study than the smaller 1st instar larva NMJs.

4.3.1.1 The genetic analysis of NMJ structure and function

Many studies have identified different mutants producing defects at the NMJ specifically affecting different aspects of the morphology or function. One class of synaptic defects affects the T-bar formation (electron dense specialization for vesicle docking) changing its shape, while others might affect their distribution at the active zone (AZ), in some cases being so severe that entire buttons are missing AZ and they are then called ghost boutons. These defects are sometimes accompanied by the corresponding defects in glutamate receptor apposition. Similar defects can be observed on the postsynaptic side, affecting GluR size and localization, mainly due to disruption of the cytoskeleton (Pielage et al. 2006). When the entire bouton is lacking receptors, those are called orphan boutons (Banovic et al. 2010). In some cases, AZ and GluR numbers are normal, but the two components are not correctly apposed and the synaptic signal cannot be properly transmitted (Graf et al. 2012).

More general defects can also be found: some mutants for a specific gene will affect specifically an aspect of the axon terminal formation, thus we see mutants with defective branching, shorter or longer terminal arbors, bouton size and/or number alteration, incorporation of satellite boutons (smaller boutons), etc. Each of those morphological defects usually results in a corresponding physiological defect in transmission and/or behavior (Menon et al. 2013).

Finally, another way of regulating synapses is through activity, which regulates morphology of the NMJ boutons or terminals. Therefore, morphological defects can also be observed following changes in activity. For example, increase activity produced by seizures increases synaptic growth (Guan et al. 2005), as does increased locomotion (Sigrist et al. 2003). Activity dependent growth is affected in larvae that are doubly deficient for Shaker (*sh*) and ether-a-gogo (*eag*), two potassium channels found in the muscle. These double mutant larvae have hyperexcitable muscles and this leads to increased bouton number and higher branching at the NMJs (Budnik et al. 1990).

4.3.2 Molecules at the *Drosophila* Neuromuscular Junction

Many synaptic molecules of the *Drosophila* NMJ have been identified and characterized, and the function of most of them is well defined. About 70-80% of those molecules are well conserved relative to the mammalian homologues, supporting that *Drosophila* and mammalian NMJs are fundamentally similar (although mammalian NMJs are cholinergic), and making *Drosophila* a great model for its study. Different proteins have different roles at the synapse and in synaptic transmission, and loss of them causes different phenotypes from strong phenotypes such as lethality to more mild ones like reduced neurotransmission.

The synaptic bouton is an enlargement of the axon terminal where the active zones (AZ) are located opposite of the GluRs. The AZ can be identified by electron microscopy as a dense T-bar structure. This structure is formed by the protein Bruchpilot (Brp). Brp is the essential scaffold protein for proper localization of the proteins needed for synaptic vesicle docking, calcium sensing and release, to locally release neurotransmitter where high concentrations of Ca^{2+} are generated. The T-bar consists of a central core anchored to the plasma membrane and filaments extending to the cytoplasm, where the synaptic vesicles can anchor. This structure helps the synaptic vesicles filled with neurotransmitter to contact and fuse with the membrane to produce exocytosis, in a very spatially controlled manner. There are several proteins involved in the specificity of place fusion, and together they form the SNARE complex (Soeller et al. 1993; Littleton et al. 1998; Chen et al. 1999): vesicle anchored v-SNARE (synaptobrevin/VAMP) and target membrane t-SNARE (syntaxin and Snap-25).

Syntaxin (Syx1A) is involved in two main pathways: it is essential for exocytosis and synaptic transmission. *Syx1A* mutants show a blockage of secretions not only from neurons, but also from many other cell types (Harrison et al. 1994; Broadie et al. 1995; Schulze et al. 1995). Loss of Syx1A causes lethality due to the inefficient post-Golgi to plasma membrane fusion of vesicles in all cell types (Schulze and Bellen 1996). More specifically, loss of Syx1A in neurons causes absence of spontaneous (mEPSP) and evoked (EPSP) neurotransmitter release.

The action potential propagates through the axon to the synaptic terminal where voltage gated calcium channels open, generating an influx of Ca^{2+} to activate the neurotransmitter release machinery. Cacophony (cac) is the presynaptic voltage-dependent Ca^{2+} channel in *Drosophila* (Littleton and Ganetzky 2000) and it is enriched at the AZ surrounding the core of Brp. Ca^{2+} sensing at the postsynaptic terminal regulates release probability: higher density in Ca^{2+} channels and therefore higher Ca^{2+} entry will give higher release probability. After an influx of calcium through voltage dependent calcium channels on the presynaptic compartment, the synaptic vesicles fuse to the membrane and their content is released. Synaptotagmin (Syt1) is a vesicular protein with two cytoplasmic Ca^{2+} binding domains (Ca^{2+} sensors) that will sense calcium influx to the terminal to promote vesicle fusion (Littleton et al. 1993; Broadie et al. 1994; DiAntonio and Schwarz 1994; Littleton et al. 1994). Basically, it binds directly to the SNARE complex to regulate neurotransmitter release. Syt1 also has Ca2+ independent roles at the synapse such as synaptic vesicle docking and endocytosis. Another calcium sensing protein is Complexin (Cpx), with a dual role by inhibiting spontaneous release of the synaptic vesicle in absence of an action potential and enhancing fusion after an evoked potential (Giraudo et al. 2006; Xue et al. 2010). Both Cpx and Syt1 proteins are supposed to modulate each other's function in synaptic vesicle fusion. For example, Cpx helps Syt1 to interact with the SNARE complex and enhances Ca^{2+} sensitivity, thus accelerating the fusion (Jorquera et al. 2012). Like in the presynaptic compartment, Ca^{2+} sensors are also present in the muscle and respond to glutamate receptor activation by neurotransmitter release.

Key molecules at the postsynaptic compartment include glutamate receptors, scaffolding proteins, adhesion molecules and ion channels. Glutamate receptors are heteroteramers formed by the subunits GluRIIC, GluRIID and GluRIIE and either GluRIIA or GluRIIB, therefore producing type-A or type-B receptors (Schuster et al. 1991; Petersen et al. 1997; Marrus and DiAntonio 2004; Marrus et al. 2004; Featherstone et al. 2005; Qin et al. 2005). Type-A and type-B receptors have different distribution (DiAntonio et al. 1999) and electrophysiological properties, with A-type showing slower desensitization kinetics than type-B. The ratio A/B type was found to be as important for correct function as the absolute levels of the receptors

themselves (Petersen et al. 1997; DiAntonio et al. 1999). Moreover, Type-A receptors tend to be enriched in new postsynaptic densities, whereas more mature ones are more balanced, meaning type-B receptors would get incorporated later in the synapses (Schmid et al. 2008).

The type-A and type-B glutamate receptors localize in the postsynaptic muscle apposed to the presynaptic AZ forming clusters of several heterotetramers. Neto is an auxiliary subunit essential in glutamate receptor cluster formation at the NMJ (Kim and Serpe 2013). At the postsynaptic compartment, the main scaffold protein is Discs large (Dlg) which recruits and regulates organization of synaptic molecules including the receptors, other scaffold proteins, and ion channels.

The extracellular matrix (ECM) is the space between motor neuron and muscle and it is filled with proteins (glycoproteins and proteoglycans) which have an important role in regulating synaptic structure and function. Correct apposition of the pre- and post-synaptic compartments (AZ and GluRs) is essential for proper transmission and requires several transynaptic proteins. Neurexin-1 (Nrx-1) is important for correct apposition and postsynaptic density organization (Owald et al. 2010; Owald et al. 2012). These molecules have also other functions: Glutamate receptor subunit composition is not arbitrary, but regulated by different pathways and one example is the Neurexin-Neuroligin (Nrx-Nlg) interaction. Historically Nrx-1 was the presynaptic partner and Nlg the post-, but it seems that, at least in the Drosophila NMJ, Nrx-1 has also a role as postsynaptic molecule (Chen et al. 2012).
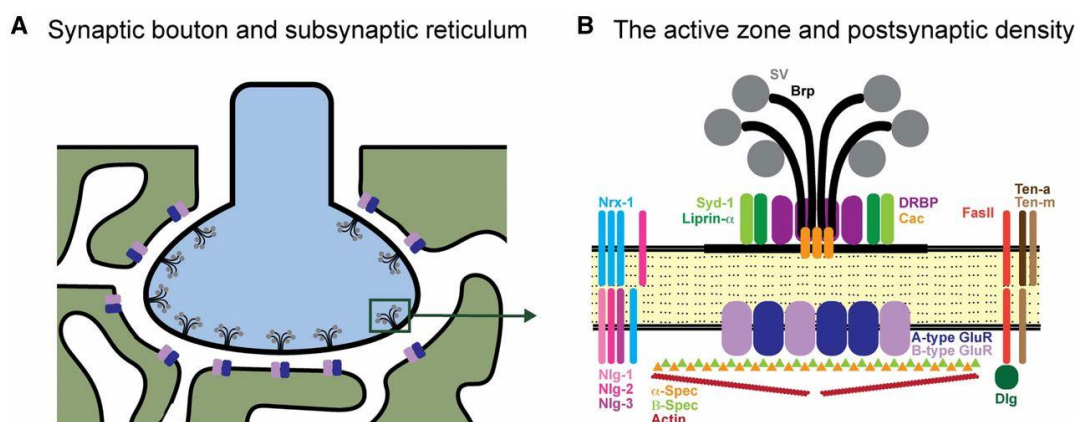
Figure 9. NMJ synapse (Modified from Kathryn P. Harris and J. Troy Littleton, 2015)

4.4 The aims of the project

Regulation of gene expression by translation control is a key driver of protein levels in a cell. Previous studies showed the implications of altered translation control in several aspects of cell and animal physiology. Canonical translation factors seem to regulate the majority of transcripts in a cell, whereas non-canonical factors could offer a way to specifically regulate certain transcripts under specific conditions. However, which exact endogenous mRNAs a certain factor controls and the mechanisms underlying of co-regulation of specific mRNAs *in vivo* remain largely unexplored.

In this project I decided to focus on the study of one of these non-canonical translation factors, eIF2D, motivated by its interesting biochemical properties and the lack of knowledge of its physiological role in a whole organism. The core hypothesis motivating my project is based on previously published data about eIF2D's biochemical properties, and unpublished data from the Duncan lab about *eIF2D^{KO}* phenotypes *in vivo*. I hypothesize that eIF2D regulates translation initiation and/or recycling of certain mRNAs in vivo to promote normal locomotion and synaptic function.

The goal of my project was to investigate the functions of eIF2D *in vivo* in a multicellular organism. My specific aims were:

1. To identify physiological processes affected by eIF2D *in vivo* and the cell types where eIF2D function is important to promote normal behavior
2. To optimize a method to study the impact of eIF2D on translation in *Drosophila* larvae
3. To identify specific endogenous mRNAs regulated by eIF2D in a multicellular organism and gain insight into how eIF2D controls their translation
4. To understand how translational regulation by eIF2D affects animal behavior

5 Material and Methods

5.1 Materials

5.1.1 Antibodies

5.1.1.1 Primary antibodies

Table 1			
Antibody	**From animal**	**Dilution**	**Sourse**
Brp (nc82)	mouse	1:100	Developmental Studies Hybridoma Bank
eIF4A	rabbit	1:1000	CST
GluRIIA (8B4D2)	mouse	1:50	Developmental Studies Hybridoma Bank
GluRIIB	rabbit	1:1000	Dr. Michaela Serpe.
GluRIIC	rabbit	1:2500	Dr. Catherine Collins
GluRIID	rabbit	1:500	Dr. Stephan Sigrist
MitoTracker™ Red CMXRos (1mM)	-	1:1000	Thermo Fisher Scientific
Syx1A	mouse	1:1000	Developmental Studies Hybridoma Bank
tubulin	mouse	1:10.000	Developmental Studies Hybridoma Bank

eIF2D antibody generation: Rabbit polyclonal anti-eIF2D antibody was produced against N- and C-terminal peptides by Thermo Fisher Scientific and affinity purified against target peptides. Western blot dilution: 1:200.

5.1.1.2 Secondary antibodies

Table 2		
Antibody	**Dilution**	**Sourse**
anti-mouse-HRP	1:4000	Thermo Scientific
anti-rabbit-HRP	1:8000	Thermo Scientific
Alexa Fluor®-labeled anti-rabbit	1:1000	Life Technologies
Alexa Fluor®- anti-mouse	1:1000	Life Technologies
Alexa Fluor® 647-conjugated goat anti-HRP	1:1000	Life Technologies

5.1.2 Fly stocks

Fly stocks were raised on standard fly food at 25°C with 70% humidity and a 12h light/12 h dark cycle. Flies were anaesthetized via a CO_2-dispensing fly pad.

Table 3		
Genotype	**Use**	**Origin**
eIF2D^{KO}	eIF2D^{KO}	Duncan lab
W$^-$	Control	Revertant line from eIF2D P-element precise excision, isogenized
w-; actin-GAL4/CyO,wee; eIF2D^{KO}/Tm6b, Tb	Ubiquitous rescue	T. Koledachkina
w-, elav-GAL4/FM7,B;; eIF2D^{KO} ,Tm3, Ser	Neuronal rescue	T. Koledachkina
w-;; Mef2-GAL4, eIF2D^{KO}/Tm6b, Tb, GB	Muscle driver	T. Koledachkina
w-; 21-7-GAL4, UAS-CD8-GFP/CyO,wee; eIF2D^{KO}/Tm6b, Tb	Sensory neuron driver	T. Koledachkina
w-; OK371-GAL4/CyO,wee; eIF2D^{KO}/Tm6b,Tb	Motor neuron driver	T. Koledachkina
UAS-eIF2D /CyO, wee; eIF2D^{KO}/TM6b,Tb,ubi-GFP	eIF2D rescue	T. Koledachkina

5.1.3 Fly food

Table 4. Ingredients for standard fly food (total volume1 L)		
Quantity	**Ingredient**	**Company**
8.75 g	Agar (strings)	Probio GmbH
0.08 g	Corn flour	Spielberger-GmbH
10 g	Soy flour	Spielberger-GmbH
25 g	Brewer's yeast (ground)	Gewürzmühle Brecht
0.08 g	Malt syrup	MeisterMarken – Ulmer Spatz
21.88 g	Treacle (molasses)	Grafschafter Krautfabrik
1.88 g	Nipagin (Methyl 4-hydroxybenzoate)	Merck

9.38 mL	Propionic acid	Roth

5.1.4   Cell lines

Table 5	
Drosophila cell line	**Source**
Schneider 2 cells (S2)	Drosophila Genomics Resourse Center (DGRC)

5.1.5   Pharmacological reagents

Table 6	
Compound	**Company / Reference**
Cycloxeximide	Sigma Aldrich
Puromycin	Sigma Aldrich
RNAsin	Promega
cOmplete, EDTA-free (Proteinase inhibitors)	Roche
PhosSTOP (Phosphatase inhibitors)	Roche
dNTPs	Invitrogen
DTT	Invitrogen
Trizol	Ambion
GlycoBlue	Ambion
Clorophorm	Roth
Methanol	Roth
Formaldehide	Sigma Aldrich

5.1.6   Enzymes and enzymes kits

Table 7		
Reagent	**Purpose / method**	**Company**
GoTaq G2 DNA polymerase	PCR	Promega
Phusion® High-Fidelity DNA Polymerase	PCR	New England Biolabs

SuperScript® II Reverse Transcriptase	cDNA Synthesis	Life Technologies
Megascript T7 Kit	Transcription reaction	Invitrogen
Proteinase K		Promega
TURBO DNase		Ambion
DNAse I, recombinant		Roche
RNAse H		NEB

5.1.7 Cell culture media and related reagents

Table 8. Media composition for S2 cell culture		
Reagent	**Volume**	**Source**
B&S Schneiders's Drosophila (ohne L-Glutamin)	500 ml	BioSell
Penicillin Streptomycin (Pen Strep)	5ml	Gibco by Life Technologies
L-Glutamin	5ml	Life Technologies
Fetal Bovine Serum (Collected in South America)	50ml	HyClone by GE Healthcare LifeSiences

Table 9. Media composition for S2 cell culture		
Reagent	**Volume**	**Source**
B&S Schneiders's Drosophila (ohne L-Glutamin)	500 ml	BioSell
Penicillin Streptomycin (Pen Strep)	5ml	Gibco by Life Technologies
L-Glutamin	5ml	Life Technologies

5.1.8 Grape Plate Recipe (For *Drosophila* embryo collection)

Table 10	
Reagent	**Volume (for 200ml)**
H2O	91.8 ml
Grape Juice	100 ml
Agar (kobe, type I)	4 g
Ethanol 95%	2.1 ml

Propionic acid	2 ml

5.1.9   Primers

Table 11		
Primer name	**Sequence**	**Gene**
OAGD301_LP1	CCA CTG AAA AAG ACA ATG AG	eIF2D
OAGD302_LP2	CGG GCC GGG CTA TGT TTT TC	eIF2D
OAGD310_LP5	GTT CCG GCA GCG CGT GGA GG	eIF2D
OAGD351_LP10	ACA CTC AAG AGG ACA GGC GG	eIF2D
OAGD1_DENR_F	CCG GTA ATA CGA CTC ACT ATA GGG AGG GGG GTA TGA CAT CGA ACA AGT CA	DENR
OAGD2_DENR_R	CCG GTA ATA CGA CTC ACT ATA GGG AGG CGT CAC CTA TCC GAT CAA GAT GA	DENR
OAGD12_EGFP_F	TAA TAC GAC TCA CTA TAG GGA GGA TGG TGA GCA AGG	GFP
OAGD13_EGFP_R	TAA TAC GAC TCA CTA TAG GGA GGA TCG CGC TTC TCG	GFP
OAGD78_eIF2D_ORF_F	TAA TAC GAC TCA CTA TAG GGG CTC CTG TGA CCT TCG CTA C	eIF2D
OAGD79_eIF2D_ORF_R	TAA TAC GAC TCA CTA TAG GGT AAA GTT CAC CAC TTC GGG G	eIF2D
OAGD1340_deIF4A_R	GACCCCTCACACAGGGAATG	eIF4A
OAGD1341_deIF4A_F	GACTGCCACCTTCTCGATTG	eIF4A
OAGD940_Shaw-F	CTG ATC AAC ATG GAC TCG G	Shaw
OAGD939_Shaw-R	CGC GTA GCC GGA ATC TTC	Shaw
OAGD1246_CG10472_RF1	GGA GGG ACA GCA GAT CAT C	CG10472
OAGD1248_CG10472_RR1	CTC AAT GGG CAC TGG CAA	CG10472

5.1.10   Commonly used buffers

Table 12		
	Buffer	**Composition**
	PBS	2.7mM KCl; 1.5mM KH_2PO_4; 8mM Na_2HPO_4 in H_2O at pH 7.4
IHC	HL3 dissection buffer	0.128M NaCl, 0.002M KCl, 0.0018M $CaCl_2$, 0.004M $MgCl_2$, 0.0355M Sucrose, 0.005M HEPES
	PBST	1xPBS, 0.1% Tween
	Blocking solution	5% goat serum in PBST

Wester blot	TBST	1xTBS (9 g NaCl, 50 mL 1M Tris pH7.4), 0.1% Tween	
	Blocking solution	5% Milk in PBS	
	Electrophoseris running gel	0,025M Tris, 0,192M glycine, 0,1% SDS	
	Wester blot transfer	0.048M Tris, 0.039M glycine, 20% methanol, 0.00375% SDS	
	SDS Sample Buffer	0.0625M Tris pH 6.8, 2% SDS, 10% glycerol, 0.1M DTT, 0.01% bromophenol blue	
DNA elecrophoresis	TBE buffer	10.8g Tris, 5.5g Boric acid, 9.3g EDTA, up to 1l with H_2O	

5.1.11 Acrylamid gels

Table 13			
Reagent	**Separating gel**		**Stacking gel**
	10%	**15%**	**5%**
H_2O	2.0 ml	1.2 ml	0.68 ml
30% Acrylamide Mix	1.7 ml	2.5 ml	0.17 ml
1.5M Tris/HCl, pH 8.8	1.3 ml	1.3 ml	0.13 ml
10% SDS	0.05 ml	0.05 ml	0.01 ml
10% APS	0.05 ml	0.05 ml	0.01 ml
TEMED	0.002 ml	0.002 ml	0.001 ml

5.1.12 Plasmids

Table 14. Plasmid name
pMT-GluRIIB_5'UTR-Rluc
pMT_park-RB_5'UTR-Rluc
pMT_Cadps-RF_5UTR-Rluc
pMT_Cadps-RD_ 5'UTR-Rluc
pMT_LanA-RA_ 5'UTR-Rluc
pMT_eIF4A-RA_5'UTR-Rluc
pMT_eIF4A-RB_5'UTR-Rluc

pMT_eIF4A-RD_5'UTR-Rluc
pMT_Mp-RG_5'UTR-Rluc
pMT_rpl41_5'UTR-Rluc
pMT_Nrx-1-RB_5'UTR-Rluc
pMT_Nrx-1-RD_5'UTR-Rluc
pMT-Fluc
pMT_1aauORF-Rluc
pMT_control-Rluc

Figure 10. Example of a plasmid with a 5'UTR followed by the Renilla Luciferase CDS
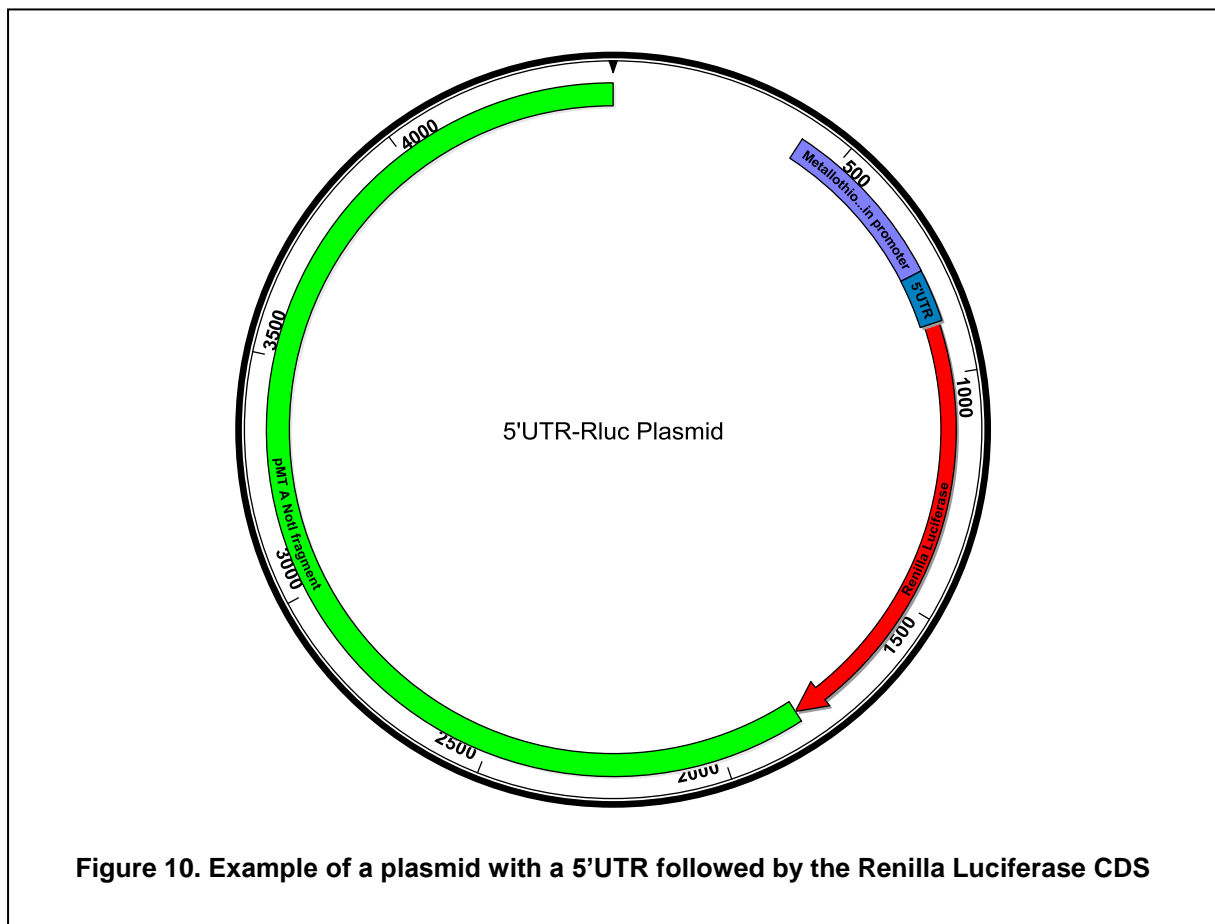
5.2 Methods

5.2.1 Genotyping of flies

To genotype flies, DNA from a single fly was extracted. A single fly was placed in a 1.5ml tube and mashed with a pipette tip containing 50µl of squishing buffer. The buffer was added to the tube and incubated at 37°C for 30min, followed by 2min incubation at 95°C to inactivate Proteinase K.

Table 15. Squishing buffer	
Reagent	**concentration**
Tris-Cl pH 8.2	10mM
EDTA	1mM
NaCl	25mM
Proteinase K	200µg/ml

This DNA was then used to perform PCR with specific primers.

In wild-type, OAGD302_LP2 and OAGD351_LP10 primers amplify a region of 2336bp whereas in eIF2D^{KO} the product is 529bp. OAGD301_LP1 and OAGD310_LP5 primers amplify a region of 400bp in wild-type and nothing in *eIF2D^{KO}*.

Table 16. PCR reaction	
Reagent	**Volume (for 1 reaction of 20µl total)**
H$_2$O	11.9µl
GoTaq 5x Buffer	4µl
dNTPs	1µl
Primer forward	1µl
Primer reverse	1µl
GoTaq polymerase	0.1µl
Single-fly DNA	1µl

Table 17. Incubation for PCR reaction		
Temperature	**Time**	
94°C	5min	
94°C	**30sec**	**x35**
55°C	**30sec**	

72°C	**2min**
72°C	7min
4°C	hold

PCR products were then visualized by 1% agarose gel (in TBE) electrophoresis with Roti®-GelStain (Carl Roth).

5.2.2 dsRNA synthesis

Templates for dsRNA production were obtained by PCR-amplification of target regions using a proof-reading *Phusion® High-Fidelity DNA Polymerase* (NEB). The amplicon sizes are 391 bps for eIF2D and 650 bps for GFP dsRNAs. Both forward and reverse primers contained T7 RNA polymerase binding sites: OAGD12_EGFP_F and OAGD13_EGFP_R for EGFP; OAGD78_eIF2D_ORF_F and OAGD79_eIF2D_ORF_R for eIF2D; OAGD1_DENR_F and OAGD2_DENR_R for DENR. Both forward and reverse primers contain T7 RNA polymerase binding sites. The PCR products were purified using QIAquick gel extraction kit (Qiagen)

For the transcription reaction the *Megascript T7 Kit (Invitrogen)* was used. Reagents were thawed on ice, briefly vortexed and spun down and assembled as indicated in Table 18. Reactions were incubated for 4-6h at 37°C in a thermocycler.

Table 18. Transcription reaction assembly	
Reagent	**Volume**
Nuclease-free Water	20µl
ATP solution	2µl
CTP solution	2µl
GTP solution	2µl
UTP solution	2µl
10x Reaction Buffer	2µl

Template DNA	0.1 – 1µg	
Enzyme	2µl	

After the incubation, the tubes were kept at 4°C for 15min. Then, 1µl *TURBO DNAse* was added to each reaction and incubated at 37°C for 20min, to eliminate template DNA from the sample. To purify the RNA, *NucleoSpin (RNAII)* kit (Machinery Nagel) was used, following the manufacturer's "*Clean up of RNA from reaction mixtures*".

5.2.3 Culturing Drosophila S2 cells and knockdown of eIF2D

Drosophila S2 cells were cultured in flasks at 25°C in complete *Schneider's Drosophila Medium* (Bio&Sell, Germany) containing *L-Glutamin*, *Penicillin/Streptomycin* and *10% FBS* (all from Life Technologies). For a knockdown treatment 2.5×10^6 cells were incubated at 25°C in 1 ml of FBS-free Schneider's medium for 1 hour or 30min with 12-15µg/millon cells of purified dsRNA (depending on the targeted gene) against *DENR, eIF2D or GFP* with constant agitation. After incubation, 4 ml of complete Schneider's medium was added and the cells were grown for 7 days at 25°C to obtain sufficient knockdown. Efficiency of eIF2D depletion was confirmed by western blot analysis of lysate dilution series compared to control GFP knockdown.

5.2.4 Protein concentration (Bradford)

Bio-Rad Protein Assay Dye Reagent Concentrate (BioRad) was diluted with water to 1X. Aliquots of 1ml per measurement were pipetted into a disposable Polystyrene Cuvette (Sarstedt). For standard curves, different amounts of 2mg/ml BSA were pipetted: 1µl, 2.5 µl, 5 µl, 7.5 µl and 10 µl of this stock to get standards at 2µg, 5µg, 10µg, 15µg, and 20µg, respectively. Samples were pipetted in separate Cuvettes. Standard curve and samples were vortexed to mix and incubated at room temperature for 5 minutes. Measure was done by measuring absorbance at 595nm with a spectrophotometer (Ultrospec3000, Pharmacia Biotech). Blank was done with the reagent alone

5.2.5 Western blot

S2 cells were lyse using *Passive Lysis Buffer* from Promega, by incubating them on ice for 20min. *Drosophila* larvae were lysed with RIPA buffer, by incubating them on ice for 20 min. Lysates were then cleared by spinning at 20.000g for 10min at 4°C. For western blot from *Drosophila* larval tissue, an extra step for protein concentration was included using a Chlorophorm/Methanol precipitation.

Samples were diluted to same concentration and 1X SDS sample buffer was added to each sample, followed by boiling the sample at 95°C for 5min.

Samples were run on a 10% or 15% Acrylamide gel at 100V max. Proteins were transferred to a PVDF membrane at 4° for 2 hours. After, membranes were blocked with 5% milk PBS for at least 30min in agitation at room temperature. Alternative, longer blocking times were performed at 4°C. Washes were performed using TBST in agitation at room temperature. Primary antibodies were diluted in TBST and the incubation was done either 2 hours at room temperature or overnight at 4°C (for eIF2D antibody). After primary antibody incubation, the membrane was washed 3 times of at least 10 minutes, followed by incubation with the corresponding secondary antibodies, also diluted in TSBT. Incubation with secondary antibodies was done for 1 hour at room temperature. Before detection, the membrane was washed at 2 times for at least 5 minutes.

Detection was done by either adding *SuperSignal™ West Dura Extended Duration Substrate* (Thermo Fischer Scientific) to the membrane when the secondary antibody was HRP conjugated or directly measuring luminescence when the secondary antibody was Alexa-Fluor conjugated.

5.2.6 Quantification of Western blot

Quantification of western blots was done using *Multi Gauge Analysis Software*. In "Measure Mode > Quant", ROI of same area was drawn around the band of interest, and intensity was quantified. ROI in areas with no band were analyzed and quantified for background subtraction. Quantifications were exported and analyzed on Excel.

5.2.7 Non-radioactive amino acid incorporation assay

The assay was performed using *Click-iT™ Protein Analysis Detection Kit* (Life Technologies) according to the manufacturer's protocol. To evaluate rates of nascent protein synthesis, 4×10^6 of S2 control (GFP-KD) or eIF2D-KD cells were incubated in 6-well plates in methionine-free and FBS-free Schneider's medium for 1 hour at 25°C to get rid of endogenous methionine. Additionally, 50 µg/ml of cycloheximide (CHX) (Sigma Aldrich) was added to CHX control samples to block elongation and estimate the dynamic range of the assay. After incubation, the synthetic Met analog L-Azidohomoalanine was added to the medium and the cells were grown for another 2 hours at 25°C. Cells were harvested and lysed according to the manufacturer's protocol and the lysates were used for the 'click' reaction to fluorescently label de novo synthesized proteins with tetramethylrhodamine (TAMRA). The proteins were then methanol-precipitated and dissolved in the sample buffer. The resulting protein samples were run on the polyacrylamide gel. The nascent protein signal was visualized by TAMRA fluorescence (light emission at 580 nm wavelength) and total protein signal was visualized by SYPRO Ruby staining using Fujifilm Fluorescent Image Analyzer FLA-9000. Both TAMRA and SYPRO Ruby signal intensities were quantified with FLA-9000 software. Relative efficiency of protein synthesis in the samples was calculated as a ratio of TAMRA to SYPRO Ruby signal.

5.2.8 Polysome profiling of S2 cells and larvae

S2 cells lysis: in order to stabilize ribosomes on mRNA prior cell lysis, 50 µg/ml of CHX was added to $20\text{-}30 \times 10^6$ S2 cells and incubated for 15 minutes at 25°C with gentle agitation. S2 cells were collected by gentle centrifugation (800g, 5min) and the cell pellets were resuspended in the lysis buffer containing 20mM Tris-HCl, pH 7.4, 100mM NaCl, 10mM MgCl$_2$, 0.4% NP-40, 350 µg/ml CHX, 100 units/ml RNasin and 1x Complete mini EDTA-free protease cocktail (Roche). The cells were lysed on ice for 10 minutes and the cell debris was then spun down at 8000g for 10 minutes at 4°C. Supernatants were collected.

Drosophila larvae lysis: 30 female larvae at 116h AEL were washed with PBS, collected in a 1,5ml tube and immediately flash frozen. Larvae were lysed with 300µl of modified Polysome buffer (50mM Tris-HCl, pH 7.4, 300mM NaCl, 30mM MgCl$_2$, 0.1% NP-40, 350 µg/ml CHX, 100 units/ml RNasin and 1x Complete mini EDTA-free

protease cocktail (Roche)) using a plastic piston. Debris was then spun down at 20.000g for 10 minutes at 4°C. Supernatants were collected.

For puromycin treated profiles CHX treatment was omitted from the lysis buffer. After lysis and spin down of the debris, supernatant was collected in a new tube. Samples were treated with 63mM of puromycin on ice for 20 min followed by an additional 20 min at 37°C.
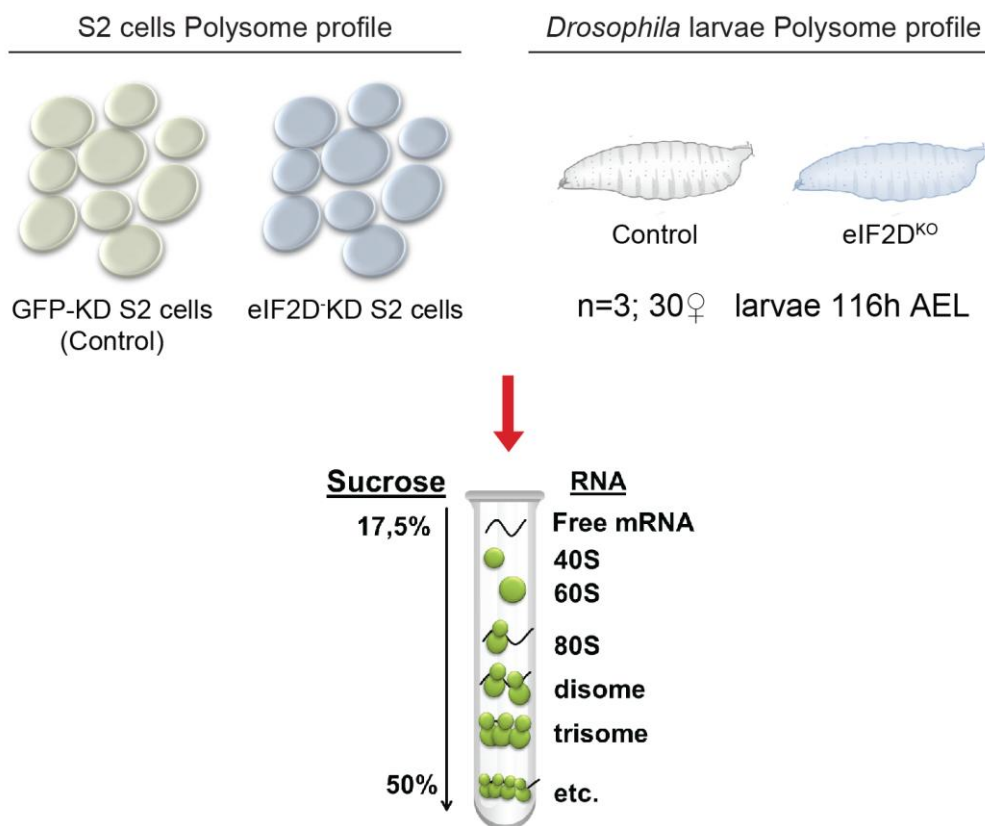
Figure 11. Scheme of Polysome profiling method from either S2 cells or *Drosophila* larvae

Total RNA concentration was defined by Nanodrop. The samples were adjusted to the same RNA concentration using the same lysis buffer. The samples were carefully layered onto prechilled 17.5% - 50% sucrose gradients (100mM NaCl, 5mM MgCl$_2$ and 20mM Tris-HCl, pH 7.4, for S2 cells polysome profile; 300mM NaCl, 30mM MgCl$_2$ and 50mM Tris-HCl, pH 7.4 for larvae polysome profile). The gradients were centrifuged at 35 000rpm in a Beckman SW40Ti rotor for 2h 15min at 4°C.

Gradients were analyzed for ribosomal content by measuring RNA absorption with a piston gradient fractionator (Biocomp Instruments).

5.2.9 Polysome/Monosome (P/M) calculation

Polysome profiles from Excel files were transferred to Adobe Illustrator to isolate the area under the Monosome or Polysome peaks. Areas were quantified using Fiji (ImageJ). Quantifications were exported and analyzed in Excel. Polysome area was divided by Monosome area. P/M ratios of all samples were normalized to Controls.

5.2.10 Total RNA isolation

To analyze distribution of mRNAs across the gradient, different fractions were combined to a total of five fractions. *TRIzol® reagent* was added to each fractions in a ratio of 3:1 followed by chloroform and a series of spins. For purification, *PureLink kit* (Ambion) was then used. The clean RNA was incubated with *TURBO DNaseI* (Ambion) to get rid of genomic DNA contamination. Finally, RNA was precipitated with sodium acetate/isopropanol. The RNA pellets were dissolved with nuclease-free water and 1 μg of total RNA was used in RT-PCR.

5.2.11 cDNA synthesis

cDNA libraries were generated using *SuperScript® II Reverse Transcriptase* (Life Technologies).

5.2.12 Quantitative real time PCR (qRT-PCR)

cDNA from whole larvae RNA was used to construct the standard curve by making a dilution series of 7 points from 1:1 to 1:68. For qRT-PCR from factions, RNA was extracted as previously described and used for cDNA synthesis.
Specific primers for each mRNA of interest were used.
The following reagents were pipetted in a 96 PCR Plate (Sarstedt).

Table 19. qRT-PCR reaction mix	
Reagent	**Volume**
Primer	5µl
Standard curve or sample cDNA	5µl
Sybr green	10µl

Table 20. qPCR reaction		
Temperature	**Time**	
95°C	10 min	Stage 1
95°C	15 sec	Stage 2 (x40)
60°C	1 min	
95°C	15 sec	Dissociating curve
60°C	15 sec	
95°C	15 sec	

Reactions were performed in an ABI 7900 HT instrument. Measurements were exported and analyzed in Excel.

5.2.13 Larval locomotion assay

Staged wandering third instar larvae were washed with distilled water. A single animal was accommodated on a 3% agarose plate of 10cm. Locomotion of the larvae was video tracked during 1 minute using either an upright SZX16 Olympus microscope and CellSense software (Olympus) or a CCD camera and Ethovision 10.0 software (Noldus). To gain consistency, each larva was tested three times and only forward locomotion events of at least 5 consecutive strides were recorded. The assay was performed at room temperature (18-22°C). Locomotion parameters were quantified for each animal automatically with Ethovision 10.0 software (Noldus). Data was exported and analyzed in Microsoft Excel.

5.2.14 ATP level assay

The ATP levels assay protocol was adapted to larvae from (Costa et al. 2013). For each genotype (control and $eIF2D^{KO}$) 10 staged larvae at 116h AEL were collected and washed in cold PBS. Next, they were homogenized with a plastic pestle in 200 µl of 6 M guanidine-HCl in extraction buffer (100 mM Tris and 4 mM EDTA, pH 7.4) to inhibit ATPases. The samples were flash frozen in liquid Nitrogen, followed by boiling at 95°C for 5 min. Samples were cleared by centrifugation 5min at 10000g. Supernatants were mixed with a luminescent solution *CellTiter-Glo Luminescent Cell Viability Assay* (Promega) and luminescence was measured. The relative ATP levels were calculated by dividing the luminescence by the total protein concentration, which was determined by Bradford assay.

5.2.15 Immunohistochemistry

Larval fillet preparation and immunostaining were performed according to Smith and Taylor (Smith and Taylor 2011). Shortly, staged 116h AEL larvae were washed in PBS, dissected in Standard saline HL3 buffer and fixed either with 4% formaldehyde in 1x phosphate-buffered saline (PBS) or *Bouin's solution* (Sigma) on ice. When required, fillets were blocked in 5% goat serum in 1x PBS. Fillets were incubated overnight in rotation or agitation with primary antibodies at 4°C. After primary antibody, the fillets were washed with 1x PBS, 0.1% Triton x100 or 0.5% Triton x100 and incubated with fluorescently labeled secondary antibodies for 1-2 hours at room temperature. The secondary antibodies were washed with the same buffer previously used, followed with a wash with PBS (no detergent). Finally, stained fillets were mounted onto microscopic slides with *SlowFade® Antifade Reagent* (Life Technologies) or 70% Glycerol and the slide edges were sealed with transparent nail polish.

For MitoTracker Red staining larval fillets were incubates with 1:1000 1mM *MitoTracker™ Red CMXRos* for 30 min at 37°C. The reagent was washed with PBS on agitation for 10min at room temperature. Fillets were fixed with 4% FA on ice for 20min and then wash again twice with PBS. Samples were mounted as above.

5.2.16 Quantification of synaptic protein levels

Images of control and eIF2D^{KO} larval NMJs and muscles were taken with Zeiss LSM 700 scanning confocal microscope (Carl Zeiss) with either 20x or 40x objectives, in the same experiment. For analysis, confocal stacks were transformed to maximum intensity projections. Quantification was performed using Volocity 6.1.1 software was used. An ROI (region of interest) around the NMJ was selected and total intensity for each channel was quantified. The data were exported to Excel for analysis.

5.2.17 Staging of larvae for Polysome profile and immunostainings

300 young (3 days) females with around 100 young males were crossed and incubate at 25°C in big vials with normal food supplemented with yeast paste. They were fliped every 24h into new vials with fresh yeast paste, twice. On the third day, they let lay eggs on a grape juice agar plate for 2 hours, and discard this plate. Then, they lay eggs on a new grape juice agar plate a new with fresh yeast paste, during max. 4 hours. After 24 hours, the first instar larvae were collected and transfer them to a vial with usual fly food and incubated at 25°C for 92 hours.

5.2.18 High-throughput Sequencing and Bioinformatics

For RNA sequencing, the samples were prepared with the "TruSeq RNA Sample Prep Kit v2" according to the manufacturer (Illumina). 50bp single end sequencing was conducted using a HiSeq 4000 (Illumina). Samples were demultiplexed with bcl2fastq2 (Illumina, version 2.17) and sequencing quality was checked with the FastQC software (Brown et al. 2017). Alignment of the reads was done to the genome reference sequence of *Drosophila melanogaster* (assembly version BDGP6,(Aken et al. 2017)) using STAR software (Dobin et al. 2013) allowing up to 2 mismatches in 51 bp. Quantification of gene expression was performed with the featureCounts program (Liao et al. 2014) (version 1.5.0) in standard configuration.

The resulting read count files were pre-processed and analyzed in the R/Bioconductor environment using the DESeq2 package (Version 1.8.2) (Love et al. 2014). Adjusted p-values in DESeq2 are calculated in terms of false discovery rate values (FDR). Differentially expressed genes expression between wild-type input and

eIF2D[KO] input samples were identified using a log2-fold change cutoff of -0.5/+0.5 and an adjusted p-value cutoff (FDR) of 0.1. Genes for fraction-specific comparisons (control vs. eIF2D[KO] for fraction pools, fraction pools vs. input) were identified using more stringent thresholds of -1/+1 (log2fc) and 0.05 (FDR). eIF2D targets were then derived by removing differentially expressed genes in the input set followed by manually removing genes with no reads in two or more fractions in either genotype. Gene annotation was performed using *Drosophila melanogaster* entries from Ensembl (Aken et al. 2017) via the biomaRt package (version 2.24.1).
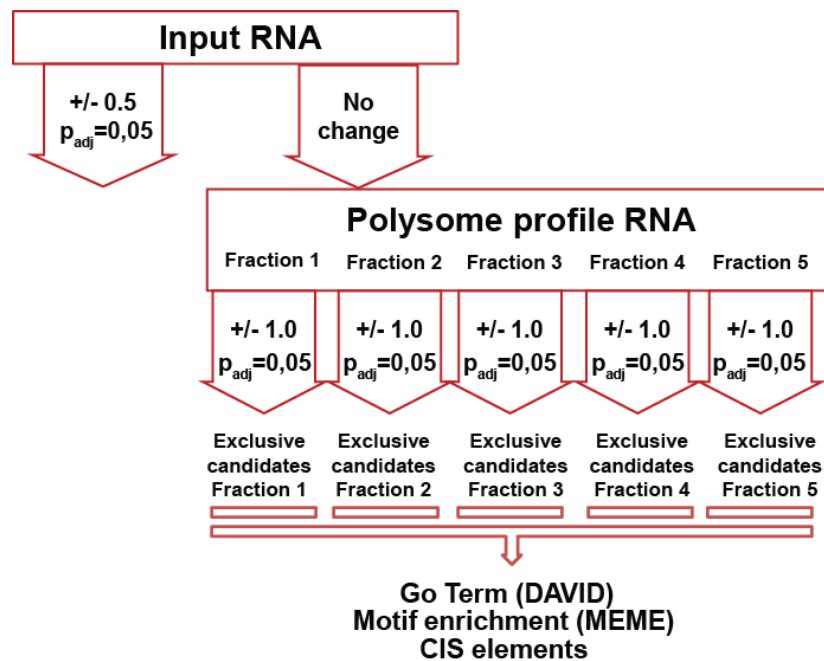
Figure 12. Bioinformatics pipeline.

Translation profiles (i.e. distribution plots) for individual eIF2D target genes were generated by calculating the fraction of normalized counts in each fraction after summing all counts across all fractions. Error bars reflect Standard Deviation from the mean of the three biological replicates.

For analysis of sequence features, whole transcripts, coding sequences (CDS), 5' and 3'UTRs were downloaded from FlyBase

(http://flybase.org/static_pages/downloads/bulkdata7.html; release 6.13, November 2016) and evaluated with respect to length. Frequency data and quality scores for uORFs were extracted from (Schleich et al. 2014). Enrichment of features in exclusive candidates relative to the whole genome or enriched genes in wild type samples were calculated in R using Wilcoxon tests.

 # Results involving these experimental procedures were obtained by Dr. Thomas Lingner.

5.2.18.1 Enriched motif analysis

To discover enriched motifs in the mRNA candidates, 5'UTR sequences from FlyBase (www.flybase.org) were analyzed in The MEME Suite (Bailey et al. 2009). MEME-ChIP was carried out analyzing the given strand, using any number of sites per sequence, count of motifs 6, motif width 3 to 8, maximum sites of motif was 300, otherwise default parameters.

5.2.18.2 Go-term analysis

The DAVID 6.7 (The Database for Annotation, Visualization and Integrated Discovery) functional annotation tool (Huang et al. 2007) was used to analyze "Biological Process" GO terms associated with exclusive candidates. The DAVID "functional annotation clustering" tool was used. The related terms are clustered into groups with enrichment scores calculated from their EASE Score (0.5 selected). We chose the ontology levels to group GOTERM_bp_all. Kappa similarity term overlap 3.

5.2.19 S2 Cell Reporter Assays

S2 Cell reporter assays with inducible 1aa or control reporters in proliferating or quiescent cell states were performed essentially as described in (Schleich et al. 2014) . Two independent transfections were performed for each KD condition. After transfection, cells were staged for either proliferating or quiescent state. Expression of the 1 aa uORF reporter was induced by incubating the cells with 100μM copper

sulfate for 6 hours. Two independent measurements were done for each treatment. Values were normalized to the control counts.

For eIF2D-target reporter assays knockdown of eIF2D and GFP (control) was performed using 1ml S2 cells at a concentration of 3×10^6 cells/ml and 15µg dsRNA for 1×10^6 cells. On the 4th day of incubation at 25°C, 500µl cells were plate at 1×10^6 cells/ml in 24-well plates. After 2 hours, transfection was done using *Effectene Transfection Reagent (*Qiagen):

Table 21	
Reagent	**Volume (for reaction of 24-well plate)**
Enhancer Buffer	60µl
Plasmid DNA (total)	0,2µg
Enhancer	1,6µl
Effectene	5µl
S2 cell culture media	350 µl

After 6 hours incubation, 100µl $CuSO_4$ was added to each well to induce expression of the plasmids. Cells were further incubated at 25°C for 44 hours.
Cells were harvest into 1.5ml tubes and washed once with PBS. Then, cells were lysed using *Passive Lysis Buffer* (Promega) by incubating on ice for 20min. Then, lysates were spun at 20.000g for 10min at 4°C.
Reporter expression was measured with the *Dual-Luciferase® Reporter Assay System* (Promega). Quantification was done by dividing the counts of Renilla/Firerly for each sample and normalized to the average of the control samples.

6 Results

6.1 eIF2D is sufficient on either side of the NMJ synapse to promote normal behavior

Previous experiments from the Duncan lab showed that lack of eIF2D protein in the *Drosophila* larvae causes a reduction of the forward locomotion speed (Koledachkina, unpublished).

In order to understand whether this locomotion phenotype was due to a general effect or rather was tissue specific, I decided to further investigate the implications of eIF2D *in vivo*. To see in which tissue eIF2D is sufficient to promote normal locomotion, I took advantage of the well-established GAL4/UAS system in *Drosophila* to express an eIF2D transgene under the UAS promoter using tissue specific Gal4 driver lines (Brand and Perrimon 1993). Flies containing eIF2D transgene expressed under the UAS promoter, in *eIF2D*^{KO} background, were crossed with different Gal4 diver lines, also in *eIF2D*^{KO} background. These experiments were done together with Dr. Tatyana Koledachina.

Ubiquitous expression using actin-Gal4 rescued the defective locomotion (Fig.13). Neuronal rescue, using an elav-Gal4 driver also rescued the locomotion (Fig.13). There are different neuron types involved in controlling behavior: motor neurons innervate and excite the muscles to promote contraction, whereas, sensory neurons detect that movement is happening and innervate the CNS to fine-tune this behavior. Motor neuron expression of eIF2D using the OK371-Gal4 driver rescued the locomotion phenotype; in contrast, expression in sensory neurons using the 21.7-Gal4 driver did not (Fig. 13). Finally, muscles need to receive the stimuli from the motor neuron and respond accordingly, producing a contraction and therefore locomotion. Transgenic expression of eIF2D in muscles using the Mef2-Gal4 driver line also rescued the locomotion (Fig. 13). Importantly, all the UAS and Gal4 lines in the eIF2D^{KO} background performed as the eIF2D^{KO} line.

Rescue experiments from either side of the synapse but not from other tissues like sensory neurons rescued the locomotion phenotype. Thus, eIF2D is sufficient in motor neurons or skeletal muscles to promote normal locomotion velocity. This result reinforces the hypothesis of a specific effect of eIF2D in the motor system.
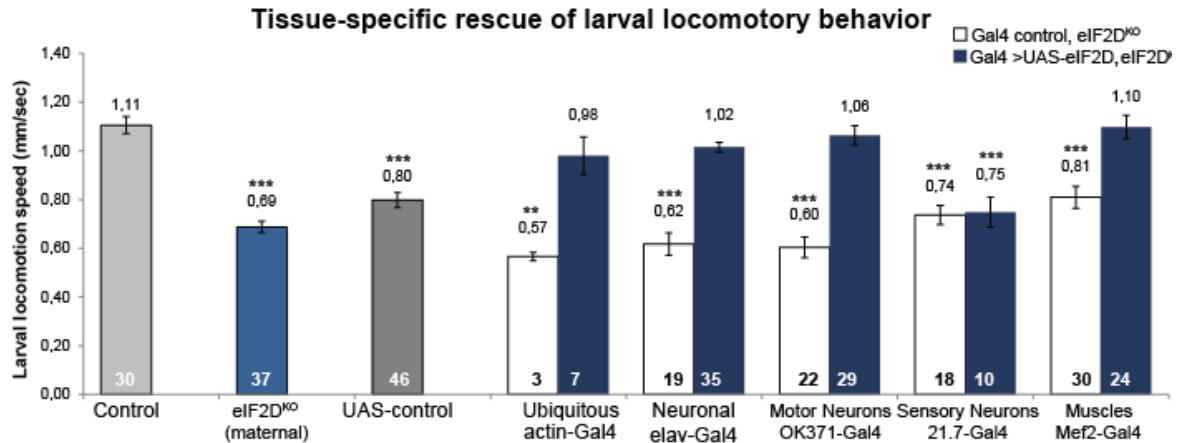
Figure 13. Tissue-specific rescue of larval locomotion behavior. Analysis of larval locomotion speed at L3 stage for different genotypes. Y-axes indicate larval speed in mm/sec. X-axes indicates the genotype. Grey bar "Control" refers to the control line used. Light blue bar "eIF2D^{KO} (Maternal)" refers to eIF2D^{KO} larvae from eIF2D^{KO} parental lines. Dark grey "UAS-Control" refers to the line expressing transgene eIF2D and crossed with the Gal4 driver lines. The white bars correspond to the GAL4 driver line on the eIF2D^{KO} background alone, whereas the dark blue bars correspond to the fly line expressing eIF2D under the UAS promoter with the Gal4 driver indicated below, resulting of crossing UAS-control with each Gal4. White numbers in the bars indicate number of larvae tested. Error bars = SEM. p-values relative to control were calculated using Mann-Whitney U-test, and are indicated on top of each bar, * p<0.05; ** p<0.01; *** p<0.001

* This data was obtained together by Dr. Tatyana Koledachina and Aida Cardona-Alberich in the Duncan lab as part of this thesis

6.2   eIF2D does not affect general translation in S2 cells

eIF2D has been identified as a translation factor with non-canonical properties *in vitro*, but knockout in *Saccharomyces cerevisiae* showed no implications in general translation or organism viability (Fleischer et al. 2006). I speculated that would also be the case in a different system. Since the behavioral data was obtained from *Drosophila* larvae, I picked a *Drosophila* cell line: Schneider's 2 cells (S2), and I looked at the effects of depleting eIF2D in S2 cells.

First, I did knockdown of *eIF2D* using dsRNA treatment in S2 cells and proved an efficient reduction (more than 90% reduction) of eIF2D protein (Fig. 14A). GFP (Green fluorescent protein) dsRNA-treated cells were used as control. GFP is a

fluorescent protein found in jellyfish but it is absent in *Drosophila,* therefore a GFP dsRNA treatment in S2 cells should have no effect. Next, I used eIF2D-KD and GFP-KD cells followed by either analysis of newly synthesized proteins or polysome profiling.

Nascent protein synthesis assays were done using click chemistry, an approach involving an azyde and a fluorescently labeled alkyne. Briefly, cells are supplied with an amino acid analog (L-azidohomoalaine or AHA) which is similar to the start amino acid Methionine (Met) with a modification of the incorporation of an azide. Due to its similarity with Met, AHA will be incorporated in all newly synthesized proteins. For detection, an alkyne tagged with TAMRA is "clicked" to the azide. The lysates are then run on an electrophoresis gel and the luminescence is quantified. Total protein staining was used for normalization between the samples. This assay showed no difference between eIF2D-KD and GFP-KD controls (Fig. 14B, CHX-free).

To verify that the assay was performing as expected, and that I was indeed quantifying true newly synthesized proteins, I included samples treated with cycloheximide (CHX) an inhibitor of translation. When treated with CHX, cells should not synthetize new protein and the signal measured should correspond to background which matched the obtained result demonstrating that the assay is measuring new protein synthesis (Fig. 14B, CHX Control).
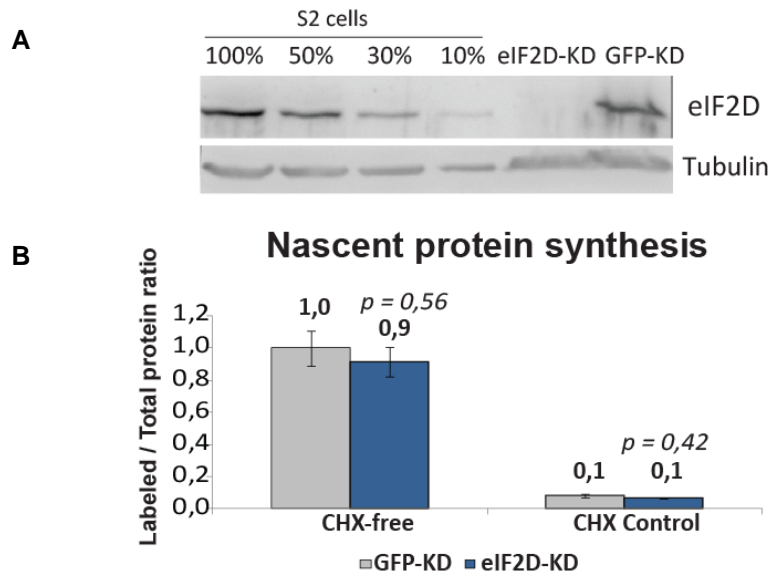
Figure 14. Nascent protein analysis in S2 cells shows no difference between eIF2D-KD cells and control. (A) Representative western blot of knockdown efficiency for eIF2D in S2 cells. Non-treated S2 cell lysate was run on the same gel using different dilutions, from 100% lysate to 10% lysate, to serve as a guide of endogenous protein levels of eIF2D. eIF2D-KD and GFP-KD (control) lysates were run on a gel in every experiment to assess eIF2D protein reduction. Tubulin staining was used as loading control. (B) Normalized average of quantification of nascent protein synthesis for GFP-KD (Control) in grey bars and eIF2D-KD in blue bars, for the experiment (CHX-free) and control (CHX control). Y-axes represent the ratio of labeled (nascent protein) to total protein. Error bars=SEM. p-values were calculated using un-paired t-test respective to GFP-KD and are indicated above each bar.

To confirm this result with an independent method, I next used eIF2D-KD cells for another classic method for studying translation: polysome profiling. This experiment separates ribosomes and mRNAs on a sucrose gradient according to their ribosome density (mRNA with fewer ribosomes on top and mRNA with more ribosomes on the bottom). Since RNA absorbs at 254nm, measure the absorbance at different points of the gradient generates a profile of the ribosomes, providing information about how many ribosomes are actively bound to mRNAs. I observed no differences between the profiles of GFP-KD control cells and eIF2D-KD cells (Fig. 15), confirming that eIF2D does not affect general translation in S2 cells.
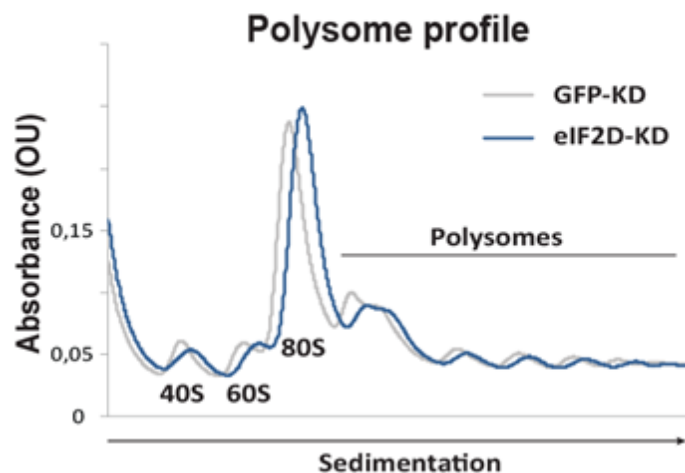
Figure 15. Polysome profile for GFP-KD and eIF2D-KD cells shows no differences. Representative traces of polysome profile of GFP-KD cells (grey) and eIF2D-KD cells (blue). Y-axes show absorbance at 254nm in optic units and X-axes represents the sedimentation on the sucrose gradient from the top with 17.5% sucrose (left) to the bottom with 50% sucrose (right).

6.3   Optimization of the polysome profiling method for *Drosophila* larvae

In order to study eIF2D's impact on translation and mRNA targets *in vivo*, I first optimized polysome profiling for whole *Drosophila* larvae together with David Schumacher as part of his Bachelor Thesis (*Establishment of a polyribosome profiling assay for* Drosophila melanogaster *larvae and assessment of eIF2D function in translation*). Briefly, we found that flash freezing the larvae in liquid nitrogen before the lysis and the additional change to the buffer composition with an increase of Magnesium, made a major difference in retaining ribosomes attached to the mRNA.

Next, I realized that correct and stringent staging of the larvae was crucial for reproducibility of the experiments. *Drosophila melanogaster* has a life cycle of about 10 days from egg eclosion to adult. The larval stage is approximately 5 days and is divided into first, second and third instars larvae, which can be further divided into feeding and wandering third instar larvae. During the first stages, larvae will feed and grow, increasing cell number and body size, and therefore in a state of high translation. When they reach the last stage of development, before pupation, they

leave the food and start crawling the sides of the vials. At this time point, larvae do not feed anymore and slow down or stop their growth, resulting in reduced translation (Fig. 16, top). Many studies ignore these differences and experiments are performed with animals over a broad time window (third instar larvae). However, I observed that only 4 hours of difference in the larval growth showed a notable difference in the polysome profile (Fig. 16). Thus, I decided to carefully stage animals for the experiments in a very tight time window of 116h after egg laying (AEL). At this point the larvae are still growing in size and show a higher general translation than the older 120h AEL larvae (Fig. 16).
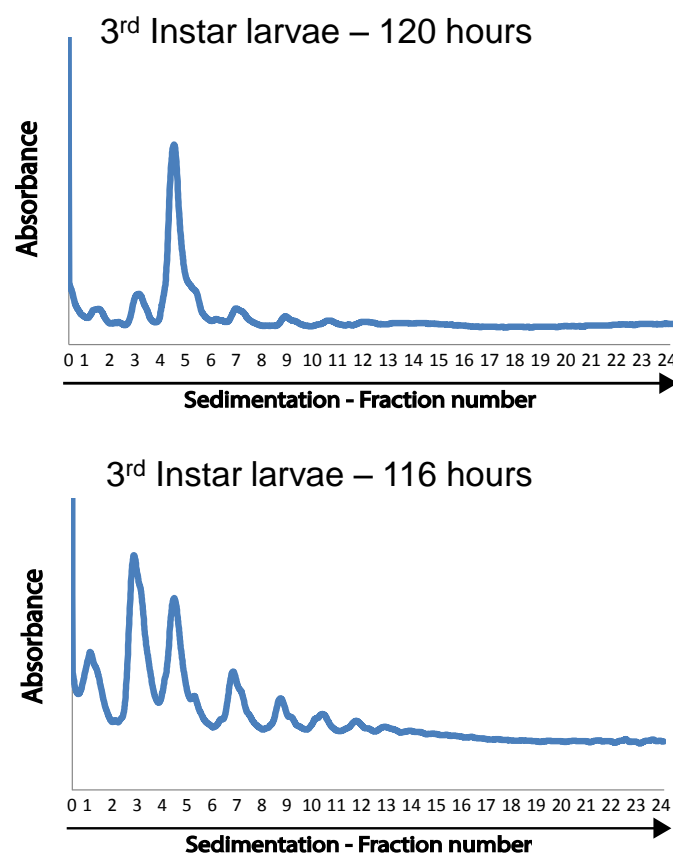
Figure 16. *Drosophila* larvae at different stages of the development show different translation profiles. Representative traces of Polysome profile of 120h AEL larvae (top) and 116h AEL larvae (bottom). Y-axes show absorbance at 254nm in optic units and X-axes represents the sedimentation on the sucrose gradient from the top with 17.5% sucrose (left) to the bottom with 50% sucrose (right), and the number of corresponding fraction.

6.4 Effects of eIF2D in translation *in vivo*

6.4.1 eIF2D affect general translation in the whole *Drosophila* larvae

Non-canonical translation factors are thought to play a role in more specific translation than the canonical ones. The observed physiologic effect was described in larvae, and more specifically in the motor system. Thus, I hypothesized that eIF2D function would be more relevant level than for a single cell, such as *Drosophila* S2 cells.

To assess if general translation was affected *in vivo* in an animal, I used eIF2D^{KO} larvae to perform polysome profiling (Fig. 17A). I calculated the relative amounts of polysome-bound mRNA (2 or more ribosomes on an mRNA) to monosome (single ribosome bound to mRNA) (Fig. 17, see Methods) of each run. Contrary to what I observed in S2 cells, the Polysome/Monosome ratio revealed that *eIF2D^{KO}* larvae have an increase in mRNA-associated ribosomes (Fig. 17B), revealing that eIF2D affects general translation *in vivo*.
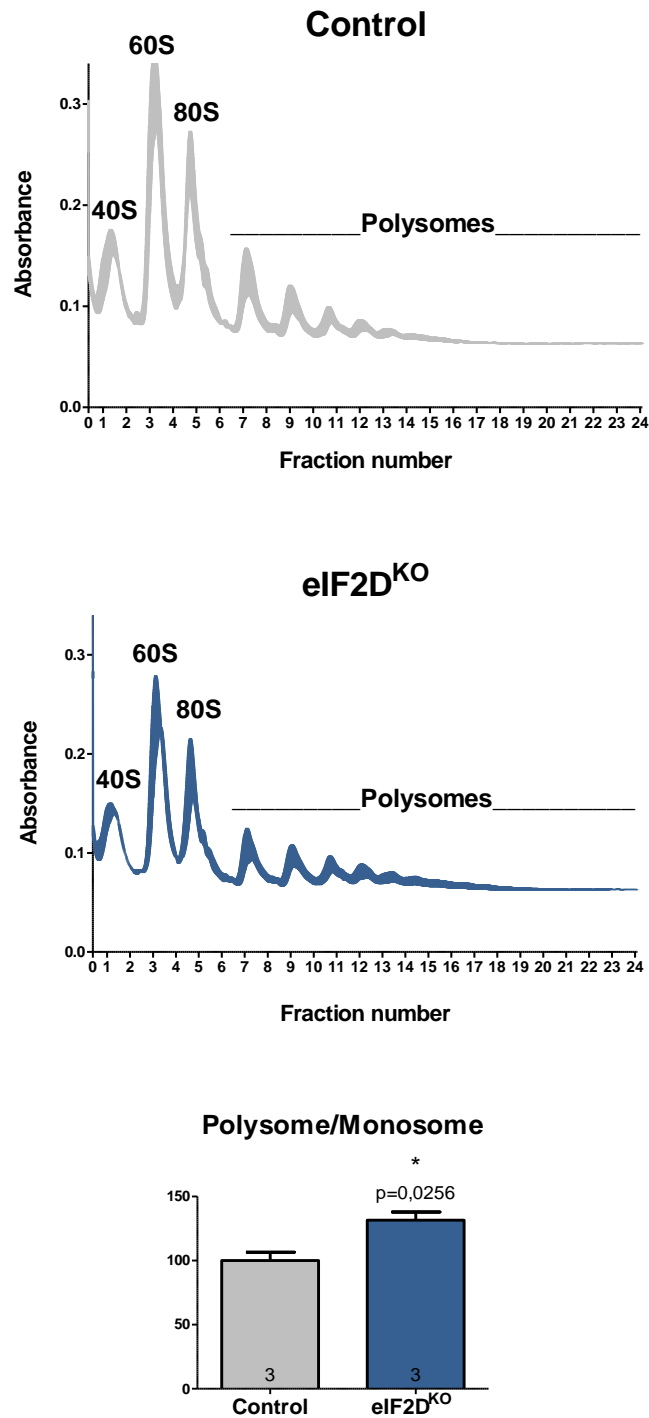
Figure 17. Polysome profile in larvae and P/M ratio. (A) Representative Polysome profiles for Control (top) and *eIF2D^{KO}* (bottom) are shown. The Y-axes shows the absorbance at 254nm and the X axes represents the fraction number from 0 to 24. The traces are the mean and SEM of three replicates for each genotype. Indicated to what corresponds each peak. (B) Quantification of the area under the curve of polysome and monosome ratio shows an increase in *eIF2D^{KO}*.
Un-paired t-test. P-value is indicated (0,026). Number of replicates is indicated in each bar.

6.4.2   *eIF2D^{KO}* larvae have an increase in translating ribosomes

There are two possible interpretations to the above mentioned result: either this increase in mRNA-associated ribosome corresponds to translating ribosomes, meaning more translation, or it corresponds to more ribosomes being stalled on the mRNA, which could result in a decreased translation. To distinguish between those two possibilities, I treated larval lysates with puromycin, a drug that selectively targets translating ribosomes and disassembles them, resulting in a decrease in ribosomes on mRNAs and polysome profiles showing only stalled ribosomes.

Polysome/Monosome ratios from puromycin treated profiles show no difference between *eIF2D^{KO}* larvae and controls (Fig. 18A, 18B), meaning that the previously observed increase in mRNA-associated ribosomes represents translating ribosomes. This implies that there is an increased number of actively translating ribosomes engaged with mRNAs in *eIF2D^{KO}* larvae and raises the question of which mRNAs are deregulated when eIF2D is missing.
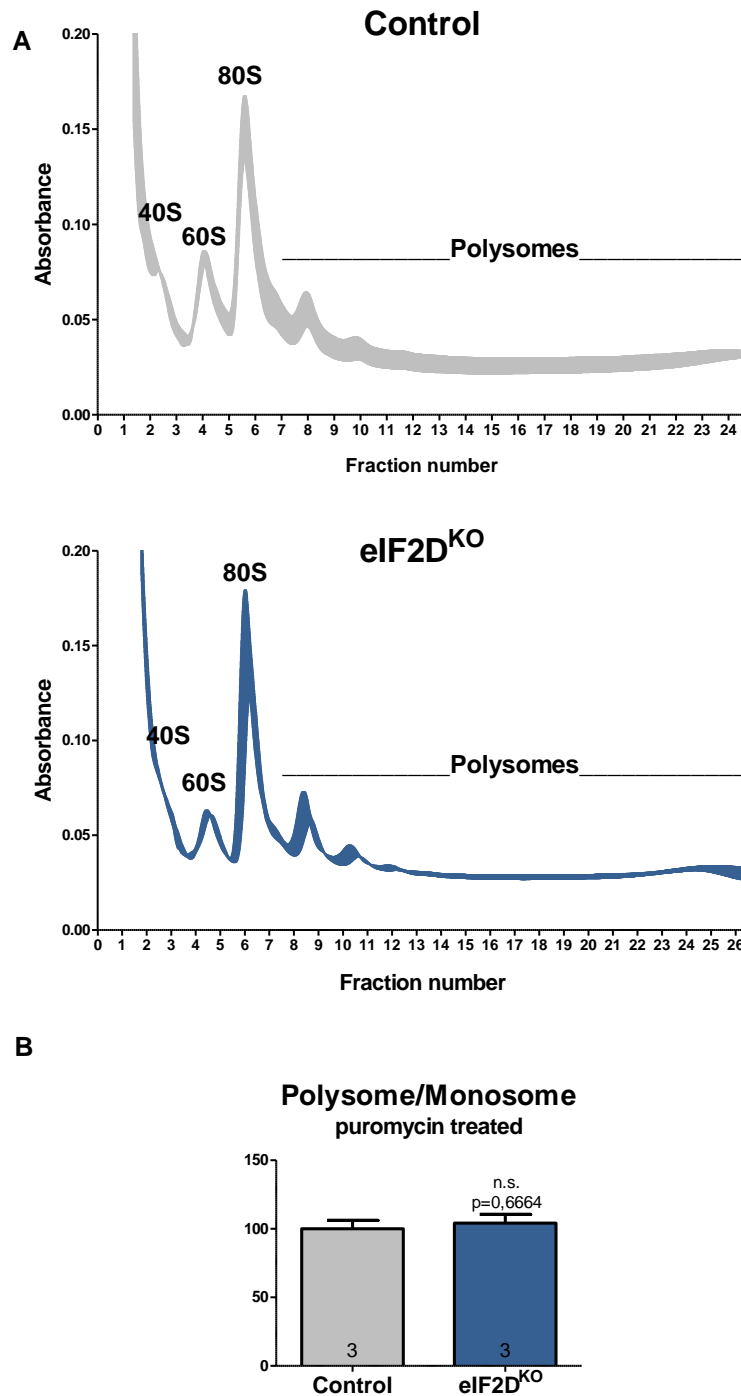
Figure 18. Effect of puromycin treatment on polysome profiles in *eIF2D^KO* larvae. (A) Profiles for control and *eIF2D^KO* larvae are shown. The Y-axis shows the absorbance at 254nm and the X axis represents the fraction number from 0 to 24. The traces are the mean and SEM of three replicates for each genotype. (B) Quantification of Polysome/Monosome ration for Control (grey) and *eIF2D^KO* (blue). p-value was calculated using un-paired t-test and it is indicated above the bar. Number of replicates is indicated in each bar.

6.5 eIF2D regulates translation of specific mRNAs *in vivo*

6.5.1 RNA deep Sequencing analysis performed with *eIF2D^{KO}* larvae

After observing that translation is affected in *eIF2D^{KO}* larvae, I wondered which specific mRNAs showed altered translation in the knockout mutants, and therefore are likely to be eIF2D mRNA targets. For that, I combined different fractions from the polysome profile fractionation into 5 fractions corresponding to 1) free mRNAs, 40S and 60S subunits, 2) 80S or monosome, 3) 2-3 mRNA-associated ribosomes, 4) 4-6 mRNA-associated ribosomes and 5) 7 or more mRNA-associated ribosomes (Fig. 19). I further performed RNA extraction and clean-up from those fractions. Finally, those samples were used for high-throughput sequencing in the Transcriptome and Genome Analysis Laboratory (TAL) at the Universitätsmedizin Göttingen by Dr. Gabriela Salinas and her team.
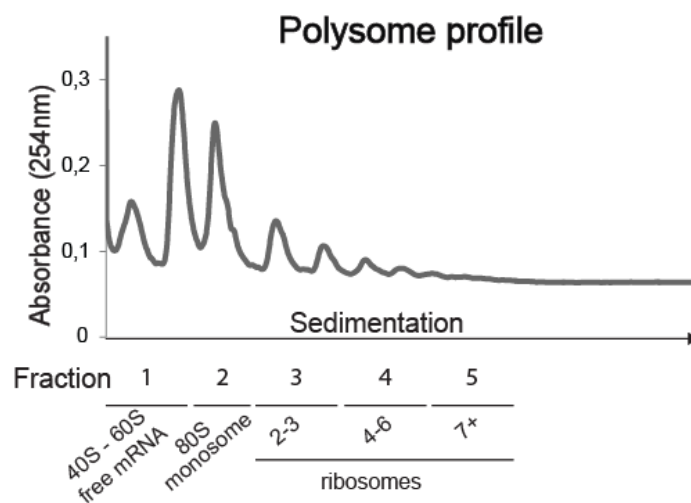
Figure 19. Example of a Polysome profile showing the fraction pooling scheme for RNA extraction and RNA-seq.

After RNA-seq, sample quality was first assessed by Dr. Thomas Lingner who reported that gene coverage was very good. We could see few reads in the intergenic and intronic regions indicating that the reads corresponded to real RNA

sequencing and not remaining DNA contamination in the samples. Additionally, the coverage was even across the exons (Fig. 20A). A Principal Component Analysis (PCA) shows the perfectly non-overlapping clusters for each fraction and a clear separation between Control (WT) and *eIF2D^{KO}* (KO) samples (Fig. 20C). The Cluster Dendrogram shows that the transcriptome profiles within some groups (input and fractions 1 and 2) are similar, whereas the profiles of fractions 4 and 5 are distant from the others corresponding to the fractions with less mRNA. However, replicate samples from Control (WT) or *eIF2D^{KO}* (KO) cluster together with the respective replicates from the same genotype, as well as samples from across the fractions independent of the genotype (Fig. 20B).

A
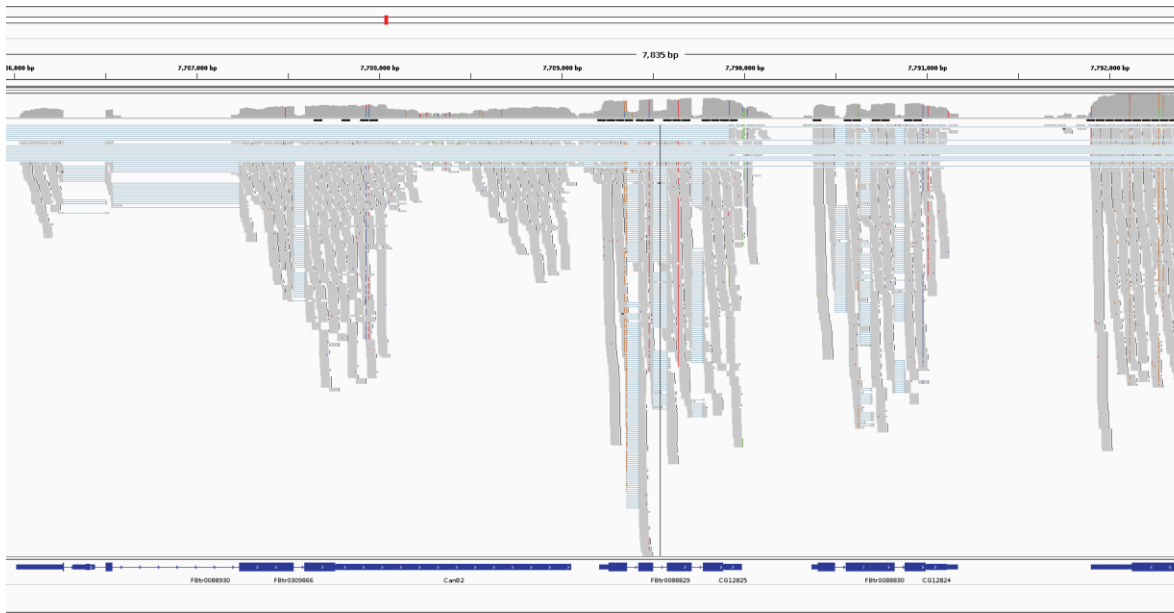
B

Cluster Dendrogram
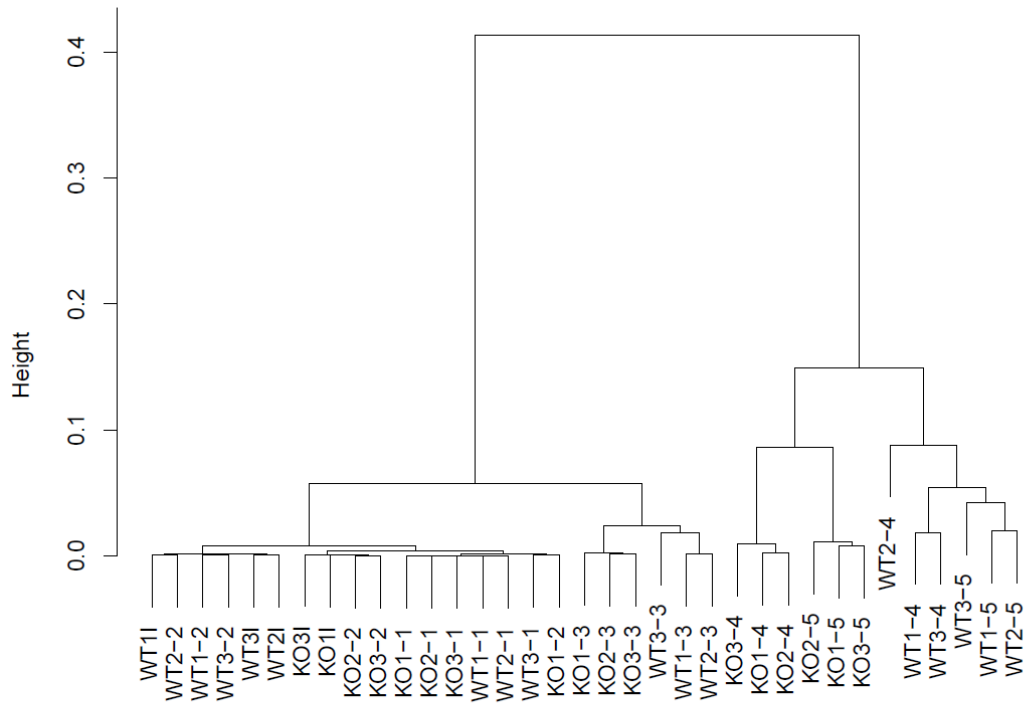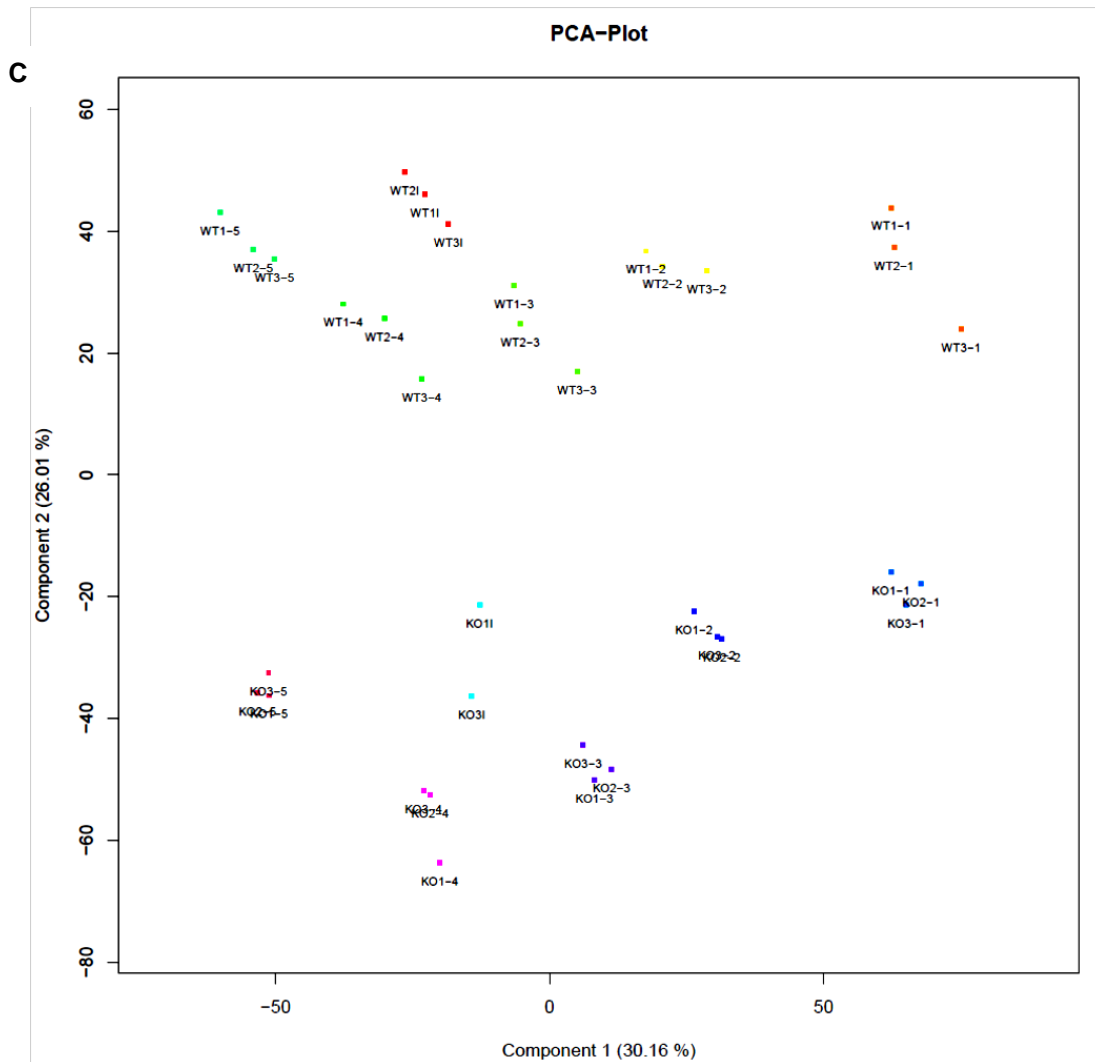
Figure 20. Basic bioinformatic analysis of RNA-seq data. (A) Plot showing the read pile-up at this region. The genes to map are pictured at the bottom as dark blue bars (introns) and thin light blue lines (exons). The more reads (grey lines), the higher the coverage (coverage/depth is also shown on extra track on top). The thin blue lines show "spliced" reads, i.e. reads that span exon junctions (the very long ones are possibly false positives from misalignments). Vertical colored lines represent SNPs and their allele-specific expression (for heterozygous ones). The exon without reads on the left is a microRNA (mir-4980) on the same strand. (B) The Cluster Dendrogram shows the position of every sequenced sample. WT corresponds to Control and KO to eIF2D^{KO} samples. The first number after the genotype indicates the number of the repeat, and the second number indicates the fraction number (1 to 5) or input sample (I). The y-axis is a measure of closeness of either individual data points or cluster: the higher the position the later the object links with others, and hence more like it is an outlier or a stray one. (C) PCA-plot (Principal component analysis) distributes the samples according to their similarities. The dots of a same color represent the replicates of a sample. The control (WT) samples are on the upper half of the plot, whereas the eIF2D^{KO} (KO) samples are on the bottom half.

This figure was provided by Thomas Lingner.

6.5.2   740 mRNAs change ribosome density in e*IF2D*^{KO}

To find those specific mRNAs with altered translation in *eIF2D*^{KO} animals, I decided to select for the targets using two-step procedure: first, we looked at every fraction separately and asked which mRNAs were differentially expressed in the eIF2D^{KO} samples in comparison to controls. Then, genes being differentially expressed also in the total mRNA levels in input samples were discarded (see Methods). The goal of the second filter was to focus only on those mRNAs with altered translation, but no significant change in transcription or mRNA turnover.

Using this procedure, we found a total of 740 differentially expressed genes in at least one fraction, although some of them changing in more than one, of the total of around 17 000 genes in the *Drosophila* genome. This corresponds to a relatively modest set of total expressed genes (~4%). Most of the changes occur in fractions 1 (free RNA) and 5 (deep polysomes - 7 or more ribosomes/mRNA), and more of the targets are downregulated than upregulated (Fig. 21).
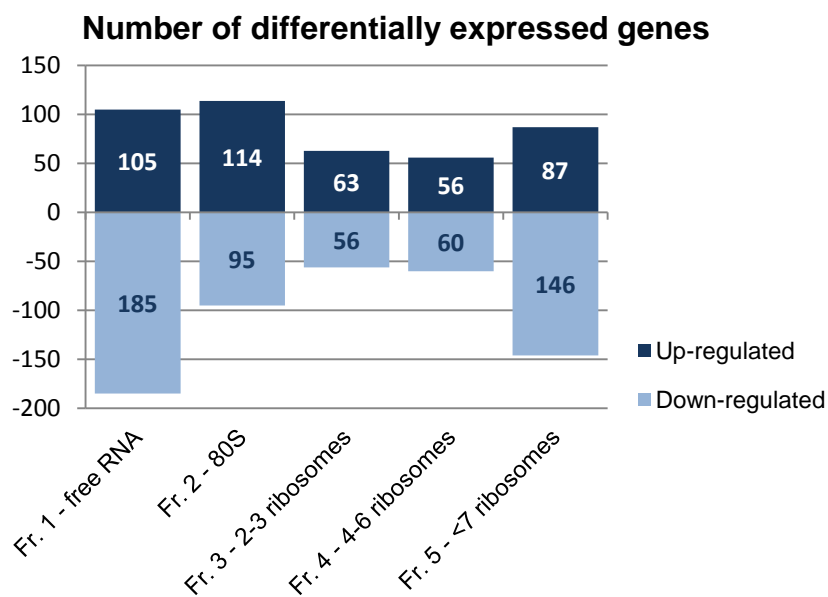
Figure 21. Number of mRNAs changed in every fraction. A number of genes were found to be altered in every fraction. The Y-axes indicates the number of genes upregulated (positive, dark blue bars) or downregulated (negative, light blue bars) for a given fraction. Exact gene numbers are indicated in the bars.

For every differentially expressed gene, we then sum the relative expression levels in all fractions to create a percentage distribution plot of every target. This provides the translation profile of every target, in control and eIF2D^{KO}.

6.5.3   Verification of the targets by qRT-PCR

Before further analyzing the RNA-seq data, I wanted to verify some of the observed results with a different method; therefore I used quantitative Reverse Transcription PCR (qRT-PCR) to confirm changes in altered expression. Using RNA from each fraction of 3 samples of each genotype, cDNA was prepared and used for qRT-PCR. For each sample, the total quantity of mRNA was calculated by adding the quantity of mRNA in the 5 fractions for a given sample. Then, the percentage amount of mRNA in every fraction was calculated. For normalization of the data, a gene showing no difference between genotypes and an average of 20% expression in every fraction was used. Finally, distribution plots across the 5 different fractions were made using the average between the 3 samples of each genotype (Fig.22).

Two examples, *Shaw* and *eIF4A* show many similarities between the results obtained with both methods. The parameters to taken into consideration were 1) the difference within one fraction between both genotypes and 2) the distribution across the 5 fractions of each genotype. Both examples fit the criteria, with the exception of fraction 1 and probably fraction 2 in *Shaw* (Fig. 22).

It is important to take into consideration that although these are both methods for RNA quantification, there are significant differences in the technique that could explain the differences observed between the two: 1) while same amount of RNA from all samples was used for RNA-seq, that was not taken into account for qRT-PCR, 2) the data was normalized to one single gene in qRT-PCR whereas in RNA-seq it was normalized to the total number of reads in that specific fraction and 3) after RNA-seq, additional filters such as excluding reads matching multiple transcripts were applied.

In sum, I considered the Deep Sequencing RNA data-set validated and proceeded to further downstream analysis.
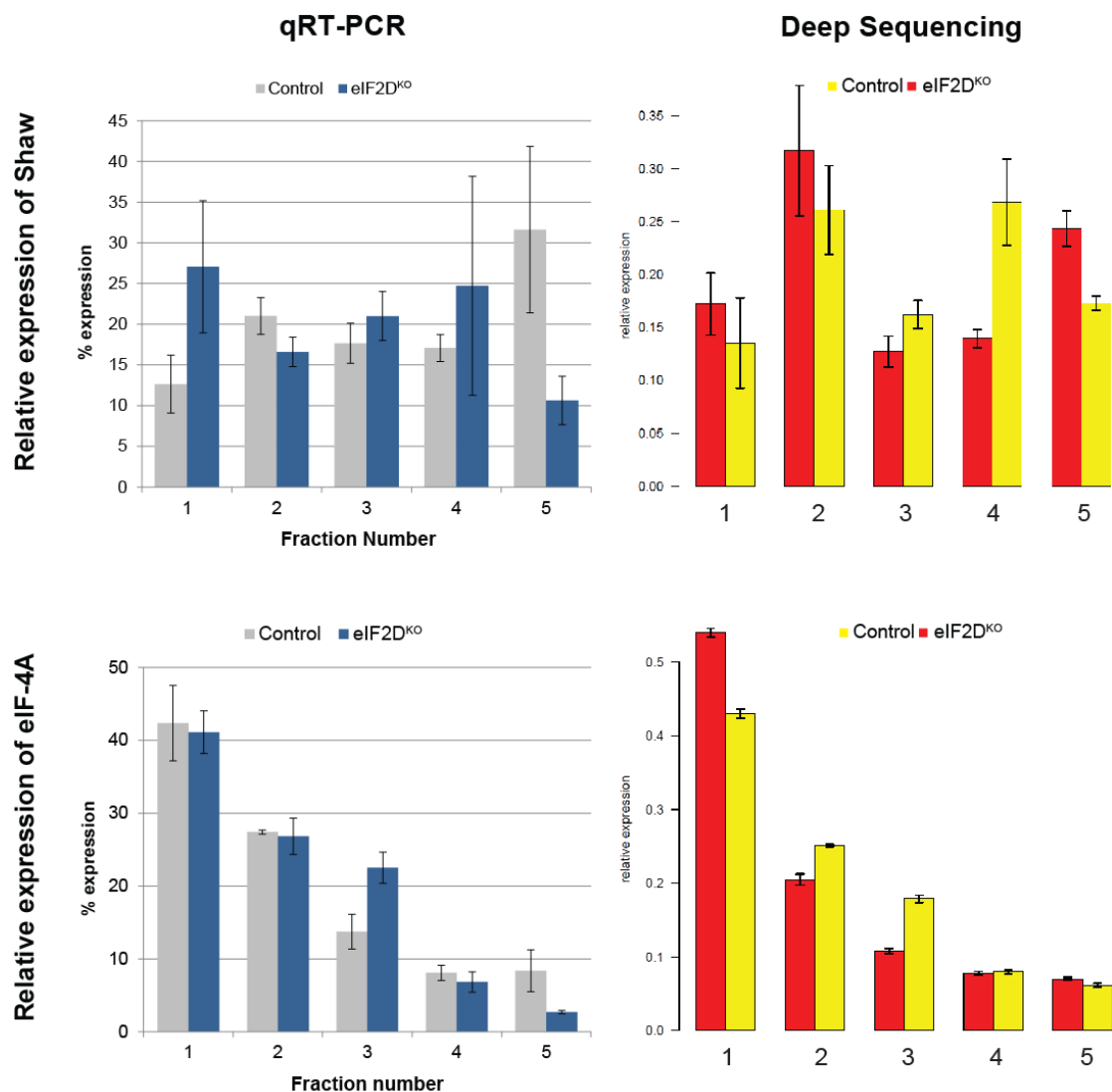
Figure 22. Percentage distribution of *Shaw* and *eIF4A* mRNA across the 5 fractions. Bar plots indicating the percentage distribution (y-axes) of the *Shaw* mRNA (top) and *eIF4A* mRNA (bottom) form the qRT-PCR (left) and Deep Sequencing (right) for each mRNA. The numbers on the x-axes indicate the fraction number of the Polysome profile fraction (see Fig. 19). Grey bars in qRT-PCR plots and red bars in Deep Sequencing plots correspond to Control samples and blue bars in qRT-PCR and yellow bars in Deep Sequencing correspond to eIF2D^{KO} samples. Error bars are STDEV in qRT-PCR plots and STDEV/SUM in Deep Sequencing plots.

6.5.4 eIF2D's in vivo translational targets are involved in specific biological processes

To try to further understand the physiological roles of eIF2D, I performed a GO term analysis of eIF2D targets focusing on the biological processes. I separately analyzed the targets from every fraction because we expected to see distribution patterns of the terms across the different fractions.

Interestingly, most of the GO-terms are synaptic and locomotion related, such as "regulation of locomotion", "neuromuscular junction development" or "locomotion rhythm", and appear in more than one fraction being especially evident in upregulated mRNAs of fraction 1 (Fig. 23, terms in red). Although the statistical significance of the relative enrichment varied across the fractions it appears in several, consistent with major phenotypes in $eIF2D^{KO}$. Other biological processes in which eIF2D targets are involved are gene expression related and ATP metabolic processes (Fig. 23.

Thus, eIF2D translational targets affect different biological processes, but mostly synaptic transmission and development, locomotion, ATP metabolic processes and gene expression control.
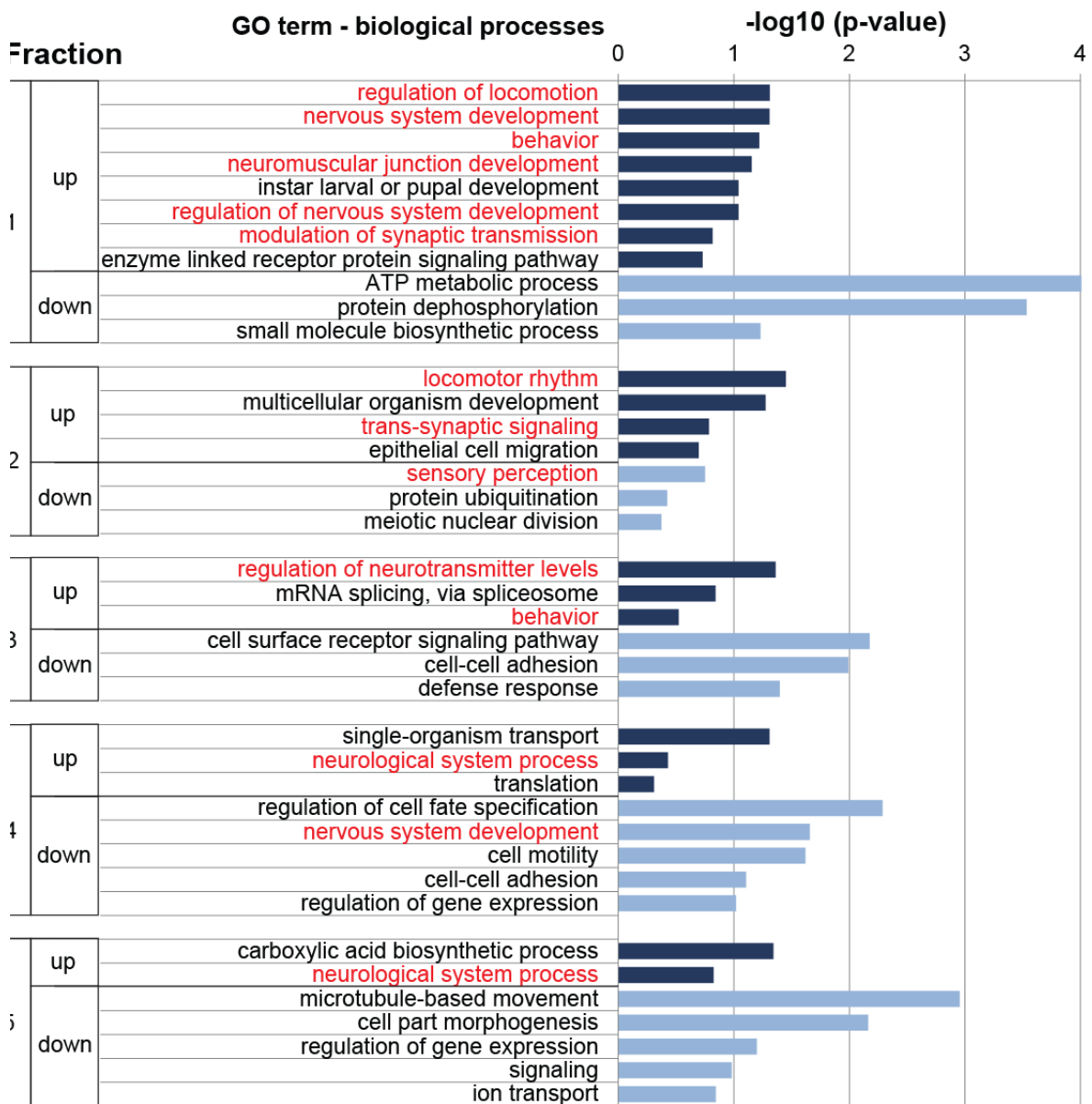
Figure 23. Gene Ontology (GO) term enrichment. Table shows the GO terms for Biological Processes enriched in the lists of up- (dark blue) and downregulated (light blue) genes in eIF2D^{KO} in each fraction, and the p-value (-log10) for each term. GO terms in red indicate those directly related to neuro-processes and behavior.

6.6 Differentially expressed genes found in deep RNA-seq might explain the observed phenotypes in *eIF2D^{KO}* larvae

6.6.1 ATP levels in whole larvae do not change

The GO-term with higher statistical significance (-log10 p-value) in the functional analysis across all fractions was "ATP metabolic process" (Fig. 23). ATP production occurs mainly in the mitochondria and is the main energy source of the cell and consequently needed for many different cellular processes, such as intracellular signaling, transcription and translation, active transport or muscle contraction. Having decreased ATP levels in the whole larvae, especially in the muscles, could explain the slow locomotion phenotype in *eIF2D^{KO}* larvae. To address whether ATP levels were changed, I performed ATP quantification from total larval lysates.

The results from ATP quantification from whole larvae showed no differences between *eIF2D^{KO}* and controls (Fig. 24), thus I discard that a major ATP deficiency is the main driver of the impaired locomotion behavior. However, I cannot exclude the possibility that ATP levels were altered in a specific cell-type or tissue as this was not directly studied.
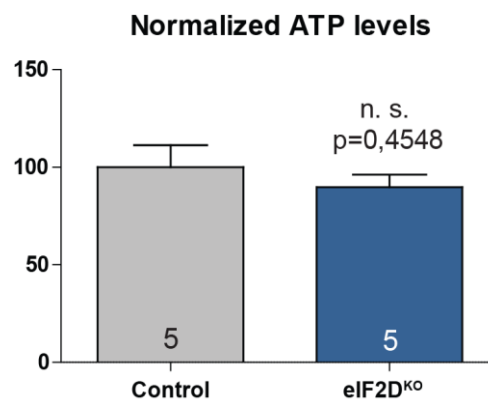
Figure 24. Normalized ATP levels for whole larvae for Control (grey) and *eIF2D^{KO}* (blue) to total protein. Number of repetitions is indicated in the bars. p-value was calculated using unpaired t-test and it is indicated above the bar. Errors bars = SEM. n.s. = not significant

6.6.2 *Parkin* is a target of eIF2D regulation and mitochondria morphology is altered

As previously mentioned, the main source of ATP's is the mitochondria but this is not the only function of mitochondria. Moreover, subcellular localization of the mitochondria and their shape are important for correct function.

Examining the eIF2D targets list derived from the RNA-seq data, I detected several mRNAs encoding mitochondrial-related proteins, one of them being *Parkin* (*park*) (Table 23). Park is a cytoplasmic E3 ubiquitin ligase involved in mitochondria fission and mitophagy. Studies of Park in *Drosophila* showed that mutations in *park* produce round shaped mitochondria leading to defective mitochondrial transport and therefore altered subcellular localization (Deng et al. 2008).

In the RNA-seq data, *Parkin* appears downregulated in fraction 3 and has an overall decreased ribosome density (Fig. 25A) suggesting reduced translation. Unfortunately, attempts to detect and quantify endogenous Parkin with 3 different antibodies either by Western blot or immunostaining were unsuccessful. Previous publications which used those antibodies were done in overexpression conditions.

I dissected and stained muscles of 116h AEL larvae with MitoTrackerRed, a marker for mitochondria. Mitochondria in *eIF2D^{KO}* larval muscles appear spherical, in contrast to the normal elongated/tubular mitochondria in control larvae. Mitochondria distribution around the nuclei is also altered in *eIF2D^{KO}*, but distribution at the muscle banding appears normal, which partially phenocopies *park* mutants (Fig. 25B).
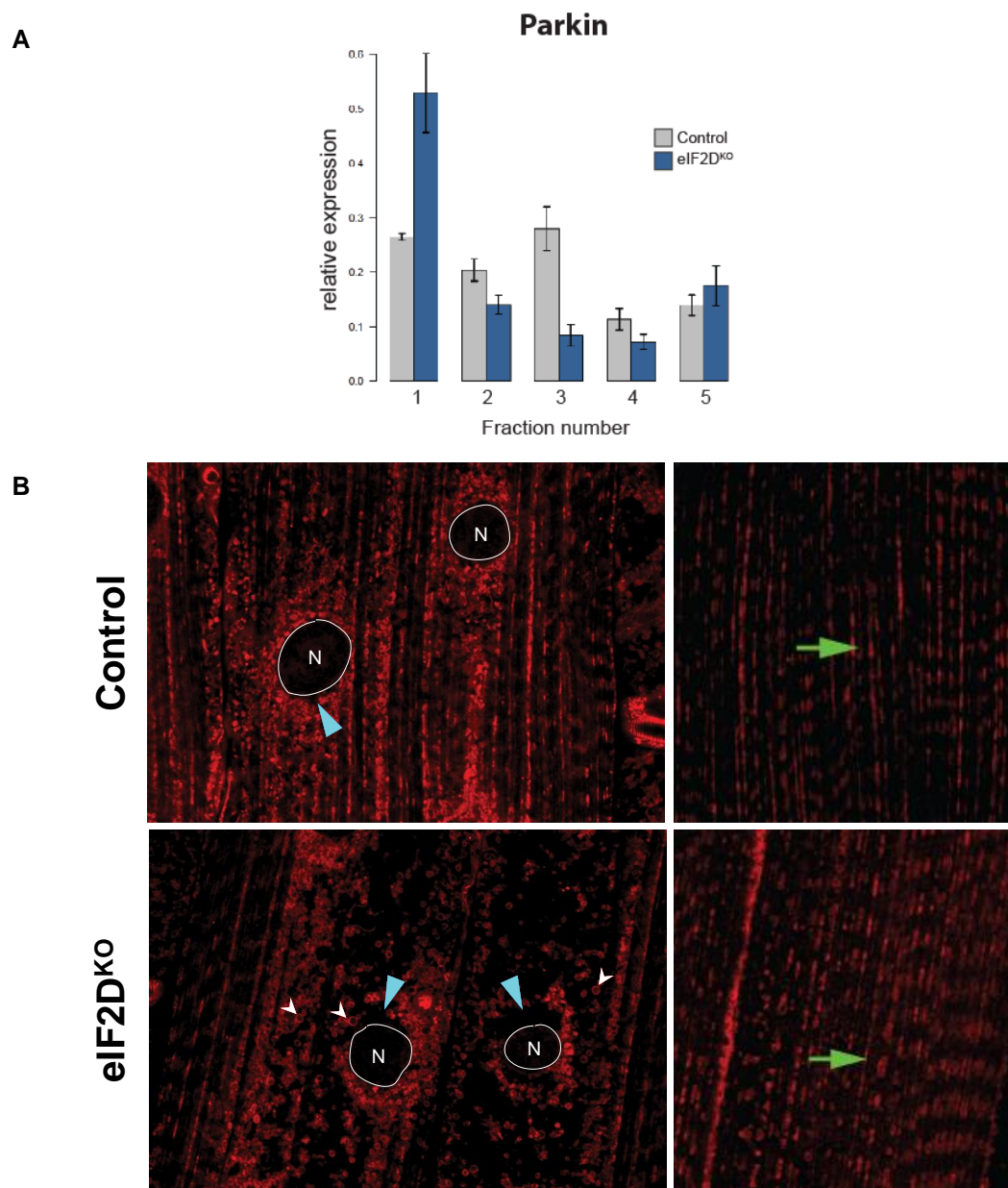
Figure 25. *Parkin* translation profile and muscle mitochondria staining. (A) Bar plots indicating the percentage distribution (y-axes) of *Parkin* mRNA form Deep Sequencing. The numbers on the x-axes indicate the fraction number of the Polysome profile. Grey bars correspond to Control samples and blue bars correspond to eIF2D^{KO} samples. Error bars are STDEV/SUM. (B) Confocal images of mitochondria (red) of the skeletal muscles (abdominal segment A3) of Control (top) and *eIF2D^{KO}* 116h AEL larvae. White circles with white "N" indicate the nuclei of the muscle, white arrowheads indicate representative single mitochondria, blue arrowheads indicate empty spaces between nuclei and mitochondria, and green arrows indicate disposition of the mitochondria between the muscle fibers.

6.6.3   Correlation between translational changes and protein levels

While it is intuitive that changes in translational status of an mRNA would affect stead-state levels of the encoded protein, the extent to which changes in translation impact on steady state protein levels is still unclear. Some groups that have directly compared steady-state protein levels and translation rates measured by polysome and/or ribosome profiling and found a low correlation. To see if translational changes affect protein level in my case, I looked at some of the potential targets to assess their protein levels. One major difficulty was the low availability of good commercial antibodies for *Drosophila* proteins in general, and for eIF2D targets in particular.

6.6.3.1   *Syntaxin-1A shows an increase in ribosome density but no differences in protein levels in eIF2D^{KO} NMJs*

One of eIF2D targets is Syntaxin-1A (Syx1A), a presynaptic protein involved in vesicle release through regulation of the SNARE complex. *Syx1A* mRNA appears upregulated in fraction 5 and overall its distribution shifts to the deeper polysomes in *eIF2D^{KO}* (Fig. 26), suggesting increased translation.
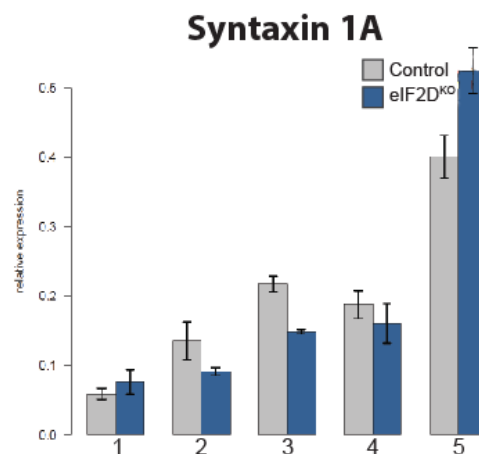
Figure 26. Increase in *Syntaxin1A* translation. Bar plots indicating the percentage distribution (y-axes) of Syx1A mRNA form Deep Sequencing. The numbers on the x-axes indicate the fraction number of the Polysome profile. Grey bars correspond to Control samples and blue bars correspond to *eIF2D^{KO}* samples. Error bars are STDEV/SUM.

I performed immunostaining of NMJ at muscle 4 of 116h AEL larvae with anti-Syx1A antibody and quantified the total intensity at the NMJ. Quantification of total intensity at the NMJ shows no differences between control animals and $eIF2D^{KO}$ (Fig. 27).

As Syx1A is a molecule found in many synapses, not only NMJs, it can be hypothesized that protein levels of Syx1A could be affected elsewhere. I performed Western blots with whole larva samples to look at total Syx1A levels, but antibody for Syx1A was not suitable for this technique (data not shown). Therefore, I cannot conclude that total Syx1A protein levels do not change. However, I can exclude a major contribution of Syx1A in the behavioral phenotype since its levels at the NMJ do not change.
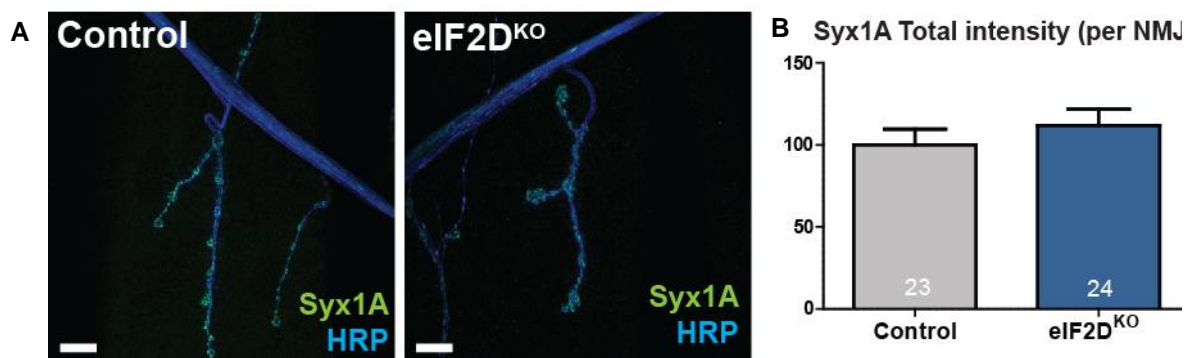
Figure 27. NMJ Staining with Syntaxin1A and quantification. (A) Representative images of Control and eIF2D^{KO} NMJs of muscles 4 of the abdominal segment A2/A3, stained with antibodies against Syx1A (green) and HRP (blue). Scale bars = 13µm (B) Quantification of total Syx1A intensity at the NMJ for Control (grey) and $eIF2D^{KO}$ (blue). P-value was calculated using non-paired t-test, p=0,391. Number of NMJs analyzed is indicated in the bars. Error bars = SEM.

6.6.3.2   eIF4A translation is upregulated in eIF2D^KO larvae

Expression levels of *eIF4A* mRNA are upregulated in fraction 3 of the RNA-seq data and its overall translation profile shows higher ribosome-bound mRNA (Fig. 22). eIF4A is a canonical translation initiation factor, very abundant protein, it is expected to be required in high amounts, hence actively translated. Therefore it was surprising to observe that it is mainly translated by monosomes (a single ribosome) in the controls, with the majority of its mRNA being in the free pool and relatively little being engaged with the ribosome. In eIF2D^KO samples, there is a shift from the free fraction to the monosome-associated, suggesting increased translation of *eIF4A* mRNA when eIF2D is lacking.

Since eIF4A is ubiquitously expressed, I decided to assess its levels by Western blot, in lysates from whole staged third instar larvae. There was a significant increase in eIF4A protein in eIF2D^KO, matching my hypothesis suggested by the increase in ribosome abundance. I conclude that eIF2D controls eIF4A protein levels by regulating its translation rates *in vivo*.
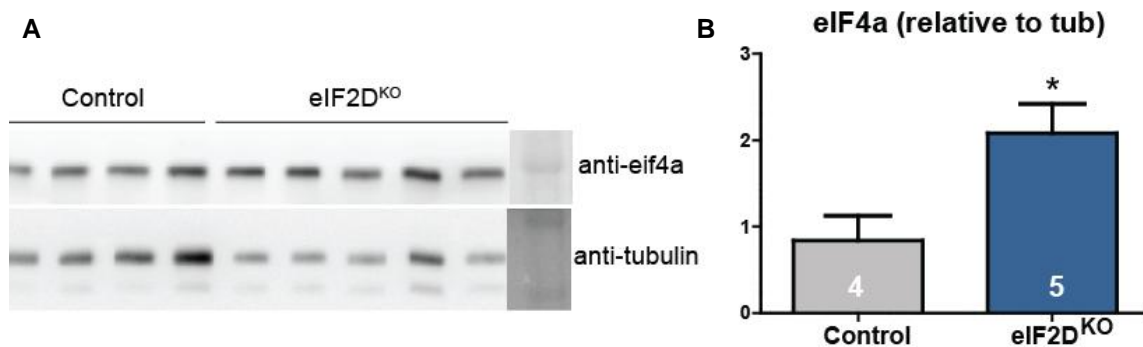
Figure 28. Protein levels of eIF4A. (A) Western blot from whole 116h AEL larvae Control and eIF2D^KO stained with antibody against eIF4A and tubulin as loading control. (B) Quantification of the Western blot of eIF4A protein levels. Tubulin levels were used to normalization. p-value was calculated using unpaired t-test, p=0.029. Number of replicates is indicated in each bar.

6.6.4 Glutamate receptors composition is affected in *eIF2D*^{KO} larvae

Next, I focused on those targets with a direct impact on synaptic function at the NMJ and locomotion behavior. Glutamate receptors are heterotetramers of with one copy of each of the obligatory subunits GluRIIC, GluRIID and GluRIIE, and one of the exchangeable subunits GluRIIA or GluRIIB. Two of those subunits appear in the RNA-seq dataset as targets of eIF2D: GluRIIB and GluRIIE. *GluRIIB* shows a decrease in ribosome-associated mRNA whereas *GluRIIE* has a mixed profile showing an increase in both the first and last fraction and a decrease in the other 3 (Fig. 29A). Interestingly, all 5 subunits have different translation profiles in the wild type.

To connect translation profiles and to protein levels, I decided to look at levels of each subunit. Unfortunately, antibodies for GluRIIE are not available. I performed immunostainings of staged third instar larvae with antibodies against GluRIIA, GluRIIB, GluRIIC and GluRIID, and imaged NMJs of muscle 4 of abdominal segments 2/3.

GluRIIA shows no difference in protein levels consistent with no significant effect on its translation profile. However, GluRIIC and GluRIID both show a decrease. This result was unexpected since translation of these subunits was not affected (Fig. 29B, 29C). To see if transcription could explain this result, I looked at the total mRNA levels of the subunits. GluRIIC mRNA is reduced by -0.84 (p-value = 0.003) in eIF2D^{KO} which might explain the reduction in protein but GluRIID has no difference. Finally, GluRIIB shows an increase in protein levels at the NMJ (Fig. 29B, 29C), which, in principle, contradicts the hypothesis of decreased protein levels due to less ribosome-associated mRNA.

These results suggest that eIF2D regulates glutamate receptor composition, by differentially regulating translation of specific subunits.
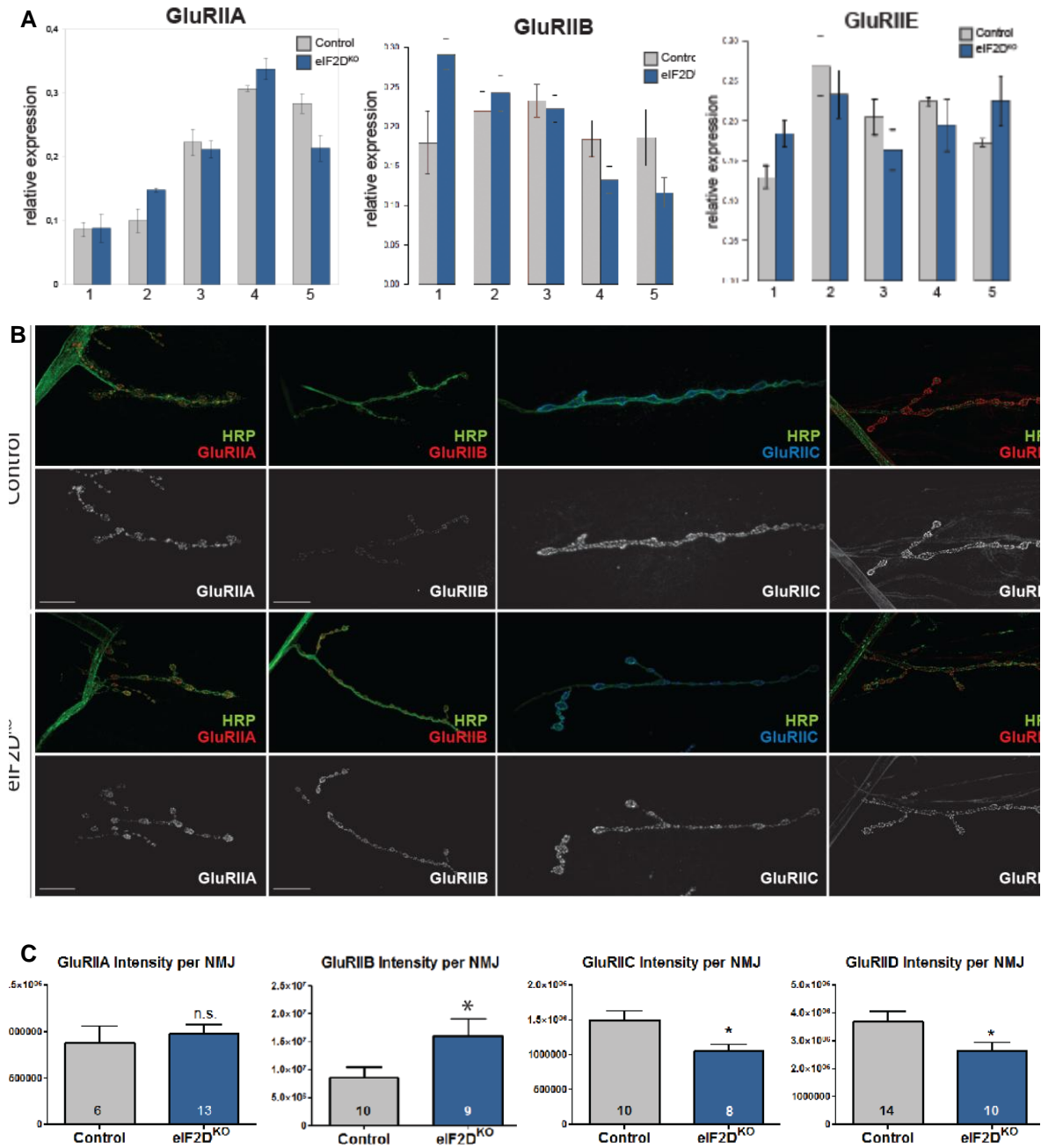
Figure 29. Glutamate receptor subunits. (A) Translation profiles of 3 GluR subunits: *GluRIIA* does not change its translation profile in eIF2D^{KO} larvae, whereas *GluRIIB* has less ribosomes-bound mRNA and shifts from the heavy to the lighter fractions. (B) Representative images of 116h AEL larval NMJs at muscle 4 stained with antibodies against different Glutamate receptor subunits (red or blue) and HRP as neuronal marker. (C) Quantification of protein levels at the NMJ for different glutamate receptor subunits: GluRIIA, GluRIIB, GluRIIC and GluRIIB. GluRIIA shows no changes, GluRIIB increases in eIF2D^{KO} and GluRIIC and GluRIID decrease in eIF2D^{KO}.

Controls are represented with grey bars and eIF2D^{KO}, with blue bars. Number of NMJs analyzed is indicated in each bar. p-values were calculated using unpaired t-test, * $p<0.05$; ** $p<0.01$; *** $p<0.001$. Error bars = SEM.

6.6.5 *eIF2D*^{KO} NMJs have fewer synaptic active zones but no defects in their apposition to post-synaptic receptors

Proper synaptic signaling requires pre- and postsynaptic components. Since glutamate receptor composition in the postsynapse was altered, I wondered whether active zone number might also be changed and to what magnitude.

I stained third instar larvae with anti-Brp antibody as a marker for active zones. Quantification of Brp total intensity shows a decrease (Fig. 30), suggesting fewer active zones in the *eIF2D*^{KO} NMJs. Moreover, a quantification of active zones to an apposed post-synaptic receptors (BRP to GluRIIC) showed no difference between control and *eIF2D*^{KO} NMJs (Fig. 30). This indicates that whereas *eIF2D*^{KO} NMJs have fewer active zones, those seem to be functional.
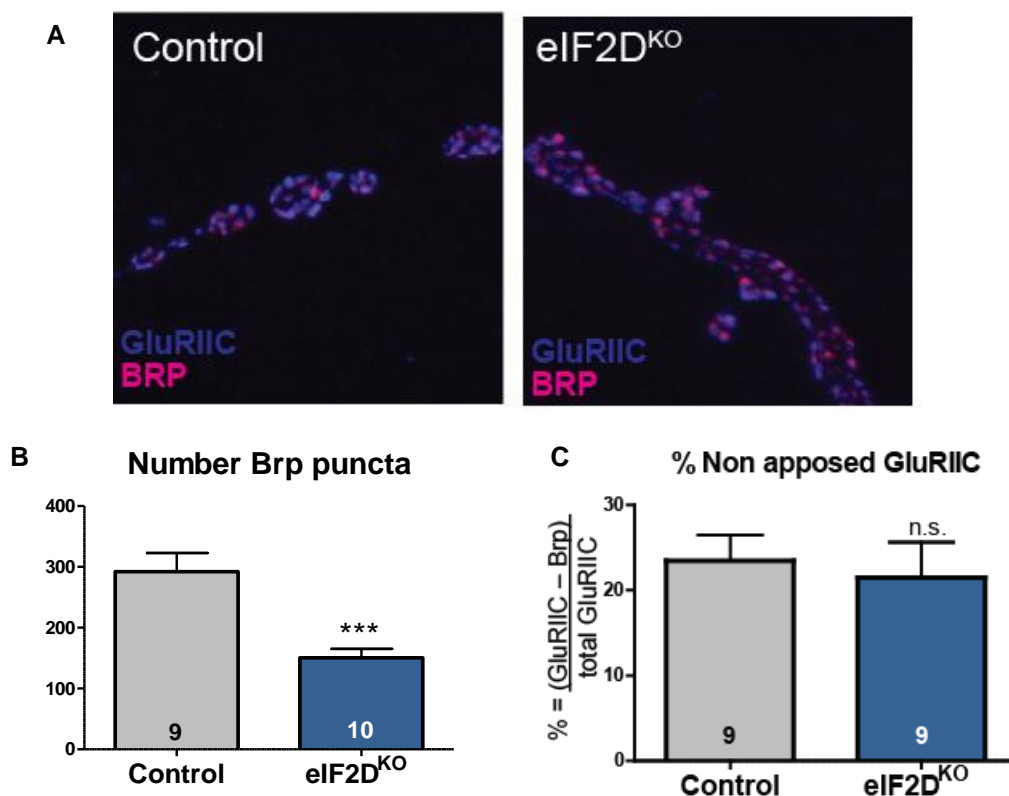
Figure 30. BRP staining and apposition to GluRIIC. (A) Representative images of 116h AEL larval NMJs at muscle 4 stained with antibodies against GluRIIC (blue) and BRP (magenta) as markers for pre- and postsynapse, respectively. (B) Quantification of BRP puncta shows a decrease in *eIF2D*^{KO}. (C) Quantification of Non-apposed GluRIIC to BRP puncta shows no difference. Controls are represented with grey bars and eIF2D^{KO}, with blue bars. Number of NMJs analyzed is indicated in each bar. p-values were calculated using unpaired t-test, * $p<0.05$; ** $p<0.01$; *** $p<0.001$. Error bars = SEM.

6.7 Specific 5'UTR features are enriched in mRNAs regulated by eIF2D *in vivo*

Next, in order to understand why these target mRNAs are regulated by eIF2D together, I examined their sequences for common features. I focused on the 5'UTRs of the mRNAs because this region is known to have a large impact in translation initiation control.

6.7.1 eIF2D regulates translation of a subset of uORF-containing mRNAs

eIF2D protein has a high homology to DENR-MCTS1 and the DENR-MCTS1 complex is involved in re-initiation after short uORFs (Schleich et al. 2014). Moreover, the Pestova lab, showed that eIF2D could promote non-directional movement of post-termination ribosomes to codons matching the final P-site tRNA and promote re-initiation there (Skabkin et al. 2010; Skabkin et al. 2013). Therefore, I wanted to know if eIF2D would regulate translation on the same or similar mRNAs as the DENR-MCTS1. To test this hypothesis, I looked for an enrichment of uORFs in eIF2D target list. For that, Thomas Lingner calculated the average number of annotated AUG uORFs per mRNA in every fraction in up- or downregulated mRNAs in $eIF2D^{KO}$ (Schleich et al. 2014) (Figure 31). I observed a different distribution between up- and down-regulated mRNAs. Those mRNAs with high number of uORF are downregulated in deep fractions (fraction 4 and 5) and upregulated in the lighter fractions (fraction 1 and 3).

Then, he calculated the average number of uORFs of all transcripts in the genome. We used this number as the genome background to which we compared the number of uORF in eIF2D targets (Figure 31, red line). Surprisingly, although absolute numbers seem very different from the genome, these differences are not statistically different in many cases, probably due to the dispersion of those values.

Next, he also calculated the average number of uORFs in the 50 most enriched mRNAs in each given fraction. uORF are known to be mostly negative regulators of translation of the mORF. Therefore, mRNAs with more uORFs would be engaged with fewer ribosomes that the ones with less or no uORFs (Heyer and Moore 2016), being enriched in the lighter fractions. Deviations from the genome average in the $eIF2D^{KO}$ samples could be driven by mRNA properties alone. Indeed, we see that

80

enriched mRNAs in fractions 1 and 2 of control samples tent to have more uORFs than the ones in polysomes. Moreover, we see differences between the genome average and the enriched genes. In the *eIF2D^{KO}*, there is a big increase in number of uORF per mRNA in fraction 3 corresponding to disome. Data from yeast have shown that when a ribosome is engaged on a uORF, all other ORFs in the mRNA tend to be unoccupied. Thus, this result suggests that in *eIF2D^{KO}* mRNAs with translating uORFs will be also translating the CDS or other uORFs. However, this is only true for fraction 3. In deeper fractions, mRNAs with more uORFs are downregulated.

In sum, uORF number per mRNA seems to have an impact on whether an mRNA translation control is affected by eIF2D. However, not every uORF containing mRNA is affected by absence of eIF2D and some of the eIF2D targets have no uORFs.
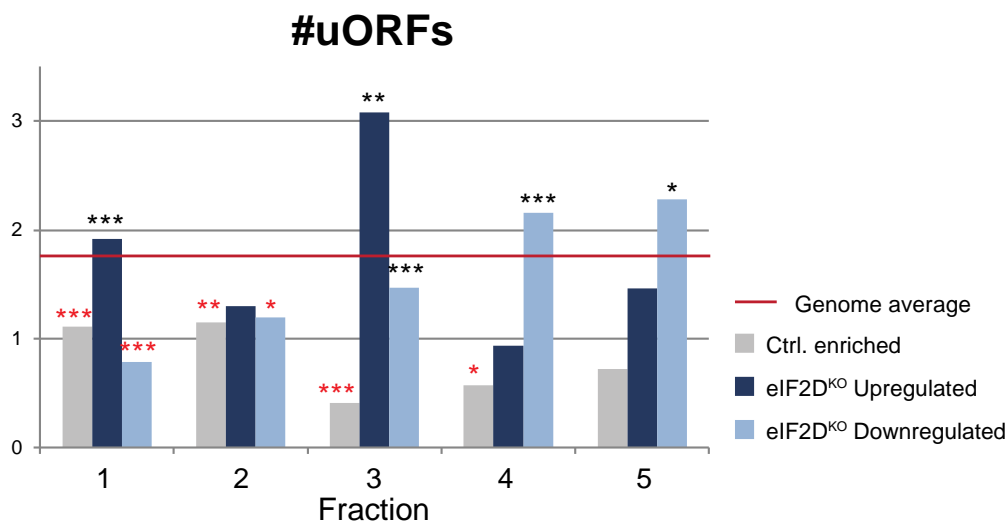
Figure 31. Number of uORF per mRNA in eIF2D targets across the fractions.
The different bars indicate the average number of uORF for the 50 enriched mRNAs in that fraction in the control samples (grey), the average number of uORF for the upregulated mRNAs in eIF2D^{KO} (dark blue), and the average number of uORF for the downregulated mRNAs in eIF2D^{KO} (light blue). The red line indicates the average of uORFs per mRNA in the whole genome. The y-axis indicates number of uORFs per mRNA. The x-axis indicates fraction number. p-values were calculated using two-sided Wilcoxon tests for comparison to the complete distribution across all transcripts* $p < 0.05$; ** $p < 0.01$; *** $p < 0.001$

Data for this figure was provided by Dr. Thomas Lingner

6.7.2   eIF2D and DENR-MCTS1 regulate different subsets of uORF-containing mRNAs

It was clear from the phenotypic characterization of *eIF2D^{KO}* flies that eIF2D and DENR have an impact on different animal functions and therefore affect translation of different mRNAs. Unlike previously suggestions from *in vitro* studies (Skabkin et al. 2010; Skabkin et al. 2013), eIF2D and DENR functions and targets might not totally overlap *in vivo*. I hypothesized that their targets could partially overlap. To address that, I studied the impact of eIF2D on the translation of DENR-dependent reporters in a cell based reporter assay.

Drosophila S2 cells were first treated with RNAi to knockdown DENR, eIF2D or both and GFP RNAi was used as control. I co-transfected reporters containing the Rluc coding sequence with a 5'UTR containing 1 amino acid long uORF (1aa uORF) and a Fluc reporter for normalization, to proliferative S2 cells. As previously reported, knockdown of DENR reduced the expression of the reporter containing the 1 amino acid long uORF (Schleich et al. 2014). Knockdown of eIF2D in S2 cells did not affect this expression (Fig. 32). Moreover, double knockdown of DENR and eIF2D did not further reduce or enhance expression compared to DENR-KD cells (Fig. 32).

Thus, although eIF2D might influence translation of uORF-containing mRNA, they are not the same mRNA type that DENR-MCTS1 regulates.
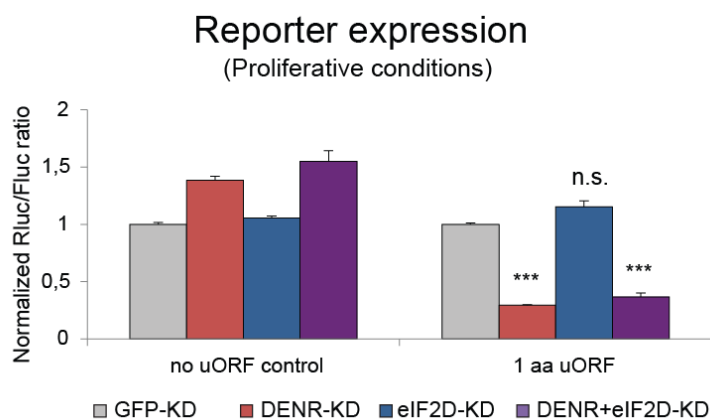
Figure 32. Reporters expression in knock down S2 cells. Normalized Rluc/Fluc expression in proliferative S2 cells with GFP-KD (Control, grey bars), DENR-KD (red bars), eIF2D-KD (blue bars) and DENR-KD+eIF2D-KD (purple bars) transfected with reporter with no uORF on its 5'UTR (left) or 1 amino acid reporter on the 5'UTR (right). p-values were calculated using unpaired t-test against GFP-KD control, * p<0.05; ** p<0.01; *** p<0.001. Error bars = SEM.

* *This data was generated together with Dr. Tatyana Koledachkina*

6.7.3   Targets of eIF2D have an enrichment of A-rich motif in their 5'UTRs

Next, I searched for common sequences within eIF2D target 5'UTRs. I analyzed the targets being up- or downregulated in each fraction separately, thus having 10 separate lists or data-sets. I used the annotated 5'UTRs from Flybase and processed all existing isoforms of an mRNA. This analysis was motivated by the expectation that different types of regulation on different mRNAs may result in some mRNAs having higher translation whereas others would have a reduced translation. Processing all mRNAs together could overshadow important features.

With the tool MEME-ChIP from MEME Suite (Timothy and Geller 2009), I performed comprehensive motif analysis including motif discovery on my data set. For every data-set I obtained a maximum of 6 different motifs. Looking across the data set, I observed that one motif appears in several fractions: an A-rich motif. This motif is enriched in mRNAs upregulated in fractions 1, 2 and 5 and downregulated in fraction 5, with different levels of significance (Fig. 33). Mainly, it consists of a sequence of 6 repeated adenosines. Because most of the mRNAs enriched in the first fractions tend to have an overall decreased translation profile, this distribution

83

suggests that eIF2D could promote translation of mRNAs containing an A-rich motif in their 5'UTRs.

Figure 33. A rich sequences. Table showing the different A-rich motifs found in the 5'UTR of eIF2D mRNA targets, organized by the fraction number where they are upregulated (UP) or downregulated (DOWN), and the E-value. Num. of sites/sequences indicates the times this motif is found in the analyzed transcripts. Because some genes have more than one transcript with different 5'UTRs, Genes with motif/in fraction indicates the number of genes containing transcripts with this motif, in the genes differentially expressed in that data set.

6.7.4   Targets of eIF2D with A-rich motif at the 5'UTR are enriched for synapse

To see if the genes with enriched A-rich motif at their transcripts' 5'UTR were part of a same functional class, I performed a GO-term enrichment analysis. The target mRNAs containing A-rich sequences from the previous analysis were subjected to GO-term enrichment analysis for cellular component (CC). Interestingly, "Synapse" is the second most enriched term which includes the genes indicated in Fig. 34. In sum, this A-rich motif in the 5'UTR could be a key element for the coordinated regulation of the synaptic mRNAs, and many more, by eIF2D in vivo.

A GO term - celular component

GO term	-log 10 (P-VALUE)
GO:0031012~extracellular matrix	
GO:0045202~synapse	
GO:0042995~cell projection	
GO:0031966~mitochondrial membrane	
GO:0005874~microtubule	
GO:0016021~integral component of membrane	

B

GO:0031012~extracellular matrix	
FBgn0260660	Mp
FBgn0033725	Cpr49Ac
FBgn0002526	LanA
FBgn0085491	CG34462
FBgn0000551	Edg78E
FBgn0032484	kek4
FBgn0039441	TwdlN
FBgn0033728	Cpr49Ae
FBgn0004956	upd1

C

GO:0045202~synapse	
FBgn0000037	mAChR-A
FBgn0002526	LanA
FBgn0030230	Rph
FBgn0038975	Nrx-1
FBgn0053653	Cadps
FBgn0083228	Frq2
FBgn0032058	CG9289
FBgn0031936	CG13794
FBgn0004882	orb
FBgn0020429	GluRIIB

Figure 34. Gene Ontology (GO) term enrichment. (A) Table shows the GO terms for "Cellular component" enriched in the genes containing an A-rich motif in the 5'UTRs, and the p-value (-log10) for each term. (B) Genes with A-rich motif in 5'UTR in the "Extracellular Matrix" group. (C) Genes with A-rich motif in 5'UTR in the "Synapse" group.

6.8 eIF2D regulates translation of several targets trough their 5'UTRs

To obtain greater mechanistic insight into eIF2D translational regulation, I decided to test the effect of 5'UTR of specific targets in luciferase reporter assays. I selected the 5'UTRs to test based on the above described 5'UTR features: 1) interesting sequence features (uORFs and/or A-rich sequence) and 2) biological processes involved. Some of those targets have more than one annotated isoform with a different 5'UTR. In those cases, I decided to assess the impact of the different isoforms. According to these criteria I used the 5'UTR of the following transcripts indicated in Table 22. The 5'UTRs of the selected mRNAs were cloned into a pMT plasmid with a metallothionein promoter inducible with $CuSO_4$ and are directly

85

upstream of the Renilla luciferase (Rluc) open reading frame, with no extra sequence in between (Fig. 10). This should recapitulate the endogenous mRNA 5'UTR structure as closely as possible. These vectors were cloned by Katrin Küchler in the Duncan lab for this project.

Table 22			
Transcript	A-rich motif	AUG uORF number	function
GluRIIB	yes	0	synapse
Cadps-RD	yes	4	synapse
Cadps-RF	yes	1	synapse
LanA	yes	1	synapse
Mp-RG (multiplexin)	yes	1	synapse
Nrx-RB	yes	6	synapse
Nrx-RD	yes	7	synapse
park	no	1	mitochondria
eIF4A-RA	yes	0	translation
eIF4A-RB	no	0	translation
eIF4A-RD	no	0	translation
rpl41	no	0	translation

Each 5'UTR-Rluc plasmid was co-transfected with a pMT-Fluc (firefly luciferase) plasmid for normalization into GFP-KD (Control) or eIF2D-KD S2 cells.

Interestingly, I could see effects on several of the reporters upon knockdown of eIF2D. GluRIIB, LanA, Multiplexin, park and rpl41 all showed no significant changes. Conversely, two genes with different transcripts, eIF4A and Nrx-1, showed a selective increase of reporter translation in eIF2D-KD cells for some isoforms but no changes for the other. Finally, Cadps showed also an increase for one of the isoforms (Cadps-RD) whereas the second isoform showed an increase (Fig. 35).

These results indicate that eIF2D regulates translation of those constructs through their 5'UTR. The fact that some constructs are upregulated and some are downregulated indicates a dual function of eIF2D as repressor and promoter of

translation. Finally, the 5'UTR alone appears not sufficient for the regulation of some targets. In those ones with no effects in the reporter assays, it might be that the sequence between 5'UTR and CDS is important, for example in case of an o-uORF (overlapping-uORF), or that eIF2D function is more essential in recycling after the CDS on these CDS. In addition, although most of these constructs have an A-rich motif or uORF in their 5'UTR, I could not detect clear correlation between those elements and the direction of regulation.
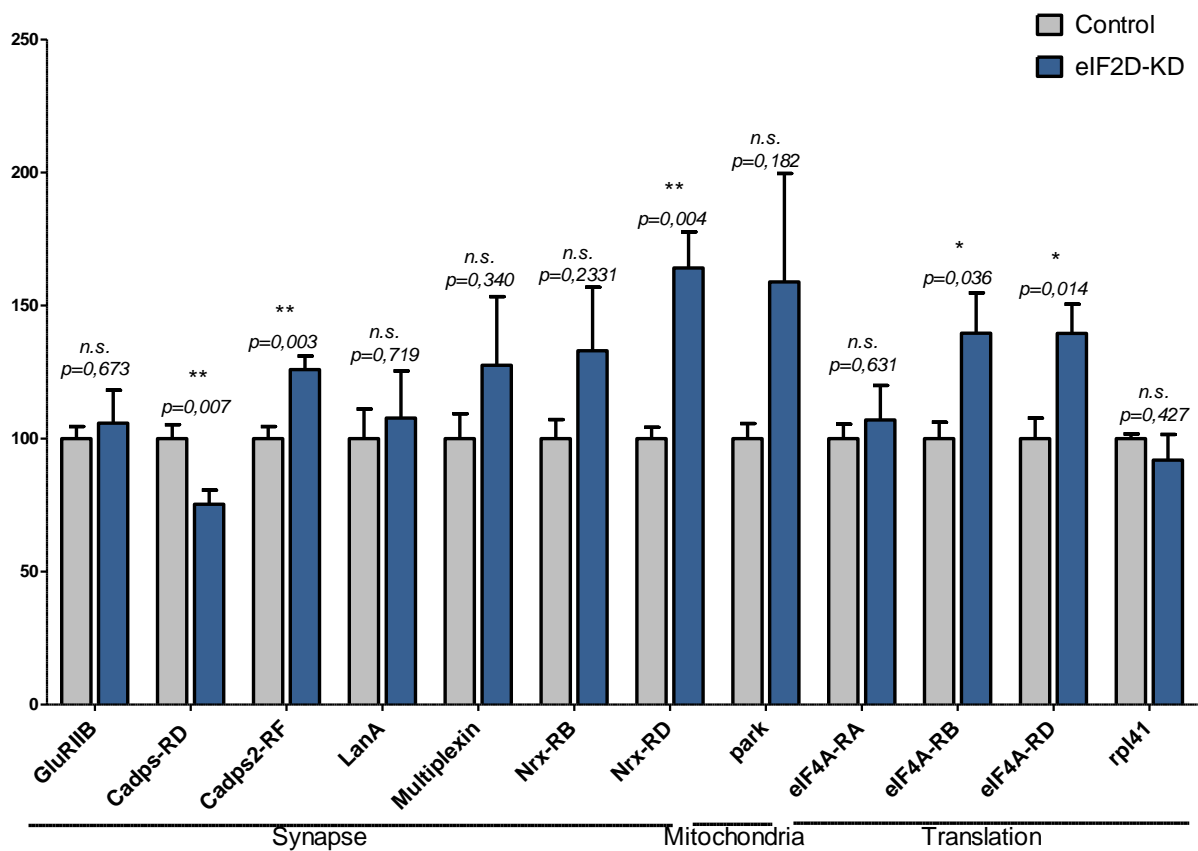
Figure 35. Reporter assays. Grey bars represent GFP-KD (Control) and blue bars represent eIF2D-KD. The Y-axes indicates the Rluc/Fluc ratio normalized to Control samples. The X-axes indicates the name of the 5'UTR reporter tested. p-values were calculated using unpaired t-test respective to Control for each reporter and are indicated above each bar, * p<0,05; ** p<0,01; *** p<0,001. Error bars = SEM

7 Discussion

Studies about translation and translation control have historically focused on studying the function of classical translation factors on. Moreover, many of these studies have been performed *in vitro* or in simple organisms like yeast.

This thesis analyzes the functional relevance of the non-canonical translation factor eIF2D for animal physiology and how this relates to regulation of translation. Taken all together, the experiments presented in this thesis show a requirement of eIF2D for motor circuit function in *Drosophila melanogaster.* eIF2D affects animal behavior by both promoting and repressing translation of specific mRNAs through their 5'UTRs, probably using non-canonical (re-)initiation and recycling mechanisms.

7.1 eIF2D is sufficient in either side of the NMJ to promote normal behavior

In this study, I used knockout flies, lacking the entire ORF of the non-canonical translation factor eIF2D, and analyzed resulting phenotypes on the behavioral level. In addition, I identified the *in vivo* mRNA targets for this factor. Previous data from the Duncan lab showed that loss of eIF2D loss has a surprisingly specific effect on the behavioral level causing a reduction of locomotion speed in larvae (Fig. 5). More interestingly, the data showed that eIF2D affects behavior by selectively affecting synaptic function without apparent defects synaptic morphology (Fig. 6). Transgenic expression of eIF2D in the whole larvae was able to rescue the deficit in locomotion. Moreover, expression of eIF2D only in muscles or motor neurons was also able to rescue this phenotype (Fig. 13).

This was a surprising finding since most of the molecules that are expressed and function in both synaptic sides would give partial rescues or no recues at all when being expressed only on one side. There are however a few examples of this type of molecules being able to rescue defects from only one side. Other molecules are cell-type specific expressed in either motor neurons or muscles and rescue the phenotypes from only one side of the synapse. eIF2D promotes normal locomotion from either the pre- or postsynaptic side of the NMJ, raising the question of which mechanisms eIF2D uses to do so.

7.2 eIF2D affects total translation *in vivo*

Since eIF2D was described as a translation factor, I hypothesized that the effects in behavior and synaptic function would be due to deregulation of translation of certain mRNAs.

Previous biochemical studies revealing non-canonical functions of eIF2D suggested a very little impact in general translation in yeast or *in vitro*. Moreover, *in vitro* studies using reconstituted translation systems showed that eIF2D promotes translation of synthetic mRNAs with very specific sequences (Dmitriev et al. 2010). In yeast, eIF2D does not have a major effect on general translation and lack of eIF2D showed no significant effects on viability (Fleischer et al. 2006). Thus, it is unclear whether eIF2D regulates translation of any mRNAs *in vivo*.

Contrary to what was initially expected based on data from yeast (Fleischer et al. 2006) and my own data from S2 cells (Fig. 14), polysome profiling revealed an increase in total translation in *eIF2D^{KO} Drosophila* larvae (Fig. 17). At first this seems contradictory to the definition of a non-canonical translation factor, which would be expected to affect only a very limited subset of mRNAs. However, it does not mean that eIF2D affects translation of all mRNAs of the animal, not even that it affects most of them. These results highlight the importance of studying eIF2D functions and targets *in vivo* in a multicellular organism.

7.3 eIF2D regulates translation of mRNAs encoding for synaptic and mitochondrial proteins

After having demonstrated that eIF2D is important for the normal translation *in vivo*, the next aim was to identify its target mRNAs. Polysome profiling followed by RNA-seq (Poly-seq) of several fractions was chosen as the best approach to answer this question. To analyze this big data set, bioinformatics analyses were required. Discussion about this method will follow in further chapters.

A total of 740 different mRNAs of the 17 000 genes of *Drosophila* were differentially expressed in at least one of the fractions in eIF2D^{KO} samples, and had altered translation profile (distribution of mRNA abundance across the fractions) (Fig.

21). I observed that many enriched GO terms for biological processes from the differentially expressed mRNAs were linked to synaptic function, synapse development or behavior. However, *in vivo* targets of eIF2D also include other general biological processes, such as those related to mitochondrial functions, transcription, protein modification or microtubule movement (Fig. 23). Whether these are connected to eIF2D's role in locomotion behavior or are independent is an interesting question for future studies.

Because eIF2D is thought to be ubiquitously expressed, several hypotheses come to our minds. The first one is that the changes observed in mRNAs' translation expressed in several cell-types, are actually deregulated in a few of them, two important ones being motor neurons and muscles. The second one is that this deregulation occurs equally in all the cell-types where the mRNA is expressed, but for a particular reason, some systems are more capable to compensate for this defect. The difference between those more sensitive systems (synapse and mitochondria) versus others resides in their complexity: motor neuron synapses need adjustments between two different cell types to properly function, whereas mitochondria need correct coordination between nuclear and mitochondrial genome. Other systems would activate alternative pathways to compensate for eIF2D loss whereas in the affected ones, those pathways would not be sufficient. The third hypothesis is that eIF2D effects in a cell-type depend on the ratio between eIF2D protein and target mRNA levels. Further experiments are needed to understand whether the effects seen in more globally expressed mRNAs are general or cell-type specific.

7.3.1 eIF2D regulates translation of several mitochondria related mRNAs but global ATP levels are not affected

The most enriched GO term was "ATP metabolic process". An experiment to address ATP levels in the larvae showed no differences between controls and *eIF2D^{KO}* mutants (Fig. 24). From this result I conclude that there are no major abnormalities in ATP production in the mutants, but I cannot discard a tissue-specific ATP deficit, for example in the muscles, that could be an explanation to the slow

locomotion phenotype. It will be important in the future to determine whether ATP levels at the motor system or other cell-types are normal.

Most of the genes in this functional category were not related to ATP production and only half were mitochondria-linked. However, a deeper look at the eIF2D targets showed several mitochondria related genes (Table 23). One of these genes was especially interesting for me. Parkin (park) is involved in mitochondria fission and has been linked to Parkinson's disease (Polymeropoulos et al. 1996; Polymeropoulos et al. 1997; Lim et al. 2002), which affects motor abilities through effects on the Dopaminergic system. Unfortunately, all attempts to address Parkin protein levels in *Drosophila* larva samples were unsuccessful, probably due to the low protein levels. However, mitochondria of the e*IF2D^{KO}* larval muscles have altered shape and distribution similar to what has been described for *park-null* mutants in the adult muscles (Deng et al. 2008), thus presenting an indirect evidence of missregulation in Parkin function (Fig. 25). Since it has been reported that mitochondrial function is highly correlated to mitochondrial shape and size, it could be that other mitochondria functions are compromised in *eIF2D^{KO}*.

Table 23. Mitochondrial related genes targets of eIF2D translation regulation		
ID	**Symbol**	**Function**
FBgn0086907	Cyt-c-d	Complex IV
FBgn0033020	COX4L	Complex IV
FBgn0029752	TrxT	Mitochondria fission
FBgn0004635	Rhomboid	Mitochondria fission
FBgn0030975	SdhBL	Complex II
FBgn0011596	fzo	Mitochondria fusion
FBgn0035124	ttm2	Protein translocation
FBgn0250816	AGO3	piRNA-guided RNA cleavage
FBgn0069354	Porin2	ion transport
FBgn0003997	hid	Apoptosis
FBgn0021765	scu	-

It is important to remember that mitochondria's function do not only include ATP production, but also other processes, one of them being calcium buffering. Mitochondria are very abundant in neurons, in particular in chemical synapses. Both molecular processes, including ATP generation and Ca^{2+} buffering by mitochondria, have been implicated in the regulation of synaptic transmission and plasticity. However, it can be challenging to understand how these more global functions of mitochondria interfere with the function of synaptic machineries (Vos et al. 2010).

In excitable cells such as neurons, action potentials trigger depolarization of the plasma membrane, followed by opening of voltage-dependent calcium-channels, leading to a rise in Ca^{2+} concentration at the synaptic terminal ((Ghosh and Greenberg 1995; Zucker 1999; Jonas 2006; Yao et al. 2009). This Ca^{2+} peak stimulates synaptic vesicle release mediated by the calcium sensor proteins of the SNARE complex (Tucker et al. 2004; Chicka et al. 2008). By taking up Ca^{2+} at the synaptic terminal, mitochondria are able to regulate synaptic vesicle release. In defective mitochondria animals, Ca^{2+} concentration at the synapse remains high thus enabling continuous synaptic vesicle release and ultimately depleting the available pool of synaptic vesicle (Vos et al. 2010). However, in a few cases such as the *Drosophila* NMJ, the mitochondrial contribution to Ca^{2+} concentration regulation seems to be minor (Guo et al. 2005; Verstreken et al. 2005; Lnenicka et al. 2006). Rather the plasma membrane Ca^{2+} ATPase (PMCA) followed by the ER lumen are the two main regulators (Sanyal et al. 2005; Lnenicka et al. 2006). Moreover, alterations in mitochondria morphology due to impaired fission results in vesicle trafficking defects, presumably due to reduced ATP levels and endocytosis which prevents synaptic vesicle recycling (Rikhy et al. 2007). Flies with inhibited mitochondrial fission or axonal transport show impaired neurotransmission only during intense neuronal activity, due to a defect in readily releasable pool mobilization (Verstreken et al. 2005).

Finally, I observed an increase in total mRNA of mitochondrial ribosomal proteins and their translation (Appendix). This suggests 3 different hypotheses: a very controversial possibility is that when eIF2D is missing, there is an increase in mitochondria ribosomes and those are then localized at the cytoplasm where they

translate cytoplasmic mRNAs. Previously, mitochondria ribosomes have been identified in the translating polysomes of in germ plasm of *Drosophila* embryos (Amikura et al. 2001). A second possibility is that eIF2D is transported to the mitochondria and has a role in mitochondrial-encoded gene translation. So far, no evidence for a role of eIF2D in mitochondrial translation has been described but I do not discard it as a possibility. Moreover, since mitochondrial protein complexes are formed by both nuclear- and mitochondrial-encoded genes, alterations in the mitochondrial translation machinery in the *eIF2D^{KO}* could reflect a compensatory mechanism that responds to altered cytoplasmic translation.

7.3.2 Poly-seq data contains mRNAs coding for proteins that might explain transynaptic behavioral rescue by eIF2D

Rescue experiments show that expression of eIF2D in a tissue-specific manner in motor neurons or muscles results in complete improvement of larval locomotion (Fig. 13). Since a motor neuron axon terminal and a muscle cell represent pre- and post-synaptic sides of larval NMJ respectively, these rescue results suggest that eIF2D may function trans-synaptically to promote normal locomotion. In molecular terms, this includes three major possibilities: (1) eIF2D itself could be secreted and transferred bidirectionaly across the synapse alone or as a part of a bigger complex such as capsids or extracellular vesicles containing mRNA (Budnik et al. 2016; Pastuzyn et al. 2018) (2) eIF2D expressed on either side promotes translation of a certain transcript or transcripts encoding proteins are able to move across the synapse in both directions, and (3) eIF2D promotes translation of different pre- or post-synaptic mRNAs, which could mutually compensate for each other's absence and result in a wild type behavior.

To study expression of eIF2D protein, the lab made a custom antibody since antibodies for eIF2D in *Drosophila* are not commercially available. Although this antibody works well in western blots from cell culture samples and larval lysates, eIF2D expression is too low to obtain informative immunostaining of larval dissections. Other biochemical techniques might be used in the future to address this question. Whether eIF2D itself is a trans-synaptic protein, remains unknown.

In order to differentiate between the second and third hypotheses, I further searched in the Poly-seq data set to identify mRNA targets in these categories. In the context of the second hypothesis, one of the targets is a synaptic protein that similar to eIF2D is functionally sufficient on either synaptic side and at the same time does not affect NMJ morphology. Endostatin is a cleavage product of Multiplexin (Mp) and is implicated in homeostatic modulation of the pre-synaptic neurotransmitter release. Transgenic Endostatin expression either pre- or post-synaptically at the NMJ was shown to rescue synaptic homeostasis in Multiplexin mutants by restoring pre-synaptic calcium influx (Wang et al. 2014).

By expressing eIF2D in muscles, it would regulate Multiplexin translation to return to normal levels and allow it to be cleaved into Endostatin to signal to the motor neuron and promote homeostatic compensation. Because synaptic function, especially homeostasis is not fully rescued, it suggests that parts of the pathways at the motor neuron might not be rescued when eIF2D is expressed only in muscle. If Endostatin functions through a presynaptic receptor or other effector that is deregulated in $eIF2D^{KO}$, Endostatin would not be able to fully work, even though its own levels are normal.

To support the third hypothesis, finding trans-synaptic adhesion molecules as translational control targets could rationalize eIF2D's ability to promote locomotion from either side of the synapse. Nrx-1 (Neurexin-1), the ortholog of vertebrate Neurexin, is a trans-synaptic adhesion molecule crucial for synaptic function and implicated in numerous human CNS disorders, including schizophrenia and Autism Spectrum Disorders (Dean et al. 2003; Li et al. 2007a; Li et al. 2007b; Clarke and Eapen 2014). Previous studies with Nrx-1 mutants show similar phenotypes to eIF2D^{KO} (Li et al. 2007b; Chen et al. 2010; Owald et al. 2012). Nrx-1 and its trans-synaptic binding partners (e.g. Neuroligins) function from both sides of some synapses, including the *Drosophila* NMJ (Sun et al. 2011; Harris and Littleton 2015).

In normal conditions, Nrx-1 would be expressed from either side of the synapse to the appropriate levels and interact with Nlg. In eIF2D^{KO}, *Nrx-1* mRNA translation decreases and protein levels would be hypothetically reduced. Transgenic

expression of eIF2D in either side of the synapse would restore Nrx-1 translation to the normal levels, as well as protein in that synaptic compartment, which would provide sufficient contact for trans-synaptic communication and active zone structure. I propose that eIF2D normally tunes translation of these mRNAs to the correct range, thereby enabling trans-synaptic protein-protein interactions important for function.

7.3.3 Glutamate receptor subunits levels at the NMJ are regulated by *eIF2D* translation in Drosophila *larvae*

Multiplexin and Neurexin-1 are only two examples of the mRNAs found in the Poly-seq data that could help to explain the observed phenotypes *in vivo*. Two other eIF2D targets were predominantly interesting: GluRIIB and GluRIIE, two subunits of the glutamate receptors, the main receptor at the larval NMJ. Glutamate receptors are heterotetramers formed with one copy of GluRIIC, GluRIID and GluRIIE subunits and a copy of either GluRIIA or GluRIIB. Mutant GluR animals have a severely reduced synaptic transmission affecting mEPSP and morphological defects such as reduction in bouton size (Choi et al. 2014). Acute pharmacological perturbations of GluR affect only synaptic transmission (EPSP if treated for a short time, and mEPSP) with no impact in morphology (Choi et al. 2014). The phenotypes observed in *eIF2D^{KO}* animals are similar to the pharmacological treatment, as mEPSP is reduced but morphology remains unchanged. Also, it is very important for correct synaptic physiology to maintain A-type to B-typre receptor ratio (Petersen et al. 1997; DiAntonio et al. 1999). Thus, changes in glutamate receptor abundance or composition could be the reason for altered behavior in *eIF2D^{KO}* larvae.

To test this hypothesis, I decided to measure the protein levels for the different GluR subunits. Unfortunately, there are no antibodies available for GluRIIE subunit, but I did obtain specific antibodies for all the other 4 subunits. GluRIIB showed an increase in protein levels at the NMJ, whereas the other exchangeable subunit, GluRIIA, was not changed. Moreover, levels of GluRIIC and GluRIID subunits are decreased (Fig. 29). Because it has been reported that a functional receptor needs one copy of each of the obligatory subunits, these results suggest a reduction in total glutamate receptors in *eIF2D^{KO}* larvae. This is further supported by the observation that active zone number at the NMJ also decreases in *eIF2D^{KO}* and explains the

reduced mEPSP amplitude phenotype. Moreover, eIF2D is necessary for the correct protein levels of the different receptor subunits, presumably by controlling translation of GluRIIB and GluRIIE.

These results opened several questions. It seems that the total glutamate receptors are decreased, without a decrease in two of the subunits which is not a commonly observed situation. One explanation is that upon altered availability of the different subunits in $eIF2D^{KO}$, glutamate receptors are no longer heterotetramers, but incorporate more than one GluRIIB. Another possibility is that those extra subunits are localized at the membrane as single subunits or as part of a receptor containing only GluRIIA and GluRIIB subunits, in any case forming part of a non-functional receptor. This situation would not alter type-A/type-B ratio. Since type-B shows faster desensitization kinetics than type-A receptor, electrophysiological experiments can be performed to assess a possible reduction in functional type-B receptors. Martin Müller lab performed experiments to answer this question. However, non-publish preliminary data suggests no differences in type-B receptor abundance.

Interestingly, homeostatic compensation only occurs after alterations in type-A receptor, and is independent of type-B receptors as depletion of type-B does not produce homeostatic compensation (Albin and Davis 2004, Heckscher et al 2007, Davis et al 1998). The fact that $eIF2D^{KO}$ larvae have impaired homeostatic mechanisms, suggests that type-A receptors might be altered. To further investigate a possible change in type-A receptor, high resolution microscopy could be used to study colocalization of the different receptor subunits. The expected observation would be that whereas overall GluRIIA do not change, the GluRIIA associate with GluRIIC and GluRIID is decreased in eIF2D^{KO}.

Finally, it is important to mention that some of the previous studies about GluRs are based on the idea that glutamate receptors strictly need to be heterotetramers to be functional. While it is not my intention to invalidate those studies, it is important to keep in mind that very few studies evaluated protein levels of all subunits together. In many cases, GluRIIC has been used to study obligatory subunits or as marker for GluRs, without taking the other subunits into account.

7.3.4 eIF2D might coordinate translation of several components of one same pathway

One important aspect of these results is the observed defect in glutamate receptor composition. Other groups have observed disconnection between subunit composition in several mutants before (Karr et al. 2009). Interestingly, there seems to be a debate about Nrx-1 function on glutamate subunit composition. On one hand, loss of Nrx-1 in the NMJ results in an increase in type-A receptors, suggesting that normal function of Nrx-1 inhibits type-A receptor clustering (Li et al. 2007b; Chen et al. 2010). On the other hand, *nrx-1* mutants are defective in early type-A incorporation (Owald et al. 2012). Interestingly, this connects two of the eIF2D targets: Nrx-1 and glutamate receptors.

Cell-type specific transcription factors may represent coordinated regulation between the motor neuron and the muscle to achieve the right expression of the synaptic components. However, only one such molecule has been identified to be specifically expressed in both cell types: eve (even skipped) (Patel et al. 1992; Bodmer 1993). Further mechanisms of coordination between cell types may be still unresolved and eIF2D regulation of translation of specific mRNAs might be one of these.

Although, a set of biochemical, electrophysiological and pharmacological experiments is still necessary to identify the exact mechanisms, eIF2D might be directly or indirectly involved in one of the pathways mediating translation of effector molecules on either side of the NMJ to modulate synaptic function and homeostasis. Thus, these data provide *in vivo* evidence for the ability of eIF2D to coordinate synthesis of proteins in multi-subunit complexes to promote synaptic function and locomotion. This would represent another of the few examples of coordinated gene expression regulation at the translation level of multiple components of one same pathway (Shi et al. 2017).

Before obtaining the eIF2D target list, I did not anticipate the complexity of the interaction between eIF2D targets. The logic interpretation is the coordinated

translation of multiple mRNAs is the cause of the abnormal behavior. Several experiments to address the impact of these proteins on the eIF2D^{KO} phenotype have been proposed in this discussion, although many more could be performed. Because Poly-seq data identified 740 targets of eIF2D, it is very difficult to assess the individual contribution to the phenotypes of every one of them. Many targets have functions that could potentially explain the phenotype. However, based on the literature, I could not find a single one that completely phenocopies *eIF2D^{KO}*. Since other groups are especially focused on the study of the individual contributions of those molecules to synaptic function, I believe that studies on eIF2D should focus their attention in discovering the mechanisms by which eIF2D interacts with and regulates its mRNA targets.

7.4 Coordinated translation regulation by eIF2D through its targets mRNA sequence

Functional analysis of the eIF2D targets show that several of them are connected as part of pathways. But how is the expression regulation of different elements of a pathway achieved at the translation level? The sequence of the mRNAs might have an impact. Several proteins affecting gene expression interact with specific sequences in the mRNAs. For example, Pumilio homolog 2 is an RNA-binding protein that acts as a post-transcriptional repressor by binding the 3-UTR of mRNA containing the consensus sequence or the Pumilio Response Element (PRE), 5-UGUANAUA-3 (Wang et al. 2002; Morris et al. 2008; Lu and Hall 2011). Another example is DENR-MCTS1 complex and its role in re-initiation after uORF translation. In this example, there is no consensus sequence but rather a structural element in the mRNA that affects translation dynamics (Schleich et al. 2014). Finally, eIF3 binds to a specific subset of messenger RNAs involved in cell growth control processes, including cell cycling, differentiation and apoptosis, via a stem loop on the mRNA 5′ UTR (Lee et al. 2015).

So far, no consensus sequence has been described for eIF2D. It was suggested from *in vitro* studies that eIF2D would have an impact on translation initiation of leaderless or short 5'UTR mRNAs. However, I could not confirm that with my Poly-seq data since only a few mRNAs are leaderless or with short 5'UTRs.

7.4.1 eIF2D regulates translation of a subset of uORF-containing mRNAs

Based on their similar protein structure, a recurrent question in the field is whether eIF2D and DENR-MCTS1 overlap in their functions and targets and to what extent,. Therefore, it was natural to address whether eIF2D targets are enriched for uORF-containing mRNAs.

Upstream Open Reading Frames (uORFs) are sequences encoded on the same mRNA, upstream of the main coding region (mORF), which usually impair translation. Because scanning starts upstream of the mORF, when a ribosome encounters a uORF and translates it, the usual procedure would be to recycle the ribosome at the end of this uORF. Thus, mRNAs containing uORFs will be more dependent on re-initiation and those factors promoting re-initiation.

My analysis of the Poly-seq data showed that differentially expressed genes in each gradient fraction have different number of uORFs in $eIF2D^{KO}$ and control samples. The results indicate a difference in the uORF number per mRNA across the fractions in eIF2D and control samples and suggest less ribosome density on those mRNAs with high uORF number (Fig. 31). As previously mentioned, uORFs are known to work as negative regulators of translation at the mORF, but the impairment seems to be even stronger when eIF2D is missing, as expected for a re-initiation factor.

However, the enrichment for uORF-containing mRNAs in eIF2D^{KO} is only mild compared to $DENR^{KO}$. Moreover, some of the targets contain no annotated or potential uORFs in their sequence. This suggests that although eIF2D might regulate re-initiation, it does not do it after all uORF-containing mRNA and it is not the only requirement for control by eIF2D. It is likely that some characteristics of the same uORF cause it to be regulated by eIF2D. Length of the uORF, distance of the uORF to the mORF, or start codon are the first ones that come to mind and are in correlation with the biochemical activities of eIF2D in translation initiation and possible start codon recognition.

7.4.1.1 The non-canonical translation factors DENR-MCTS1 and eIF2D regulate translation of a different subset of mRNAs in vivo

Previous publications studied eIF2D and DENR-MCTS1 together. Even though some of their biochemical properties are different, still some researchers suggest a big overlap between them. For example, both eIF2D and DENR MCTS1 promote tRNA recruitment to the 40S ribosomal subunit (Dmitriev et al. 2010; Skabkin et al. 2010; Skabkin et al. 2013). However, eIF2D targets found in Poly-seq data do not overlap with the described DNER-MCTS1 targets.

eIF2D domain homology to MCTS1 and DENR (Skabkin et al. 2010). MCTS1, like eIF2D, carries a PUA domain and was shown to bind RNA (Nandi et al., 2007). DENR possesses a SUI1 domain, like eIF2D and eIF1. MCTS1 and DENR function as a complex that structurally resembles eIF2D (Reinert et al. 2006; Skabkin et al. 2010; Schleich et al. 2014). Comparing the structures of eIF2D or DENR-MCTS1 complex in association with the 40S subunit revealed some differences. For example, eIF2D has a domain inexistent in the DENR-MCTS1 complex (the winged helix) which interacts with the central part of helix 44 (h44) of the ribosome and would impede the joining of the 60S to the 40S (Introduction, Fig. 4).

In vivo, DENR is important for proliferating cells in *Drosophila* and affects neocortical development in mice (Schleich et al. 2014; Haas et al. 2016). Moreover, a previous study from the Duncan and Teleman labs showed that the DENR-MCTS1 complex is important for the correct development of the *Drosophila* development. Intriguingly, characterization of the $eIF2D^{KO}$ flies already showed fundamental differences between those two factors: lack of eIF2D affects more specific physiological functions, already suggesting regulation of a different subset of mRNA targets. $DENR^{KO}$ flies die early in adulthood while $eIF2D^{KO}$ flies are completely viable and fertile. $DENR^{KO}$ flies show some morphological defects not present in $eIF2D^{KO}$: impaired proliferation of histoblast cells, crooked legs and rotated genitals (Schleich et al. 2014). As the authors commented, these phenotypes suggest that DENR affects translation of mRNAs involved in cell proliferation and signaling, due to the phenotypic similarities to mutants with reduced cell cycle regulators.

These phenotypic differences seen in the flies could be partially explained be the expression patterns of the two translation factors. In flies, RNA-seq data indicates lower levels for eIF2D than DENR in all the tissues and developmental stages (Flybase, Gelbart and Emmert, 2013). In human, DENR and MCTS1 mRNAs are detected in brain at all stages of development. In mice, DENR and MCTS1 proteins are detected throughout the mouse brain development, with DENR constantly increasing with brain age and MCTS1 peaking at age P10 (Haas et al. 2016). In contrast, eIF2D expression is very weak in human brain compared to DENR and MCTS1 (Haas et al. 2016).

Looking into general effects on translation of both factors, polysome profiles from $DENR^{KO}$ larvae and DENR-KD S2 cells showed a reduction in P/M ratio (polysome/monosome) (Schleich et al. 2014) whereas I observed an increase in $eIF2D^{KO}$ larvae and no effects in cell culture. This confirms that DENR might be involved in translation of a subset of mRNAs with more general functions for the cell, such as cell cycle regulators, while eIF2D would regulate mRNAs involved in functions characteristic of a specialized cell type, such as synaptic function in neurons.

In the above-mentioned study, Schleich et al. demonstrated that the DENR-MCTS1 complex mediates selective translation re-initiation on mRNAs with strong Kozak upstream ORFs (stuORFs) in 5'UTR. Interestingly, this translational regulation was found to be especially important in actively proliferating tissues in *Drosophila*. Therefore homozygous DENR mutants are developmentally lethal. Furthermore, DENR and eIF2D were shown to genetically interact *in vivo* suggesting that they have overlapping biological functions (Schleich et al. 2014). While the specific differences between mechanisms used by the two factors remain unclear, analysis of the Poly-seq data revealed differences in the translational targets of both factors with enrichment for different CIS-elements.

7.4.2   A-rich motif at the 5'UTRs of the mRNA might serve as regulatory CIS-element for eIF2D translation regulation

Motif discovery analysis of eIF2D 5'UTRs targets revealed enrichment for A-rich motif. This A-rich motif appeared in more than one data set (Fig. 33). As for uORFs, having an A-rich motif in the 5'UTR seems neither necessary nor sufficient for eIF2D regulation in vivo. Adenosine-rich elements in the 5'-UTR can selectively reduce translation due to PABP binding (Melo et al. 2003). One hypothesis is that an A-rich motif would make the 40S subunits stall and eIF2D would function in resumption of the scanning, thus increasing translation on those mRNAs. Another idea is that those A-rich motifs might be imbedded in a uORF, coding for lysine. Multiple consecutive lysines can cause protein translation machinery to stall on mRNAs (Arthur et al. 2015). In this case, eIF2D would promote either recycling of the stalled ribosomes or resumption of elongation.

7.4.3 Reporter assays suggest a dual function of eIF2D in promoting and repressing translation

To test whether eIF2D controls translation through its targets 5'UTRs, I performed dual luciferase reporter assays in *Drosophila* S2 cells. Results show a response of some of the constructs to eIF2D depletion, whereas other are not affected (Fig. 35). This suggests that translation regulation by eIF2D does not only involve the 5'UTR. Indeed, one of the functions described for eIF2D was post-termination ribosome recycling (Pisarev et al. 2010; Skabkin et al. 2010), which would more likely be dependent on the coding sequence or the 3'UTR. Another possibility is that the sequence between 5'UTR and CDS is important for regulation. One example would be an o-uORF (overlapping-uORF), a special type of uORF with its start codon on the 5'UTR and the stop codon overlapping with the CDS.

The fact that some constructs are upregulated and one is downregulated indicates a dual function of eIF2D as repressor and promoter of translation, depending on the 5'UTR sequence. In addition, although most of these constructs have an A-rich motif or uORF in their 5'UTR, there is no evident correlation between these elements and the direction of regulation. The hypothesis that eIF2D promotes translation re-initiation could be supported by the decrease in Cadps-RD which contains 4 uORFs. However, Nrx-RD and Cadps-RF also contain uORFs and show an upregulation of translation. Moreover the three 5'UTRs have an A-rich motif. The

difference between them is that the A-rich motif of Nrx-RD and Cadps-RF is part of one of the uORFs, whereas in Cadps-RD is not.

To understand the specific contribution to each one of the elements to the translation regulation, several experiments involving mutations of these constructs should be performed. For example, mutating each start codon of the Cadps-RD uORFs to abolish uORF translation would indicate which one, if any, of the uORFs is responsible for translation decrease in eIF2D^{KO}. A second experiment would be to delete the A-rich motif in those 5'UTR that already contain one or insert it in the ones without.

Taken together, these experiments presented in this thesis show a requirement of eIF2D for motor circuit function in *Drosophila* by selectively regulating translation of specific mRNAs through their 5'UTRs using non-canonical initiation and re-initiation mechanisms.
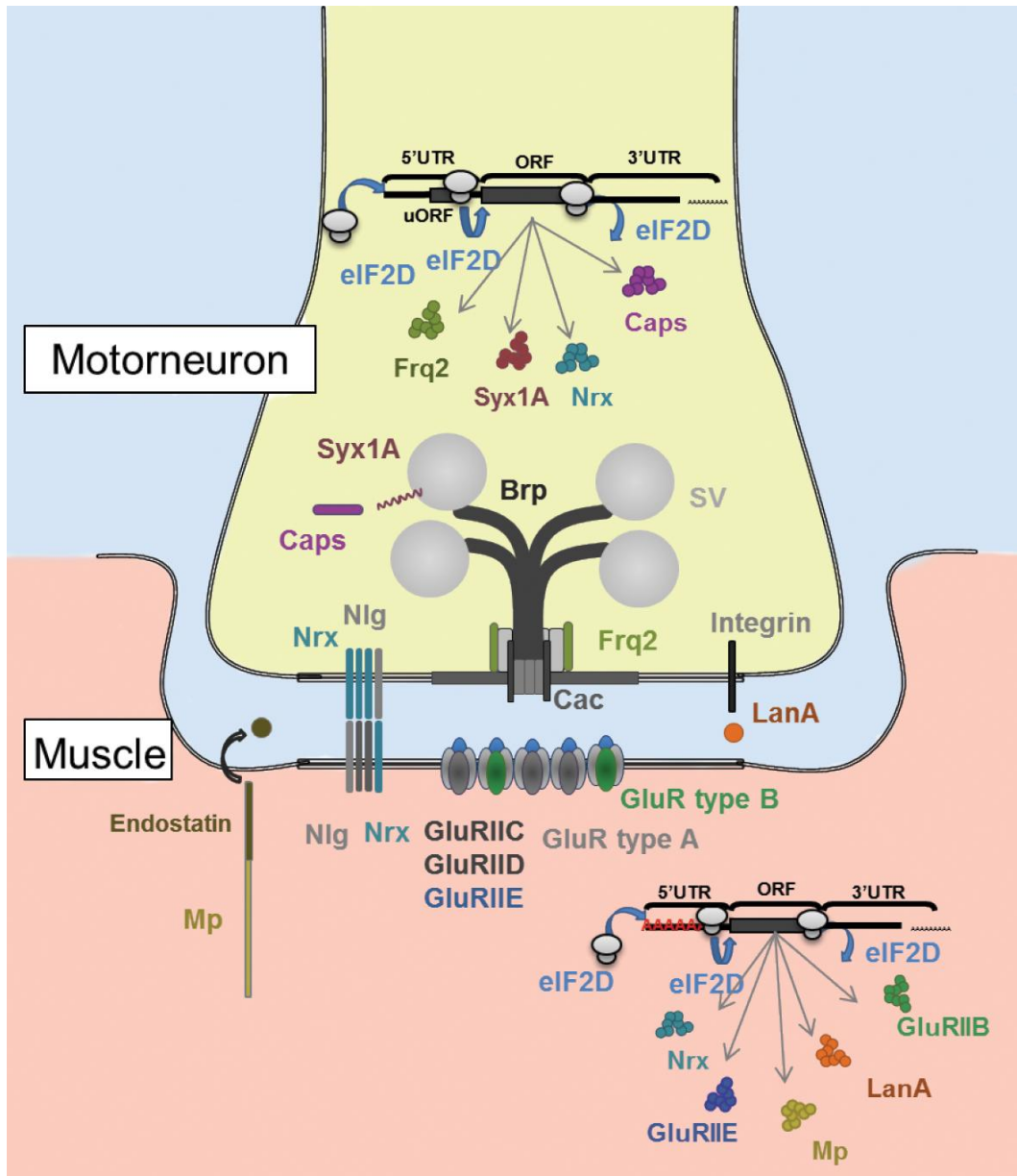
Figure 37. Working model for eIF2D functions at the NMJ. eIF2D protein is expressed on both sides of the NMJ synapse (Motor neuron and Muscle). Although some of its targets are expressed in either side (i.e. *Nrx-1*) most of them seem to be cell-type specific. On both cells, eIF2D regulates translation by affecting different steps on each mRNA. It affects translation initiation on leaderless or short 5'UTR mRNAs or non-AUG uORFs, re-initiation after specific uORFs or pausing sequences such as A-rich motifs, and termination thus promoting translation of some mRNAs while repressing it on others. This dual function in translation allows coordinated translation regulation of multiple synaptic components. In the motor neuron eIF2D regulates translation of Frequenin2 (Frq2), Calcium-dependent secretion activator (Caps) and Syntaxin1A (Syx1A) among others. Some examples of targets expressed in the muscle are Glutamate receptor Subunits E and B (GluRIIE and GluRIIB), LamininA (LanA) and Multiplexin (Mp) which is cleaved to Endostatin.

7.5 Potential molecular mechanism of eIF2D by competing with the initiation factor eIF1

Another factor with partial homology to eIF2D is eIF1, which also contain a SUI1 domain. This SUI1 domain forms a loop that interacts with the codon-anticodon duplex and controls the fidelity of start codon recognition (Hinnebusch 2011; Weisser et al. 2017). eIF1 is also and implicated in 40S subunit binding and start codon recognition (Mitchell and Lorsch 2008; Nanda et al. 2009; Weisser et al. 2013; Martin-Marcos et al. 2014). Several mutations that reduce eIF1 and 40S binding, increase translation initiation at non-AUG codons (Martin-Marcos et al. 2011; Martin-Marcos et al. 2013; Martin-Marcos et al. 2014). Moreover, overexpression of eIF1 suppresses initiation ant non-AUG codons and AUG in poor context (Valasek et al. 2004; Alone et al. 2008; Martin-Marcos et al. 2011).

Recently, structural studies of eIF1 in complex with the 40S ribosomal subunit showed that eIF1 and part of eIF2D interact with the same pocket. This observation has led to the idea that eIF1 and eIF2D would compete for the same binding site on the 40S. eIF2D-containing ribosomes would allow initiation at non-AUG codons or AUG codons in a suboptimal context due to the absence of eIF1. Thus, eIF2D would be involved in the regulation of specific ORFs with non-AUG start codon or AUG in poor context. In the absence of eIF2D is missing, more eIF1 could bind to the ribosome thus increasing stringency for AUG start codon recognition in the optimal context. This would change which uORFs are translated and therefor the ribosome density on a particular mRNA. To test this, relative levels of ribosome-associated eIF1 with and without eIF2D could be measured.

7.6 Poly-seq (Polysome profiling followed by High throughput RNA-sequencing) is a powerful method to study translation *in vivo*

In order to reveal the mRNA targets for eIF2D, I established a new approach that combines of two classic methods (polysome profiling and RNA-sequencing, Poly-seq) and could be easily used in many other RNA-biochemistry labs for similar purposes. The main novelty of this approach is the processing of multiple fractions separately instead of combining them into only two fractions (free pool and Polysome pool) that give us information about the translation profile of a particular mRNA, as

well as the development of a pipeline using differential expression analysis to analyze this type of data/results. This big data set generated in this experiment allows the study of translation profiles of the different mRNAs of the whole genome, not only in our mutants but also in the WT conditions, and relates them to the mRNA characteristics.

7.6.1 Optimization of polysome profiling for *Drosophila* larvae

Polysome profiling is a popular method to study translation. Different labs have optimized the method for different purposes and sample types, and it even has been used in *Drosophila* larvae before. However, the results obtained using those published protocols were the expected: polysomes seem disassembled and a very big 80S peak was seen, suggesting loss of translating ribosomes. For this project, I optimized the method to study translation of the impact of a specific factor on specific mRNAs in the *Drosophila* larvae.

7.6.1.1 *Magnesium concentration and lysis conditions are key elements for optimized polysome profiling*

Together with David Schumacher's as part of his Bachelor Thesis (*Establishment of a polyribosome profiling assay for* Drosophila melanogaster *larvae and assessment of eIF2D function in translation*), we found out that changes in magnesium concentration and flash freezing in liquid nitrogen were giving us better results for larval polysome profiling.

Magnesium is a cofactor for ribosome binding. Higher or lower intracellular concentrations of Magnesium can force the association of ribosomal subunits or dissociate and unfold ribosomes, respectively (Gavrilova et al. 1966; Gesteland 1966). In this case, intracellular concentrations of magnesium were not changed, since only lysis buffer was high in Mg but larvae diet was not supplemented with Mg in any way. One concern could be that after the cells opened and were put in contact with high magnesium concentrations, empty 80S would form (ribosomes without any mRNA attached). Although I think this concern is valid, it would probably not happen for the majority of free subunits. Polysome profiles actually show that the free

subunits exceed the 80S under these conditions (Fig. 17). Moreover, these condition is applied in both genotypes, thus the resulting differences would not be entirely explained by this possible artifact. On the other hand, since those ribosomes would not be attached to mRNA, this would not influence further downstream analysis of RNA-seq.

Flash freezing the larvae in liquid nitrogen resulted also in a big change in the profiles. Larvae contain two tissues with high enzymatic content: the salivary glands and the gut. Although the lysis buffer contains proteinases inhibitors and RNAse inhibitors, those concentrations might be not sufficient to stop all the enzymatic activity occurring after lysing the larvae at room temperature. On the other hand, a key step of polysome profile from cells is the incubation with cycloheximide before harvest and lysis, to chemically freeze the translating ribosomes on place. This step is not possible in larvae since CHX is toxic and would kill the larvae before it has an effect on every ribosome of the organism. By flash freezing we are able to stop all the enzymatic activity of the cells. On one hand the activity of proteinases and RNAses that will degrade the mRNAs and ribosomes and on the other hand, the enzymatic activity of the ribosome to continue translating.

7.6.1.2 *Staging and sexing the larvae is essential to avoid detection of developmental or sex specific translation changes*

Different proteins need to be expressed at different moments of the life of an organism. Growing stages require high rates of translation in the whole organisms, whereas memory consolidation requires translation activation of certain mRNAs more specific in neurons. Therefore, by comparing translation in animals at different stages or grown under different conditions we would be evaluating which mRNAs are differentially translated under those circumstances. To avoid finding altered translated mRNAs as a result of different ages and therefore, finding false positives of eIF2D regulation, it was crucial to carefully stage the larvae. This question was already relevant in my experiment plan but became even more evident after observing that the general translation status of the larvae was dramatically different with only a few hours of difference between them (Fig. 16).

The same concern is relevant for the sex. Even though larvae are not yet sexually active, they already possess the precursors of the reproductive organs of the adult and express some genes differently. Moreover, some genes are exclusively masculine or feminine. I observed that both female and male larvae and adults are viable, but for a reason that I do not yet understand, males hatch later from the eggs (data not shown). I worried that by randomly collecting larvae from both genotypes, I would collect more females than males for the *eIF2D^{KO}* samples. For now, I decided to focus on female larvae since they have a hatching time more similar to the controls.

7.6.2   Poly-seq data might help to understand the phenotypes

The risk of using a new approach to answer one of the main aims raised many questions. Before looking into differences between the controls and the KO samples, I wondered if I could obtain relevant information and how to interpret the data.

One idea is that a gene with high protein levels would have high translation rates. I observed many different translation profiles that indicate a poor correlation between the expected abundance of the protein or physiological importance of the protein in the cell and ribosome density. Because mRNAs are not always occupied to their full capacity, that suggests a possible point of gene regulation: since the mRNA is available in the cell, a rapid demand in the protein levels could be satisfied by increasing translation without a need in activating transcription, which would be slower. That means, that in some cases mRNAs are not being translated to its full capacity either because a single mRNA strand could allocate more ribosomes or because the free pool of that transcript is more abundant than the translated one. This offers an opportunity for fast regulation under certain conditions.

An interesting coordination effect that has been described in gene expression known as potentiation. Several groups have reported that highly transcribed mRNAs that become in different conditions also become more efficiently translated (Preiss et al. 2003; Serikawa et al. 2003). Although mRNA with significant transcriptional changes were intentionally excluded from the differential expression analysis, looking at the unfiltered data set, I observe several examples of potential potentiation, one

being the mitochondrial ribosomal proteins. It would be interesting in the future to examine eIF2D's potential role in this phenomenon in coordination of different steps of gene expression.

7.6.3 Differential expression analysis by DESeq2 could be complemented with mRNA clustering according to their expression distribution

In order to select eIF2D targets from the RNA sequencing data, together with Dr. Thomas Lingner we decided to use the common approach in RNA-seq data analysis which is the differential expression package (DESeq2). DESeq2 is a very powerful analysis method specially developed to find differentially expressed genes or transcripts in RNA-seq datasets.

Although this analysis revealed alterations in mRNAs that I validated as eIF2D targets, this approach might introduce many false negatives. By using DESeq2 I identified as targets those mRNAs with different expression in a given fraction. However, some mRNAs show changes their distribution across the fractions (translation profile) without being statistically significant altered in any of them and thus not appearing as targets. Moreover, by introducing a requirement of no changes in the total mRNA levels I might miss eIF2D targets which translation is also altered. However, since it was the first time someone generated this type of complex dataset, it was not clear yet which would be the best approach to analyze it. Therefore we gave preference to obtain false negatives over false positives, arguing that in this case, false negatives are less harmful than false positives.

A more sophisticated analysis of this dataset could help us to find other eIF2D targets silent in this analysis. Using a clustering method for mRNAs according to their translation profiles in the control samples and then by the changes in the eIF2D^{KO} samples. This would allow us not only to look at changes in individual mRNAs but create clusters of genes that behave similarly and study them together.

7.6.4 Poly-seq in comparison to other alternative methods to study translation

Besides polysome profiling, two other powerful methods exist to study translation: ribosome footprint profile and Translating Ribosome Affinity Purification (TRAP).

Ribosome footprint profiling is based on the fact that a translating ribosome typically protects an approximately 30nt of the mRNA that is being translated from RNAse digestion. This can allow determination of the position of the translating ribosomes on the different mRNAs, and to correlate ribosome density to RNA sequence in order to reveal novel translational regulatory features (e.g., uORFs, start and termination sites, ribosome stall position). However, it does not have the possibility to study changes in isoforms whereas Poly-seq does.

Translating ribosome affinity purification (TRAP) allows studying the translatome of a cell-type specific in a cell mix population. Genetically modified ribosomes containing a tag are expressed in the tissue of interest and by immunoprecipitation those can be separated from the non-tagged ribosomes (from other cell types). The RNA associated with those ribosomes can be sequenced and analyzed for differential expression. This method does not give any information about the position of the ribosomes on the mRNA and studies ribosome access in opposition to ribosome density changes.

Those three methods could probably be combined to gain more precision and overcome some of the disadvantages that each one alone has. For example, in the case of this study, Poly-seq was performed in the whole animal, mixing translatomes of all cell types together and analyzing it as a whole. Since changes in one mRNA might happen in one cell type without any effect on the others, it would be interesting to combine the Poly-seq method with TRAP, to separately study change in muscles and motor neurons. Finally, position information of the ribosomes on mRNAs could determine if eIF2D promotes translation initiation at non-AUG codons, as suggested above.
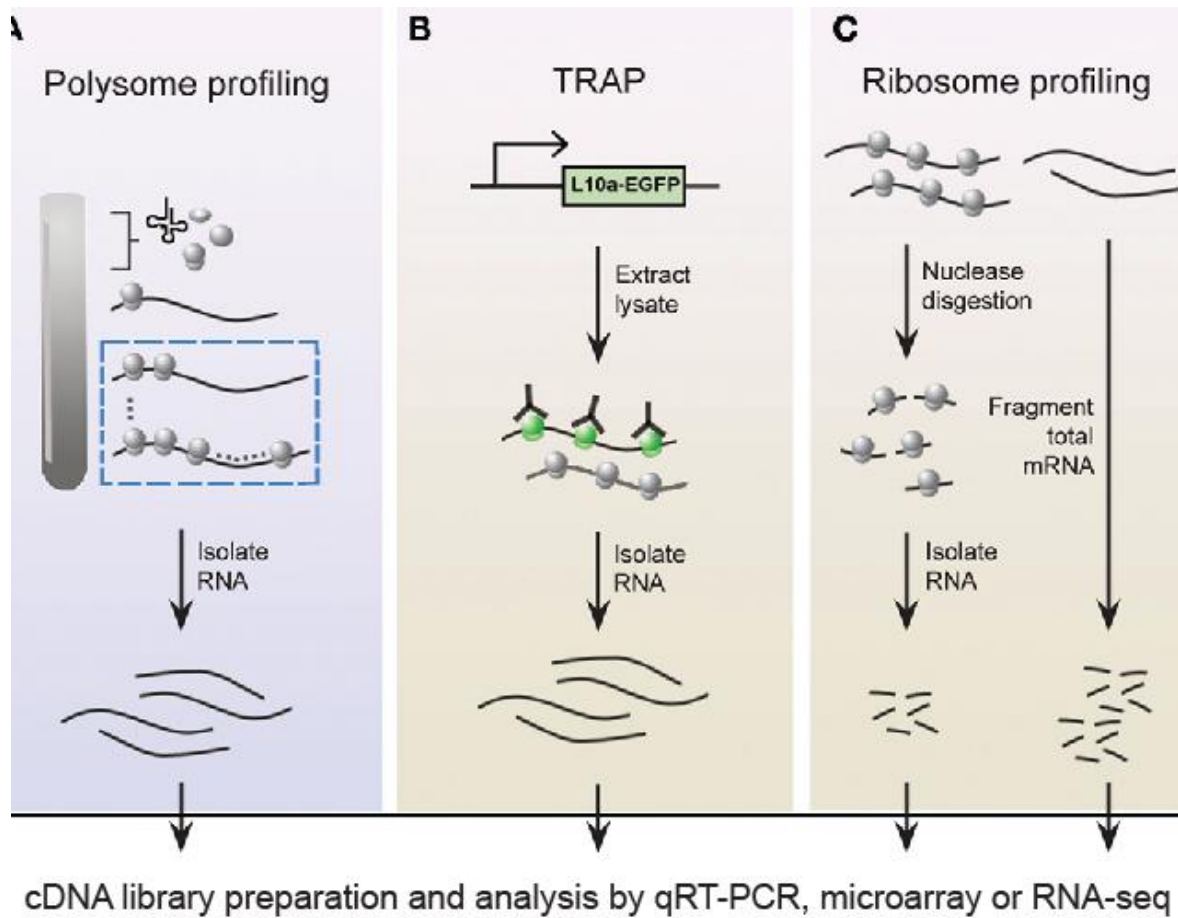
Figure 38. Scheme of different genome-wide methods for translation study. (A) Polysome profiling separates mRNAs according to their ribosome density on a sucrose gradient. mRNAs from different fractions can be isolated for further analysis. (B) BacTRAP animals drive expression of tagged ribosomal protein in cell-type specific manner. Tagged-ribosome complexes are immunopurified and associated mRNAs are identified by various techniques. (C) Ribosome profiling is used to identify ribosome occupancy on mRNAs, based on the fact that translating ribosomes protect a length-known fragment of the mRNA. Lysates are digested by RNAses to remove the unprotected. The resulting monosome complexes are purified and ribosome-protected fragments are recovered. Total mRNA from a similar preparation is usually used in parallel in the different methods to address possible transcriptional changes. The purified RNA can then be analyzed using different RNA quantification methods.

Modified from (Kapeli and Yeo 2012).

7.6.4.1 *Future perspectives of Poly-seq. How to further develop the method*

Reporter assays revealed a different regulation of the isoforms of one same gene by eIF2D. There are many existing evidences of differential regulation of transcripts driven by the 5'UTR and 3'UTR sequences. That evidences the importance of analyzing the isoforms separately instead of combining them together. This should be easily resolved by mapping the reads from the RNA-seq to the transcriptome instead of to the genome. A similar approach to what was described as Transcript Isoforms in Polysomes sequencing (TrIP-seq) (Floor and Doudna 2016) could be applied to the eIF2D RNA-seq data.

Next, I realized that some of eIF2D translational targets might be silent in the traditional DESeq2 analysis that we performed. A better analysis would focus on the distribution of a particular mRNA across the fractions (Floor and Doudna 2016) and how this distribution is altered in the eIF2D^{KO} samples. Then, the different mRNAs with similar distribution and changes in their distribution would be grouped together in a cluster. The mRNAs in the different clusters would then be analyzed together for motif enrichment. I believe that this would provide more information about the correlation between the enriched motifs and the direction of the regulation (promotion or repression of translation).

Protein levels at steady state do not always correlate with translation rates, as it has previously reported (Liu et al. 2016). Even if we could find enough antibodies, the resources and the time to test protein levels of the 740 targets is incalculable. As for finding the mRNA targets of eIF2D, to see how this deregulation of translation affects protein levels, I would need to assess protein levels in a proteome wide manner. The simplest way would be to do mass spectrometry with the same *eIF2D^{KO}* larvae and cross-analyze this data with the Poly-seq data clustering. Changes in the mRNA distribution across the gradient would be then linked to changes in protein abundance.

Finally, the all above mentioned could be done in a sell-type specific manner. Polysome profile followed by TRAP would allow to study changes in translation of

specific mRNAs expressed in a specific cell-type. In parallel, the BONCAT technology allows selective marking of nascent proteins in a cell-type specific manner by integration of a modified amino acid. This modification allows conjugation to either a fluorescent or biotin tag, commonly known as "click reaction" (Dieterich et al. 2006). These proteins can then be visualized in the cells or western blots, or affinity purified and identified by mass spectrometry (Muller et al. 2015). The combination of polysome-TRAP and BONCAT-Mass-spec would allow to correlate translational to protein changes in cell-type specific manner.

In an ideal situation, one could perform a Polysome-profile followed by TRAP method, map the RNA reads to the transcriptome and cross this data with the cell-type specific Mass-spec.

These suggested changes could be applied to the RNA-sequencing data generated in this thesis, to further understand eIF2D effects on translation. Moreover, although this method was optimized for study translation *in vivo* using *Drosophila* larvae, polysome profiling can be used with all kinds of animal tissue. This method could be used in other labs or in other projects to study impact of different translation regulators on specific mRNAs.

8   Abbreviations

ABCE-1	ATP-binding cassette protein
AEL	After egg laying
ATF4	Activating Transcription Factor 4
AZ	Active zone
BRP	bruchpilot
Cadps	Calcium-dependent secretion activator
CDS	Coding sequence
CHX	Cycloheximide
CNS	Central nervous system
Cpx	Complexin
DENR	density-regulated Protein
eIF1	eukaryotic initiation factor 1
eIF1A	eukaryotic initiation factor 1A
eIF2	eukaryotic initiation factor 2
eIF2D	eukaryotic initiation factor 2D
eIF3	eukaryotic initiation factor 3
eIF4A	eukaryotic initiation factor 4A
eIF4F	eukaryotic initiation factor 4F
eIF4G	eukaryotic initiation factor 4G
eIF5	eukaryotic initiation factor 5
EPSPs	excitatory postsynaptic potentials
eRF1	Eukaryotic release factor 1
eRF3	Eukaryotic release factor 3
GCN2	General control non-depressible 2
GCN4	General control protein 4
GFP	Green fluorescent protein
GluR	glutamate receptor
GluRIIA	glutamate receptor subunit IIA
GluRIIB	glutamate receptor subunit IIB
GluRIIC	glutamate receptor subunit IIC
GluRIID	glutamate receptor subunit IID
GluRIIE	glutamate receptor subunit IIE

GO	Gene ontology
HRI	Haem-regulated inhibitor
LanA	lamininA
MCTS1	multiple copies in T-cell lymphoma-1
mEPSPs	miniature excitatory postsynaptic potentials
mORF	main Open Reading Frame
Mp	multiplexin
mRNA	Messenger RNA
Nlg	Neuroligin
NMJ	Neuromuscular junction
Nrx-1	neurexin-1
ORF	Open reading frame
o-uORF	overlapping upstream Rreading Frame
P/M	Polysome/Monosome
PABP	Poly(A)-binding protein
Park	parkin
PERK	PKR-like ER kinase
PIC	Pre-initiation complex
PKR	RNA-dependent protein kinase
PUA	PseudoUridine synthase and Archaeosine transglycosylase
Rpl41	Ribosomal protein L41
stuORF	upstream ORFs with strong Kozak sequences
SUI1	Suppressor of Initiator codon
SV	Synaptic vesicle
Syt1	Synaptotagmin
Syx1A	syntaxin1A
TC	Ternary complex
TRAP	Translating ribosome affinity purification
tRNA	Transfer RNA
uORF	upstream Open Reading Frame
WH	winged helix

9 Apendix

9.1 Percentage distribution of Mitochondria ribosomal proteins across the fractions

gene_name		Control					eIF2D^KO				
		Fr 1	Fr 2	Fr 3	Fr 4	Fr 5	Fr 1	Fr 2	Fr 3	Fr 4	Fr 5
mRpL41	FBgn0034001	14,09%	15,25%	17,40%	25,28%	27,97%	7,75%	10,27%	15,50%	27,79%	38,69%
mRpL24	FBgn0031651	15,74%	13,94%	17,37%	24,84%	28,12%	11,19%	12,21%	15,96%	25,11%	35,53%
mRpS34	FBgn0260460	21,72%	13,11%	17,90%	22,39%	24,89%	13,31%	11,20%	14,88%	26,30%	34,30%
mRpL15	FBgn0036990	18,12%	14,92%	16,76%	25,49%	24,72%	12,63%	10,45%	15,92%	27,64%	33,36%
mRpL32	FBgn0039835	20,86%	14,08%	21,59%	20,26%	23,20%	13,34%	13,56%	16,59%	24,30%	32,21%
mRpL21	FBgn0036853	15,15%	13,41%	14,80%	26,39%	30,25%	10,97%	11,86%	17,06%	27,99%	32,12%
mRpL28	FBgn0031660	14,57%	12,34%	19,18%	26,93%	26,98%	9,68%	9,66%	18,74%	30,25%	31,67%
mRpL3	FBgn0030686	19,68%	15,43%	17,52%	21,86%	25,50%	15,11%	13,52%	16,63%	23,73%	31,00%
mRpL9	FBgn0038319	16,38%	15,12%	19,74%	24,95%	23,82%	12,86%	12,80%	17,46%	26,25%	30,63%
mRpL11	FBgn0038234	19,81%	14,93%	20,49%	21,92%	22,85%	13,53%	10,65%	18,27%	27,00%	30,55%
mRpL46	FBgn0035272	28,11%	17,21%	17,40%	17,85%	19,42%	18,42%	15,34%	16,66%	19,31%	30,27%
mRpL16	FBgn0023519	21,12%	15,59%	17,39%	21,91%	23,99%	13,08%	14,05%	17,60%	25,51%	29,75%
mRpS23	FBgn0260407	17,83%	16,14%	18,18%	25,69%	22,16%	12,89%	12,84%	16,79%	27,83%	29,65%
mRpS24	FBgn0039159	20,78%	9,65%	18,64%	26,28%	24,64%	11,93%	8,69%	15,74%	34,43%	29,20%
mRpL47	FBgn0014023	14,76%	20,01%	21,34%	21,19%	22,70%	15,33%	16,05%	17,71%	21,92%	28,98%
mRpS17	FBgn0034986	12,66%	14,70%	19,11%	30,10%	23,43%	8,94%	12,15%	17,58%	32,73%	28,61%
mRpL35	FBgn0038923	14,52%	12,16%	21,84%	24,57%	26,91%	11,06%	13,38%	19,44%	27,93%	28,18%
mRpL2	FBgn0036135	19,09%	14,87%	19,75%	22,58%	23,71%	15,36%	13,68%	18,08%	24,99%	27,89%
mRpL44	FBgn0037330	26,40%	16,02%	16,74%	19,22%	21,62%	19,63%	13,27%	17,41%	22,35%	27,33%
mRpL12	FBgn0011787	20,20%	15,28%	20,31%	24,99%	19,23%	13,77%	12,04%	19,25%	28,63%	26,31%
mRpL51	FBgn0032053	20,82%	17,06%	18,34%	24,83%	18,96%	11,40%	11,16%	17,17%	34,04%	26,22%
mRpL27	FBgn0053002	22,81%	17,91%	19,85%	21,80%	17,63%	11,77%	15,35%	19,19%	27,64%	26,05%
mRpL4	FBgn0001995	18,55%	20,60%	19,64%	20,00%	21,21%	17,71%	16,25%	19,04%	20,96%	26,03%
mRpS9	FBgn0037529	40,89%	15,54%	13,72%	13,69%	16,17%	28,78%	14,40%	13,07%	18,05%	25,71%
mRpS35	FBgn0035374	12,17%	20,23%	25,98%	23,09%	18,53%	9,05%	14,48%	23,99%	27,15%	25,33%
mRpL43	FBgn0034893	14,18%	16,87%	21,00%	25,70%	22,25%	10,87%	13,88%	20,48%	29,64%	25,12%
mRpS2	FBgn0031639	20,07%	17,30%	20,11%	21,54%	20,98%	17,44%	14,13%	19,86%	23,70%	24,88%
mRpL22	FBgn0030786	18,01%	16,26%	17,88%	24,54%	23,31%	14,15%	12,99%	18,96%	29,10%	24,80%
mRpL45	FBgn0263863	21,52%	19,16%	19,95%	20,09%	19,28%	18,06%	16,02%	19,86%	21,46%	24,59%
mRpL49	FBgn0030433	30,52%	14,64%	15,71%	21,40%	17,73%	18,61%	11,96%	16,31%	29,41%	23,71%
mRpL19	FBgn0037608	19,18%	14,71%	19,90%	25,60%	20,61%	15,03%	13,31%	21,44%	26,51%	23,71%
mRpL39	FBgn0036462	27,25%	18,25%	17,09%	19,74%	17,67%	20,01%	15,76%	18,11%	22,52%	23,60%
mRpL38	FBgn0030552	23,29%	20,33%	19,67%	19,21%	17,50%	18,58%	16,87%	20,09%	20,92%	23,54%
mRpL17	FBgn0035122	15,51%	16,76%	22,04%	23,61%	22,07%	13,63%	15,24%	20,60%	27,11%	23,42%
mRpL10	FBgn0031231	18,13%	18,05%	24,08%	21,83%	17,91%	11,27%	15,43%	23,80%	26,09%	23,42%
mRpL18	FBgn0026741	18,66%	16,47%	21,43%	25,98%	17,45%	13,28%	16,60%	20,52%	26,35%	23,24%

mRpS25	FBgn0030572	13,14%	12,84%	20,02%	32,80%	21,21%	10,65%	10,29%	20,06%	35,83%	23,16%
mRpS31	FBgn0036557	28,99%	20,35%	17,75%	15,80%	17,11%	22,72%	15,83%	18,84%	19,54%	23,06%
mRpL40	FBgn0037892	20,18%	15,48%	22,56%	23,21%	18,57%	15,20%	13,95%	18,87%	29,13%	22,85%
mRpL37	FBgn0261380	21,72%	20,63%	20,91%	20,34%	16,39%	17,05%	16,53%	20,79%	23,29%	22,34%
mRpS18B	FBgn0032849	28,89%	18,04%	19,41%	18,28%	15,37%	18,75%	14,57%	18,66%	25,74%	22,28%
mRpS30	FBgn0030692	14,90%	21,55%	22,96%	20,63%	19,96%	11,29%	19,10%	23,44%	23,94%	22,24%
mRpL1	FBgn0037566	28,06%	19,42%	18,43%	17,82%	16,26%	19,43%	16,64%	19,01%	22,94%	21,97%
mRpL54	FBgn0034579	14,62%	17,58%	24,29%	25,34%	18,17%	10,12%	15,66%	22,19%	30,30%	21,74%
mRpS11	FBgn0038474	28,47%	14,93%	20,05%	19,60%	16,95%	18,90%	16,31%	21,42%	21,93%	21,44%
mRpL36	FBgn0042112	19,73%	16,91%	18,36%	26,08%	18,91%	14,00%	13,23%	20,28%	31,12%	21,37%
mRpS26	FBgn0036774	15,64%	16,84%	21,84%	27,38%	18,29%	11,44%	12,38%	20,93%	34,17%	21,09%
mRpS7	FBgn0032236	22,89%	16,25%	19,92%	21,95%	18,99%	16,85%	13,95%	21,93%	26,29%	20,99%
mRpS6	FBgn0035534	26,17%	15,70%	18,15%	23,17%	16,82%	16,93%	14,35%	19,09%	29,22%	20,41%
mRpS18C	FBgn0039765	10,74%	15,00%	23,91%	30,98%	19,37%	9,23%	12,18%	23,43%	34,96%	20,20%
mRpS28	FBgn0034361	46,77%	16,87%	13,84%	11,59%	10,92%	28,50%	14,82%	14,90%	21,68%	20,11%
mRpL20	FBgn0036335	12,32%	16,94%	22,48%	29,04%	19,22%	11,91%	14,43%	20,95%	32,61%	20,09%
mRpL30	FBgn0029718	12,40%	13,64%	24,95%	32,18%	16,83%	9,93%	10,88%	22,83%	36,54%	19,83%
mRpL48	FBgn0031357	24,49%	14,57%	19,98%	22,31%	18,65%	14,19%	13,28%	21,78%	31,92%	18,83%
mRpL52	FBgn0033208	15,04%	17,22%	25,50%	26,18%	16,07%	10,21%	14,04%	24,54%	32,94%	18,26%
mRpS22	FBgn0039555	41,14%	17,61%	14,77%	13,40%	13,07%	30,47%	16,27%	17,46%	17,92%	17,88%
mRpL23	FBgn0035335	19,23%	12,48%	19,65%	29,40%	19,25%	16,05%	14,50%	19,70%	31,91%	17,84%
mRpS5	FBgn0044510	19,61%	24,30%	23,47%	16,38%	16,24%	17,42%	24,50%	24,17%	16,86%	17,05%
mRpS14	FBgn0044030	16,50%	13,45%	20,99%	31,89%	17,17%	10,62%	13,26%	23,62%	35,84%	16,66%
mRpS29	FBgn0034727	41,95%	19,55%	15,15%	11,45%	11,92%	36,38%	18,35%	14,56%	14,34%	16,38%
mRpS18A	FBgn0051450	14,19%	13,13%	24,56%	32,65%	15,48%	10,76%	11,90%	24,85%	36,41%	16,07%
mRpL13	FBgn0032720	16,97%	17,67%	23,79%	28,37%	13,20%	11,14%	15,60%	23,77%	33,90%	15,60%
mRpL14	FBgn0040389	17,11%	19,00%	24,44%	25,81%	13,64%	12,60%	15,34%	23,97%	33,97%	14,12%
mRpS21	FBgn0044511	13,63%	11,11%	22,52%	37,69%	15,05%	7,51%	10,67%	24,91%	43,75%	13,16%
mRpS10	FBgn0038307	17,66%	23,89%	25,54%	19,83%	13,08%	13,44%	21,89%	26,47%	25,43%	12,78%
mRpL50	FBgn0028648	20,47%	20,86%	23,26%	21,63%	13,78%	14,72%	17,90%	27,09%	27,87%	12,42%
mRpS33	FBgn0038426	13,31%	15,90%	26,27%	31,74%	12,78%	10,15%	12,51%	29,04%	36,90%	11,41%
mRpL33	FBgn0040907	21,94%	14,19%	21,47%	32,39%	10,01%	14,23%	14,62%	24,47%	36,10%	10,57%
mRpS16	FBgn0033907	21,94%	21,41%	27,72%	19,97%	8,96%	16,67%	16,60%	29,82%	28,21%	8,69%
mRpL55	FBgn0038678	26,58%	19,70%	25,75%	19,17%	8,79%	16,80%	17,02%	31,85%	25,87%	8,46%
mRpL42	FBgn0033480	38,41%	20,74%	17,77%	15,45%	7,63%	25,84%	21,46%	23,03%	21,30%	8,37%
mRpL34	FBgn0083983	17,25%	27,07%	31,57%	19,17%	4,95%	14,14%	20,14%	36,81%	23,14%	5,76%

9.2 Total mRNA of mitochondria ribosomal proteins

ensembl_gene_id	gene_name	description	log2FoldChange	Padj
FBgn0031231	mRpL10	mitochondrial ribosomal protein L10	1,06	2,20E-06
FBgn0038234	mRpL11	mitochondrial ribosomal protein L11	1,17	2,77E-15
FBgn0011787	mRpL12	mitochondrial ribosomal protein L12	1,21	1,73E-15
FBgn0032720	mRpL13	mitochondrial ribosomal protein L13	1,39	7,20E-12
FBgn0040389	mRpL14	mitochondrial ribosomal protein L14	1,38	2,37E-10
FBgn0036990	mRpL15	mitochondrial ribosomal protein L15	1,09	9,88E-08
FBgn0023519	mRpL16	mitochondrial ribosomal protein L16	1,21	7,98E-13
FBgn0035122	mRpL17	mitochondrial ribosomal protein L17	1,12	1,52E-07
FBgn0026741	mRpL18	mitochondrial ribosomal protein L18	1,23	1,52E-15
FBgn0037608	mRpL19	mitochondrial ribosomal protein L19	0,78	8,33E-06
FBgn0036135	mRpL2	mitochondrial ribosomal protein L2	0,84	1,53E-05
FBgn0036335	mRpL20	mitochondrial ribosomal protein L20	1,30	4,26E-25
FBgn0036853	mRpL21	mitochondrial ribosomal protein L21	1,17	2,58E-06
FBgn0030786	mRpL22	mitochondrial ribosomal protein L22	0,49	2,51E-03
FBgn0035335	mRpL23	mitochondrial ribosomal protein L23	1,07	1,48E-09
FBgn0031651	mRpL24	mitochondrial ribosomal protein L24	0,92	7,12E-11
FBgn0053002	mRpL27	mitochondrial ribosomal protein L27	0,58	1,25E-02
FBgn0031660	mRpL28	mitochondrial ribosomal protein L28	0,41	5,78E-04
FBgn0030686	mRpL3	mitochondrial ribosomal protein L3	0,29	3,77E-02
FBgn0029718	mRpL30	mitochondrial ribosomal protein L30	1,20	9,07E-11
FBgn0039835	mRpL32	mitochondrial ribosomal protein L32	1,83	2,24E-26
FBgn0040907	mRpL33	mitochondrial ribosomal protein L33	1,14	1,43E-06
FBgn0083983	mRpL34	mitochondrial ribosomal protein L34	1,39	9,20E-09
FBgn0038923	mRpL35	mitochondrial ribosomal protein L35	0,86	6,40E-04
FBgn0042112	mRpL36	mitochondrial ribosomal protein L36	1,05	9,73E-07
FBgn0261380	mRpL37	mitochondrial ribosomal protein L37	1,23	6,66E-11
FBgn0030552	mRpL38	mitochondrial ribosomal protein L38	0,46	1,95E-02
FBgn0036462	mRpL39	mitochondrial ribosomal protein L39	0,24	2,41E-01
FBgn0001995	mRpL4	mitochondrial ribosomal protein L4	0,59	8,29E-04
FBgn0037892	mRpL40	mitochondrial ribosomal protein L40	1,40	5,01E-12
FBgn0034001	mRpL41	mitochondrial ribosomal protein L41	1,25	2,93E-10
FBgn0033480	mRpL42	mitochondrial ribosomal protein L42	1,02	5,60E-06
FBgn0034893	mRpL43	mitochondrial ribosomal protein L43	0,65	2,84E-05
FBgn0037330	mRpL44	mitochondrial ribosomal protein L44	0,69	1,18E-03
FBgn0263863	mRpL45	mitochondrial ribosomal protein L45	0,46	1,93E-02
FBgn0035272	mRpL46	mitochondrial ribosomal protein L46	0,59	6,39E-04
FBgn0014023	mRpL47	mitochondrial ribosomal protein L47	1,06	2,47E-15
FBgn0031357	mRpL48	mitochondrial ribosomal protein L48	1,09	2,43E-08
FBgn0030433	mRpL49	mitochondrial ribosomal protein L49	0,78	1,79E-04
FBgn0028648	mRpL50	mitochondrial ribosomal protein L50	1,48	5,22E-16
FBgn0032053	mRpL51	mitochondrial ribosomal protein L51	1,52	7,31E-14
FBgn0033208	mRpL52	mitochondrial ribosomal protein L52	0,90	8,87E-07
FBgn0050481	mRpL53	mitochondrial ribosomal protein L53		
FBgn0034579	mRpL54	mitochondrial ribosomal protein L54	1,26	2,98E-10
FBgn0038678	mRpL55	mitochondrial ribosomal protein L55	1,42	2,17E-11
FBgn0038319	mRpL9	mitochondrial ribosomal protein L9	1,06	1,30E-08
FBgn0038307	mRpS10	mitochondrial ribosomal protein S10	1,30	9,80E-17
FBgn0038474	mRpS11	mitochondrial ribosomal protein S11	1,22	1,12E-09

FBgn0044030	mRpS14	mitochondrial ribosomal protein S14	1,53	6,83E-13
FBgn0033907	mRpS16	mitochondrial ribosomal protein S16	1,32	3,50E-13
FBgn0034986	mRpS17	mitochondrial ribosomal protein S17	1,04	7,02E-09
FBgn0051450	mRpS18A	mitochondrial ribosomal protein S18A	1,34	4,65E-14
FBgn0032849	mRpS18B	mitochondrial ribosomal protein S18B	1,02	5,63E-09
FBgn0039765	mRpS18C	mitochondrial ribosomal protein S18C	1,49	8,14E-14
FBgn0031639	mRpS2	mitochondrial ribosomal protein S2	1,16	1,31E-07
FBgn0044511	mRpS21	mitochondrial ribosomal protein S21	1,00	1,22E-03
FBgn0039555	mRpS22	mitochondrial ribosomal protein S22	0,14	4,37E-01
FBgn0260407	mRpS23	mitochondrial ribosomal protein S23	1,43	1,60E-17
FBgn0039159	mRpS24	mitochondrial ribosomal protein S24	1,41	3,74E-07
FBgn0030572	mRpS25	mitochondrial ribosomal protein S25	1,24	1,32E-09
FBgn0036774	mRpS26	mitochondrial ribosomal protein S26	0,73	2,97E-04
FBgn0034361	mRpS28	mitochondrial ribosomal protein S28	0,50	1,29E-02
FBgn0034727	mRpS29	mitochondrial ribosomal protein S29	0,46	6,36E-03
FBgn0030692	mRpS30	mitochondrial ribosomal protein S30	1,15	5,27E-13
FBgn0036557	mRpS31	mitochondrial ribosomal protein S31	0,32	2,01E-01
FBgn0038426	mRpS33	mitochondrial ribosomal protein S33	1,71	2,51E-16
FBgn0260460	mRpS34	mitochondrial ribosomal protein S34	0,97	1,72E-08
FBgn0035374	mRpS35	mitochondrial ribosomal protein S35	1,06	5,66E-11
FBgn0044510	mRpS5	mitochondrial ribosomal protein S5	-0,33	5,11E-01
FBgn0035534	mRpS6	mitochondrial ribosomal protein S6	1,53	3,95E-12
FBgn0032236	mRpS7	mitochondrial ribosomal protein S7	1,02	3,87E-13
FBgn0037529	mRpS9	mitochondrial ribosomal protein S9	0,07	7,22E-01

10 References

Abastado JP, Miller PF, Hinnebusch AG. 1991a. A quantitative model for translational control of the GCN4 gene of Saccharomyces cerevisiae. *New Biol* **3**: 511-524.

Abastado JP, Miller PF, Jackson BM, Hinnebusch AG. 1991b. Suppression of ribosomal reinitiation at upstream open reading frames in amino acid-starved cells forms the basis for GCN4 translational control. *Mol Cell Biol* **11**: 486-496.

Aken BL, Achuthan P, Akanni W, Amode MR, Bernsdorff F, Bhai J, Billis K, Carvalho-Silva D, Cummins C, Clapham P et al. 2017. Ensembl 2017. *Nucleic Acids Res* **45**: D635-D642.

Algire MA, Maag D, Lorsch JR. 2005. Pi release from eIF2, not GTP hydrolysis, is the step controlled by start-site selection during eukaryotic translation initiation. *Mol Cell* **20**: 251-262.

Alkalaeva EZ, Pisarev AV, Frolova LY, Kisselev LL, Pestova TV. 2006. In vitro reconstitution of eukaryotic translation reveals cooperativity between release factors eRF1 and eRF3. *Cell* **125**: 1125-1136.

Alone PV, Cao C, Dever TE. 2008. Translation initiation factor 2gamma mutant alters start codon selection independent of Met-tRNA binding. *Mol Cell Biol* **28**: 6877-6888.

Amikura R, Kashikawa M, Nakamura A, Kobayashi S. 2001. Presence of mitochondria-type ribosomes outside mitochondria in germ plasm of Drosophila embryos. *Proc Natl Acad Sci U S A* **98**: 9133-9138.

Arthur L, Pavlovic-Djuranovic S, Smith-Koutmou K, Green R, Szczesny P, Djuranovic S. 2015. Translational control by lysine-encoding A-rich sequences. *Sci Adv* **1**.

Bailey TL, Boden M, Buske FA, Frith M, Grant CE, Clementi L, Ren J, Li WW, Noble WS. 2009. MEME SUITE: tools for motif discovery and searching. *Nucleic Acids Res* **37**: W202-208.

Banovic D, Khorramshahi O, Owald D, Wichmann C, Riedt T, Fouquet W, Tian R, Sigrist SJ, Aberle H. 2010. Drosophila neuroligin 1 promotes growth and postsynaptic differentiation at glutamatergic neuromuscular junctions. *Neuron* **66**: 724-738.

Bodmer R. 1993. The gene tinman is required for specification of the heart and visceral muscles in Drosophila. *Development* **118**: 719-729.

Brand AH, Perrimon N. 1993. Targeted gene expression as a means of altering cell fates and generating dominant phenotypes. *Development* **118**: 401-415.

Brar GA, Yassour M, Friedman N, Regev A, Ingolia NT, Weissman JS. 2012. High-resolution view of the yeast meiotic program revealed by ribosome profiling. *Science* **335**: 552-557.

Broadie K, Bate M. 1993a. Activity-dependent development of the neuromuscular synapse during Drosophila embryogenesis. *Neuron* **11**: 607-619.

-. 1993b. Innervation directs receptor synthesis and localization in Drosophila embryo synaptogenesis. *Nature* **361**: 350-353.

-. 1993c. Muscle development is independent of innervation during Drosophila embryogenesis. *Development* **119**: 533-543.

Broadie K, Bellen HJ, DiAntonio A, Littleton JT, Schwarz TL. 1994. Absence of synaptotagmin disrupts excitation-secretion coupling during synaptic transmission. *Proc Natl Acad Sci U S A* **91**: 10727-10731.

Broadie K, Prokop A, Bellen HJ, O'Kane CJ, Schulze KL, Sweeney ST. 1995. Syntaxin and synaptobrevin function downstream of vesicle docking in Drosophila. *Neuron* **15**: 663-673.

Broadie KS, Bate M. 1993d. Development of the embryonic neuromuscular synapse of Drosophila melanogaster. *J Neurosci* **13**: 144-166.

Brown J, Pirrung M, McCue LA. 2017. FQC Dashboard: integrates FastQC results into a web-based, interactive, and extensible FASTQ quality control tool. *Bioinformatics*.

Budnik V, Ruiz-Canada C, Wendler F. 2016. Extracellular vesicles round off communication in the nervous system. *Nat Rev Neurosci* **17**: 160-172.

Budnik V, Zhong Y, Wu CF. 1990. Morphological plasticity of motor axons in Drosophila mutants with altered excitability. *J Neurosci* **10**: 3754-3768.

Bugiani M, Boor I, Powers JM, Scheper GC, van der Knaap MS. 2010. Leukoencephalopathy with vanishing white matter: a review. *J Neuropathol Exp Neurol* **69**: 987-996.

Calvo SE, Pagliarini DJ, Mootha VK. 2009. Upstream open reading frames cause widespread reduction of protein expression and are polymorphic among humans. *Proc Natl Acad Sci U S A* **106**: 7507-7512.

Cantera R, Nassel DR. 1992. Segmental peptidergic innervation of abdominal targets in larval and adult dipteran insects revealed with an antiserum against leucokinin I. *Cell Tissue Res* **269**: 459-471.

Cash S, Chiba A, Keshishian H. 1992. Alternate neuromuscular target selection following the loss of single muscle fibers in Drosophila. *J Neurosci* **12**: 2051-2064.

Chen K, Gracheva EO, Yu SC, Sheng Q, Richmond J, Featherstone DE. 2010. Neurexin in embryonic Drosophila neuromuscular junctions. *PLoS One* **5**: e11115.

Chen YA, Scales SJ, Patel SM, Doung YC, Scheller RH. 1999. SNARE complex formation is triggered by Ca2+ and drives membrane fusion. *Cell* **97**: 165-174.

Chen YC, Lin YQ, Banerjee S, Venken K, Li J, Ismat A, Chen K, Duraine L, Bellen HJ, Bhat MA. 2012. Drosophila neuroligin 2 is required presynaptically and postsynaptically for proper synaptic differentiation and synaptic transmission. *J Neurosci* **32**: 16018-16030.

Cheung YN, Maag D, Mitchell SF, Fekete CA, Algire MA, Takacs JE, Shirokikh N, Pestova T, Lorsch JR, Hinnebusch AG. 2007. Dissociation of eIF1 from the 40S ribosomal subunit is a key step in start codon selection in vivo. *Genes Dev* **21**: 1217-1230.

Chicka MC, Hui E, Liu H, Chapman ER. 2008. Synaptotagmin arrests the SNARE complex before triggering fast, efficient membrane fusion in response to Ca2+. *Nat Struct Mol Biol* **15**: 827-835.

Choi BJ, Imlach WL, Jiao W, Wolfram V, Wu Y, Grbic M, Cela C, Baines RA, Nitabach MN, McCabe BD. 2014. Miniature neurotransmission regulates Drosophila synaptic structural maturation. *Neuron* **82**: 618-634.

Clarke RA, Eapen V. 2014. Balance within the Neurexin Trans-Synaptic Connexus Stabilizes Behavioral Control. *Front Hum Neurosci* **8**: 52.

Costa AC, Loh SH, Martins LM. 2013. Drosophila Trap1 protects against mitochondrial dysfunction in a PINK1/parkin model of Parkinson's disease. *Cell Death Dis* **4**: e467.

Currie DA, Truman JW, Burden SJ. 1995. Drosophila glutamate receptor RNA expression in embryonic and larval muscle fibers. *Dev Dyn* **203**: 311-316.

Davis GW, Muller M. 2015. Homeostatic control of presynaptic neurotransmitter release. *Annu Rev Physiol* **77**: 251-270.

Dean C, Scholl FG, Choih J, DeMaria S, Berger J, Isacoff E, Scheiffele P. 2003. Neurexin mediates the assembly of presynaptic terminals. *Nat Neurosci* **6**: 708-716.

Deng H, Dodson MW, Huang H, Guo M. 2008. The Parkinson's disease genes pink1 and parkin promote mitochondrial fission and/or inhibit fusion in Drosophila. *Proc Natl Acad Sci U S A* **105**: 14503-14508.

DiAntonio A, Petersen SA, Heckmann M, Goodman CS. 1999. Glutamate receptor expression regulates quantal size and quantal content at the Drosophila neuromuscular junction. *J Neurosci* **19**: 3023-3032.

DiAntonio A, Schwarz TL. 1994. The effect on synaptic physiology of synaptotagmin mutations in Drosophila. *Neuron* **12**: 909-920.

Dieterich DC, Link AJ, Graumann J, Tirrell DA, Schuman EM. 2006. Selective identification of newly synthesized proteins in mammalian cells using bioorthogonal noncanonical amino acid tagging (BONCAT). *Proc Natl Acad Sci U S A* **103**: 9482-9487.

Dmitriev SE, Terenin IM, Andreev DE, Ivanov PA, Dunaevsky JE, Merrick WC, Shatsky IN. 2010. GTP-independent tRNA delivery to the ribosomal P-site by a novel eukaryotic translation factor. *J Biol Chem* **285**: 26779-26787.

Dobin A, Davis CA, Schlesinger F, Drenkow J, Zaleski C, Jha S, Batut P, Chaisson M, Gingeras TR. 2013. STAR: ultrafast universal RNA-seq aligner. *Bioinformatics* **29**: 15-21.

Featherstone DE, Rushton E, Broadie K. 2002. Developmental regulation of glutamate receptor field size by nonvesicular glutamate release. *Nat Neurosci* **5**: 141-146.

Featherstone DE, Rushton E, Rohrbough J, Liebl F, Karr J, Sheng Q, Rodesch CK, Broadie K. 2005. An essential Drosophila glutamate receptor subunit that functions in both central neuropil and neuromuscular junction. *J Neurosci* **25**: 3199-3208.

Fijalkowska D, Verbruggen S, Ndah E, Jonckheere V, Menschaert G, Van Damme P. 2017. eIF1 modulates the recognition of suboptimal translation initiation sites and steers gene expression via uORFs. *Nucleic Acids Res* **45**: 7997-8013.

Fleischer TC, Weaver CM, McAfee KJ, Jennings JL, Link AJ. 2006. Systematic identification and functional screens of uncharacterized proteins associated with eukaryotic ribosomal complexes. *Genes Dev* **20**: 1294-1307.

Floor SN, Doudna JA. 2016. Tunable protein synthesis by transcript isoforms in human cells. *Elife* **5**.

Gavrilova LP, Ivanov DA, Spirin AS. 1966. Studies on the structure of ribosomes. 3. Stepwise unfolding of the 50 s particles without loss of ribosomal protein. *J Mol Biol* **16**: 473-489.

Gesteland RF. 1966. Isolation and characterization of ribonuclease I mutants of Escherichia coli. *J Mol Biol* **16**: 67-84.

Ghosh A, Greenberg ME. 1995. Calcium signaling in neurons: molecular mechanisms and cellular consequences. *Science* **268**: 239-247.

Giraudo CG, Eng WS, Melia TJ, Rothman JE. 2006. A clamping mechanism involved in SNARE-dependent exocytosis. *Science* **313**: 676-680.

Gorczyca M, Augart C, Budnik V. 1993. Insulin-like receptor and insulin-like peptide are localized at neuromuscular junctions in Drosophila. *J Neurosci* **13**: 3692-3704.

Graf ER, Valakh V, Wright CM, Wu C, Liu Z, Zhang YQ, DiAntonio A. 2012. RIM promotes calcium channel accumulation at active zones of the Drosophila neuromuscular junction. *J Neurosci* **32**: 16586-16596.

Grant CM, Hinnebusch AG. 1994. Effect of sequence context at stop codons on efficiency of reinitiation in GCN4 translational control. *Mol Cell Biol* **14**: 606-618.

Guan Z, Saraswati S, Adolfsen B, Littleton JT. 2005. Genome-wide transcriptional changes associated with enhanced activity in the Drosophila nervous system. *Neuron* **48**: 91-107.

Gunisova S, Hronova V, Mohammad MP, Hinnebusch AG, Valasek LS. 2018. Please do not recycle! Translation reinitiation in microbes and higher eukaryotes. *FEMS Microbiol Rev* **42**: 165-192.

Guo X, Macleod GT, Wellington A, Hu F, Panchumarthi S, Schoenfield M, Marin L, Charlton MP, Atwood HL, Zinsmaier KE. 2005. The GTPase dMiro is required for axonal transport of mitochondria to Drosophila synapses. *Neuron* **47**: 379-393.

Haas MA, Ngo L, Li SS, Schleich S, Qu Z, Vanyai HK, Cullen HD, Cardona-Alberich A, Gladwyn-Ng IE, Pagnamenta AT et al. 2016. De Novo Mutations in DENR Disrupt Neuronal Development and Link Congenital Neurological Disorders to Faulty mRNA Translation Re-initiation. *Cell Rep* **15**: 2251-2265.

Harbison CT, Gordon DB, Lee TI, Rinaldi NJ, Macisaac KD, Danford TW, Hannett NM, Tagne JB, Reynolds DB, Yoo J et al. 2004. Transcriptional regulatory code of a eukaryotic genome. *Nature* **431**: 99-104.

Harris KP, Littleton JT. 2015. Transmission, Development, and Plasticity of Synapses. *Genetics* **201**: 345-375.

Harrison SD, Broadie K, van de Goor J, Rubin GM. 1994. Mutations in the Drosophila Rop gene suggest a function in general secretion and synaptic transmission. *Neuron* **13**: 555-566.

Hershey JW. 1991. Translational control in mammalian cells. *Annu Rev Biochem* **60**: 717-755.

Heyer EE, Moore MJ. 2016. Redefining the Translational Status of 80S Monosomes. *Cell* **164**: 757-769.

Hinnebusch AG. 2005. Translational regulation of GCN4 and the general amino acid control of yeast. *Annu Rev Microbiol* **59**: 407-450.

-. 2011. Molecular mechanism of scanning and start codon selection in eukaryotes. *Microbiol Mol Biol Rev* **75**: 434-467, first page of table of contents.

Huang DW, Sherman BT, Tan Q, Collins JR, Alvord WG, Roayaei J, Stephens R, Baseler MW, Lane HC, Lempicki RA. 2007. The DAVID Gene Functional Classification Tool: a novel biological module-centric algorithm to functionally analyze large gene lists. *Genome Biol* **8**: R183.

Ingolia NT, Ghaemmaghami S, Newman JR, Weissman JS. 2009. Genome-wide analysis in vivo of translation with nucleotide resolution using ribosome profiling. *Science* **324**: 218-223.

Ingolia NT, Lareau LF, Weissman JS. 2011. Ribosome profiling of mouse embryonic stem cells reveals the complexity and dynamics of mammalian proteomes. *Cell* **147**: 789-802.

Jackson RJ, Hellen CU, Pestova TV. 2010. The mechanism of eukaryotic translation initiation and principles of its regulation. *Nat Rev Mol Cell Biol* **11**: 113-127.

Jia MH, Larossa RA, Lee JM, Rafalski A, Derose E, Gonye G, Xue Z. 2000. Global expression profiling of yeast treated with an inhibitor of amino acid biosynthesis, sulfometuron methyl. *Physiol Genomics* **3**: 83-92.

Jonas E. 2006. BCL-xL regulates synaptic plasticity. *Mol Interv* **6**: 208-222.

Jorquera RA, Huntwork-Rodriguez S, Akbergenova Y, Cho RW, Littleton JT. 2012. Complexin controls spontaneous and evoked neurotransmitter release by regulating the timing and properties of synaptotagmin activity. *J Neurosci* **32**: 18234-18245.

Kapeli K, Yeo GW. 2012. Genome-wide approaches to dissect the roles of RNA binding proteins in translational control: implications for neurological diseases. *Front Neurosci* **6**: 144.

Karr J, Vagin V, Chen K, Ganesan S, Olenkina O, Gvozdev V, Featherstone DE. 2009. Regulation of glutamate receptor subunit availability by microRNAs. *J Cell Biol* **185**: 685-697.

Kim YJ, Serpe M. 2013. Building a synapse: a complex matter. *Fly (Austin)* **7**: 146-152.

Kozak M. 1987. An analysis of 5'-noncoding sequences from 699 vertebrate messenger RNAs. *Nucleic Acids Res* **15**: 8125-8148.

-. 2001. Constraints on reinitiation of translation in mammals. *Nucleic Acids Res* **29**: 5226-5232.

-. 2002. Pushing the limits of the scanning mechanism for initiation of translation. *Gene* **299**: 1-34.

Lawless C, Pearson RD, Selley JN, Smirnova JB, Grant CM, Ashe MP, Pavitt GD, Hubbard SJ. 2009. Upstream sequence elements direct post-transcriptional regulation of gene expression under stress conditions in yeast. *BMC Genomics* **10**: 7.

Lee AS, Kranzusch PJ, Cate JH. 2015. eIF3 targets cell-proliferation messenger RNAs for translational activation or repression. *Nature* **522**: 111-114.

Li C, Han D, Zhang F, Zhou C, Yu HM, Zhang GY. 2007a. Preconditioning ischemia attenuates increased neurexin-neuroligin1-PSD-95 interaction after transient cerebral ischemia in rat hippocampus. *Neurosci Lett* **426**: 192-197.

Li J, Ashley J, Budnik V, Bhat MA. 2007b. Crucial role of Drosophila neurexin in proper active zone apposition to postsynaptic densities, synaptic growth, and synaptic transmission. *Neuron* **55**: 741-755.

Li W, Wang X, Van Der Knaap MS, Proud CG. 2004. Mutations linked to leukoencephalopathy with vanishing white matter impair the function of the eukaryotic initiation factor 2B complex in diverse ways. *Mol Cell Biol* **24**: 3295-3306.

Liao Y, Smyth GK, Shi W. 2014. featureCounts: an efficient general purpose program for assigning sequence reads to genomic features. *Bioinformatics* **30**: 923-930.

Lim KL, Dawson VL, Dawson TM. 2002. The genetics of Parkinson's disease. *Curr Neurol Neurosci Rep* **2**: 439-446.

Littleton JT, Chapman ER, Kreber R, Garment MB, Carlson SD, Ganetzky B. 1998. Temperature-sensitive paralytic mutations demonstrate that synaptic exocytosis requires SNARE complex assembly and disassembly. *Neuron* **21**: 401-413.

Littleton JT, Ganetzky B. 2000. Ion channels and synaptic organization: analysis of the Drosophila genome. *Neuron* **26**: 35-43.

Littleton JT, Stern M, Perin M, Bellen HJ. 1994. Calcium dependence of neurotransmitter release and rate of spontaneous vesicle fusions are altered in Drosophila synaptotagmin mutants. *Proc Natl Acad Sci U S A* **91**: 10888-10892.

Littleton JT, Stern M, Schulze K, Perin M, Bellen HJ. 1993. Mutational analysis of Drosophila synaptotagmin demonstrates its essential role in Ca(2+)-activated neurotransmitter release. *Cell* **74**: 1125-1134.

Liu Y, Beyer A, Aebersold R. 2016. On the Dependency of Cellular Protein Levels on mRNA Abundance. *Cell* **165**: 535-550.

Lnenicka GA, Grizzaffi J, Lee B, Rumpal N. 2006. Ca2+ dynamics along identified synaptic terminals in Drosophila larvae. *J Neurosci* **26**: 12283-12293.

Love MI, Huber W, Anders S. 2014. Moderated estimation of fold change and dispersion for RNA-seq data with DESeq2. *Genome Biol* **15**: 550.

Lu G, Hall TM. 2011. Alternate modes of cognate RNA recognition by human PUMILIO proteins. *Structure* **19**: 361-367.

Luukkonen BG, Tan W, Schwartz S. 1995. Efficiency of reinitiation of translation on human immunodeficiency virus type 1 mRNAs is determined by the length of the upstream open reading frame and by intercistronic distance. *J Virol* **69**: 4086-4094.

MacIsaac KD, Wang T, Gordon DB, Gifford DK, Stormo GD, Fraenkel E. 2006. An improved map of conserved regulatory sites for Saccharomyces cerevisiae. *BMC Bioinformatics* **7**: 113.

Marrus SB, DiAntonio A. 2004. Preferential localization of glutamate receptors opposite sites of high presynaptic release. *Curr Biol* **14**: 924-931.

Marrus SB, Portman SL, Allen MJ, Moffat KG, DiAntonio A. 2004. Differential localization of glutamate receptor subunits at the Drosophila neuromuscular junction. *J Neurosci* **24**: 1406-1415.

Martin-Marcos P, Cheung YN, Hinnebusch AG. 2011. Functional elements in initiation factors 1, 1A, and 2beta discriminate against poor AUG context and non-AUG start codons. *Mol Cell Biol* **31**: 4814-4831.

Martin-Marcos P, Nanda J, Luna RE, Wagner G, Lorsch JR, Hinnebusch AG. 2013. beta-Hairpin loop of eukaryotic initiation factor 1 (eIF1) mediates 40 S ribosome binding to regulate initiator tRNA(Met) recruitment and accuracy of AUG selection in vivo. *J Biol Chem* **288**: 27546-27562.

Martin-Marcos P, Nanda JS, Luna RE, Zhang F, Saini AK, Cherkasova VA, Wagner G, Lorsch JR, Hinnebusch AG. 2014. Enhanced eIF1 binding to the 40S ribosome impedes conformational rearrangements of the preinitiation complex and elevates initiation accuracy. *RNA* **20**: 150-167.

Melo EO, de Melo Neto OP, Martins de Sa C. 2003. Adenosine-rich elements present in the 5'-untranslated region of PABP mRNA can selectively reduce the abundance and translation of CAT mRNAs in vivo. *FEBS Lett* **546**: 329-334.

Menon KP, Carrillo RA, Zinn K. 2013. Development and plasticity of the Drosophila larval neuromuscular junction. *Wiley Interdiscip Rev Dev Biol* **2**: 647-670.

Mitchell SF, Lorsch JR. 2008. Should I stay or should I go? Eukaryotic translation initiation factors 1 and 1A control start codon recognition. *J Biol Chem* **283**: 27345-27349.

Monastirioti M, Gorczyca M, Rapus J, Eckert M, White K, Budnik V. 1995. Octopamine immunoreactivity in the fruit fly Drosophila melanogaster. *J Comp Neurol* **356**: 275-287.

Morris AR, Mukherjee N, Keene JD. 2008. Ribonomic analysis of human Pum1 reveals cis-trans conservation across species despite evolution of diverse mRNA target sets. *Mol Cell Biol* **28**: 4093-4103.

Mueller PP, Hinnebusch AG. 1986. Multiple upstream AUG codons mediate translational control of GCN4. *Cell* **45**: 201-207.

Muller A, Stellmacher A, Freitag CE, Landgraf P, Dieterich DC. 2015. Monitoring Astrocytic Proteome Dynamics by Cell Type-Specific Protein Labeling. *PLoS One* **10**: e0145451.

Nanda JS, Cheung YN, Takacs JE, Martin-Marcos P, Saini AK, Hinnebusch AG, Lorsch JR. 2009. eIF1 controls multiple steps in start codon recognition during eukaryotic translation initiation. *J Mol Biol* **394**: 268-285.

Natarajan K, Meyer MR, Jackson BM, Slade D, Roberts C, Hinnebusch AG, Marton MJ. 2001. Transcriptional profiling shows that Gcn4p is a master regulator of gene expression during amino acid starvation in yeast. *Mol Cell Biol* **21**: 4347-4368.

Owald D, Fouquet W, Schmidt M, Wichmann C, Mertel S, Depner H, Christiansen F, Zube C, Quentin C, Korner J et al. 2010. A Syd-1 homologue regulates pre- and postsynaptic maturation in Drosophila. *J Cell Biol* **188**: 565-579.

Owald D, Khorramshahi O, Gupta VK, Banovic D, Depner H, Fouquet W, Wichmann C, Mertel S, Eimer S, Reynolds E et al. 2012. Cooperation of Syd-1 with Neurexin synchronizes pre- with postsynaptic assembly. *Nat Neurosci* **15**: 1219-1226.

Paradis S, Sweeney ST, Davis GW. 2001. Homeostatic control of presynaptic release is triggered by postsynaptic membrane depolarization. *Neuron* **30**: 737-749.

Pastuzyn ED, Day CE, Kearns RB, Kyrke-Smith M, Taibi AV, McCormick J, Yoder N, Belnap DM, Erlendsson S, Morado DR et al. 2018. The Neuronal Gene Arc Encodes a Repurposed Retrotransposon Gag Protein that Mediates Intercellular RNA Transfer. *Cell* **173**: 275.

Patel NH, Ball EE, Goodman CS. 1992. Changing role of even-skipped during the evolution of insect pattern formation. *Nature* **357**: 339-342.

Patil CK, Li H, Walter P. 2004. Gcn4p and novel upstream activating sequences regulate targets of the unfolded protein response. *PLoS Biol* **2**: E246.

Paulin FE, Campbell LE, O'Brien K, Loughlin J, Proud CG. 2001. Eukaryotic translation initiation factor 5 (eIF5) acts as a classical GTPase-activator protein. *Curr Biol* **11**: 55-59.

Pestova TV, Borukhov SI, Hellen CU. 1998. Eukaryotic ribosomes require initiation factors 1 and 1A to locate initiation codons. *Nature* **394**: 854-859.

Pestova TV, Kolupaeva VG. 2002. The roles of individual eukaryotic translation initiation factors in ribosomal scanning and initiation codon selection. *Genes Dev* **16**: 2906-2922.

Pestova TV, Kolupaeva VG, Lomakin IB, Pilipenko EV, Shatsky IN, Agol VI, Hellen CU. 2001. Molecular mechanisms of translation initiation in eukaryotes. *Proc Natl Acad Sci U S A* **98**: 7029-7036.

Pestova TV, Lomakin IB, Lee JH, Choi SK, Dever TE, Hellen CU. 2000. The joining of ribosomal subunits in eukaryotes requires eIF5B. *Nature* **403**: 332-335.

Petersen SA, Fetter RD, Noordermeer JN, Goodman CS, DiAntonio A. 1997. Genetic analysis of glutamate receptors in Drosophila reveals a retrograde signal regulating presynaptic transmitter release. *Neuron* **19**: 1237-1248.

Pielage J, Fetter RD, Davis GW. 2006. A postsynaptic spectrin scaffold defines active zone size, spacing, and efficacy at the Drosophila neuromuscular junction. *J Cell Biol* **175**: 491-503.

Pisarev AV, Skabkin MA, Pisareva VP, Skabkina OV, Rakotondrafara AM, Hentze MW, Hellen CU, Pestova TV. 2010. The role of ABCE1 in eukaryotic posttermination ribosomal recycling. *Mol Cell* **37**: 196-210.

Polymeropoulos MH, Higgins JJ, Golbe LI, Johnson WG, Ide SE, Di Iorio G, Sanges G, Stenroos ES, Pho LT, Schaffer AA et al. 1996. Mapping of a gene for Parkinson's disease to chromosome 4q21-q23. *Science* **274**: 1197-1199.

Polymeropoulos MH, Lavedan C, Leroy E, Ide SE, Dehejia A, Dutra A, Pike B, Root H, Rubenstein J, Boyer R et al. 1997. Mutation in the alpha-synuclein gene identified in families with Parkinson's disease. *Science* **276**: 2045-2047.

Preiss T, Baron-Benhamou J, Ansorge W, Hentze MW. 2003. Homodirectional changes in transcriptome composition and mRNA translation induced by rapamycin and heat shock. *Nat Struct Biol* **10**: 1039-1047.

Preiss T, M WH. 2003. Starting the protein synthesis machine: eukaryotic translation initiation. *Bioessays* **25**: 1201-1211.

Qin D, Liu Q, Devaraj A, Fredrick K. 2012. Role of helix 44 of 16S rRNA in the fidelity of translation initiation. *RNA* **18**: 485-495.

Qin G, Schwarz T, Kittel RJ, Schmid A, Rasse TM, Kappei D, Ponimaskin E, Heckmann M, Sigrist SJ. 2005. Four different subunits are essential for expressing the synaptic glutamate receptor at neuromuscular junctions of Drosophila. *J Neurosci* **25**: 3209-3218.

Reinert LS, Shi B, Nandi S, Mazan-Mamczarz K, Vitolo M, Bachman KE, He H, Gartenhaus RB. 2006. MCT-1 protein interacts with the cap complex and modulates messenger RNA translational profiles. *Cancer Res* **66**: 8994-9001.

Rikhy R, Kamat S, Ramagiri S, Sriram V, Krishnan KS. 2007. Mutations in dynamin-related protein result in gross changes in mitochondrial morphology and affect synaptic vesicle recycling at the Drosophila neuromuscular junction. *Genes Brain Behav* **6**: 42-53.

Sanyal S, Consoulas C, Kuromi H, Basole A, Mukai L, Kidokoro Y, Krishnan KS, Ramaswami M. 2005. Analysis of conditional paralytic mutants in Drosophila sarco-endoplasmic reticulum calcium ATPase reveals novel mechanisms for regulating membrane excitability. *Genetics* **169**: 737-750.

Schleich S, Acevedo JM, Clemm von Hohenberg K, Teleman AA. 2017. Identification of transcripts with short stuORFs as targets for DENR*MCTS1-dependent translation in human cells. *Sci Rep* **7**: 3722.

Schleich S, Strassburger K, Janiesch PC, Koledachkina T, Miller KK, Haneke K, Cheng YS, Kuechler K, Stoecklin G, Duncan KE et al. 2014. DENR-MCT-1 promotes translation re-initiation downstream of uORFs to control tissue growth. *Nature* **512**: 208-212.

Schmid A, Hallermann S, Kittel RJ, Khorramshahi O, Frolich AM, Quentin C, Rasse TM, Mertel S, Heckmann M, Sigrist SJ. 2008. Activity-dependent site-specific changes of glutamate receptor composition in vivo. *Nat Neurosci* **11**: 659-666.

Schulze KL, Bellen HJ. 1996. Drosophila syntaxin is required for cell viability and may function in membrane formation and stabilization. *Genetics* **144**: 1713-1724.

Schulze KL, Broadie K, Perin MS, Bellen HJ. 1995. Genetic and electrophysiological studies of Drosophila syntaxin-1A demonstrate its role in nonneuronal secretion and neurotransmission. *Cell* **80**: 311-320.

Schuster CM, Ultsch A, Schloss P, Cox JA, Schmitt B, Betz H. 1991. Molecular cloning of an invertebrate glutamate receptor subunit expressed in Drosophila muscle. *Science* **254**: 112-114.

Serikawa KA, Xu XL, MacKay VL, Law GL, Zong Q, Zhao LP, Bumgarner R, Morris DR. 2003. The transcriptome and its translation during recovery from cell cycle arrest in Saccharomyces cerevisiae. *Mol Cell Proteomics* **2**: 191-204.

Shi Z, Fujii K, Kovary KM, Genuth NR, Rost HL, Teruel MN, Barna M. 2017. Heterogeneous Ribosomes Preferentially Translate Distinct Subpools of mRNAs Genome-wide. *Mol Cell* **67**: 71-83 e77.

Sigrist SJ, Reiff DF, Thiel PR, Steinert JR, Schuster CM. 2003. Experience-dependent strengthening of Drosophila neuromuscular junctions. *J Neurosci* **23**: 6546-6556.

Skabkin MA, Skabkina OV, Dhote V, Komar AA, Hellen CU, Pestova TV. 2010. Activities of Ligatin and MCT-1/DENR in eukaryotic translation initiation and ribosomal recycling. *Genes Dev* **24**: 1787-1801.

Skabkin MA, Skabkina OV, Hellen CU, Pestova TV. 2013. Reinitiation and other unconventional posttermination events during eukaryotic translation. *Mol Cell* **51**: 249-264.

Smith R, Taylor JP. 2011. Dissection and imaging of active zones in the Drosophila neuromuscular junction. *J Vis Exp*.

Soeller WC, Oh CE, Kornberg TB. 1993. Isolation of cDNAs encoding the Drosophila GAGA transcription factor. *Mol Cell Biol* **13**: 7961-7970.

Sun M, Xing G, Yuan L, Gan G, Knight D, With SI, He C, Han J, Zeng X, Fang M et al. 2011. Neuroligin 2 is required for synapse development and function at the Drosophila neuromuscular junction. *J Neurosci* **31**: 687-699.

Tarun SZ, Jr., Sachs AB. 1997. Binding of eukaryotic translation initiation factor 4E (eIF4E) to eIF4G represses translation of uncapped mRNA. *Mol Cell Biol* **17**: 6876-6886.

Tarun SZ, Jr., Wells SE, Deardorff JA, Sachs AB. 1997. Translation initiation factor eIF4G mediates in vitro poly(A) tail-dependent translation. *Proc Natl Acad Sci U S A* **94**: 9046-9051.

Timothy J, Geller T. 2009. SURF-1 gene mutation associated with leukoencephalopathy in a 2-year-old. *J Child Neurol* **24**: 1296-1301.

Tucker WC, Schwarz A, Levine T, Du Z, Gromet-Elhanan Z, Richter ML, Haran G. 2004. Observation of calcium-dependent unidirectional rotational motion in recombinant photosynthetic F1-ATPase molecules. *J Biol Chem* **279**: 47415-47418.

Unbehaun A, Borukhov SI, Hellen CU, Pestova TV. 2004. Release of initiation factors from 48S complexes during ribosomal subunit joining and the link between establishment of codon-anticodon base-pairing and hydrolysis of eIF2-bound GTP. *Genes Dev* **18**: 3078-3093.

Valasek L, Nielsen KH, Zhang F, Fekete CA, Hinnebusch AG. 2004. Interactions of eukaryotic translation initiation factor 3 (eIF3) subunit NIP1/c with eIF1 and eIF5 promote preinitiation complex assembly and regulate start codon selection. *Mol Cell Biol* **24**: 9437-9455.

Vattem KM, Wek RC. 2004. Reinitiation involving upstream ORFs regulates ATF4 mRNA translation in mammalian cells. *Proc Natl Acad Sci U S A* **101**: 11269-11274.

Verstreken P, Ly CV, Venken KJ, Koh TW, Zhou Y, Bellen HJ. 2005. Synaptic mitochondria are critical for mobilization of reserve pool vesicles at Drosophila neuromuscular junctions. *Neuron* **47**: 365-378.

Vos M, Lauwers E, Verstreken P. 2010. Synaptic mitochondria in synaptic transmission and organization of vesicle pools in health and disease. *Front Synaptic Neurosci* **2**: 139.

Wang T, Hauswirth AG, Tong A, Dickman DK, Davis GW. 2014. Endostatin is a trans-synaptic signal for homeostatic synaptic plasticity. *Neuron* **83**: 616-629.

Wang X, McLachlan J, Zamore PD, Hall TM. 2002. Modular recognition of RNA by a human pumilio-homology domain. *Cell* **110**: 501-512.

Weisser M, Schafer T, Leibundgut M, Bohringer D, Aylett CHS, Ban N. 2017. Structural and Functional Insights into Human Re-initiation Complexes. *Mol Cell* **67**: 447-456 e447.

Weisser M, Voigts-Hoffmann F, Rabl J, Leibundgut M, Ban N. 2013. The crystal structure of the eukaryotic 40S ribosomal subunit in complex with eIF1 and eIF1A. *Nat Struct Mol Biol* **20**: 1015-1017.

Wells SE, Hillner PE, Vale RD, Sachs AB. 1998. Circularization of mRNA by eukaryotic translation initiation factors. *Mol Cell* **2**: 135-140.

Xue M, Craig TK, Xu J, Chao HT, Rizo J, Rosenmund C. 2010. Binding of the complexin N terminus to the SNARE complex potentiates synaptic-vesicle fusogenicity. *Nat Struct Mol Biol* **17**: 568-575.

Yao CK, Lin YQ, Ly CV, Ohyama T, Haueter CM, Moiseenkova-Bell VY, Wensel TG, Bellen HJ. 2009. A synaptic vesicle-associated Ca2+ channel promotes endocytosis and couples exocytosis to endocytosis. *Cell* **138**: 947-960.

Zucker RS. 1999. Calcium- and activity-dependent synaptic plasticity. *Curr Opin Neurobiol* **9**: 305-313.

11 Acknowledgments

I would like to express my sincere gratitude to those people who gave me support, advice and inspiration during this Thesis.

To my supervisor Dr. Kent Duncan for creating this project and giving me the opportunity to work on it.

To my thesis committee Dr. Peter Soba and Dr. Hans-Jürgen Kreienkamp for advice during the thesis and on the writing of the thesis.

To the Duncan lab members and former member for all the fruitful discussions during progress report presentations, journal club, lunch and coffee break. Especially, to Dr. Tatyana Koledachkina for all the work she did in this project before I took over and for guidance during my first months in the lab. To David Schumacher for trusting me on being his co-supervisor during his Bachelor thesis and contributing to optimize the polysome profiling method. To Christoph Janiesch for teaching me many of the biochemical experiments I used. To Katrin Küchler for all the cloning she did for this project. To Nagammal Neelagandan for the many discussions we had about our results.

To Dr. Thomas Lingner at the University of Göttingen for all the bioinformatics analysis that he did for this project, especially for making all the bioinformatics seem so easy.

To Dr. Martin Müller and Jennifer Keim, for all the electrophysiology experiments that they performed for this project. And as important, for taking the time to explain me what the results mean.

To the Soba lab for all the help with the flies. And together with the Calderon de Anda lab for the discussions in the joint group meetings. And to many of the other groups and members of the ZMNH. In particular to the members of the ZMNH PhD Program Dr. Sabine Fleischer, Dr. Irm Hermans-Borgmeyer, Dr. Guido Hermey and Dr. Anne Willing. To my friend and colleague Brenna Fearey to reading and giving comments on this thesis.

To Catherine Collins at the University of Michigan and her lab, especially Elham Adib and Jiaxing Li, for receiving me in her lab and teaching me NMJ microscopy.

To my family, my mother Teresa Alberich and my sister Judit Cardona. Gràcies per donar-me suport i creure en mi sempre.

To my friends and colleagues, here and there: Steffen, Eva, Justine, Ana, Aleix, les meues Bionenes (Núria, Maria, Laia, Marta and Sandra), Maru and Silvia, Bene, you all inspire me.

Because this thesis wouldn't be this thesis without all these people.

Declaration on oath

Hiermit erkläre ich an Eides statt, das sich die vorliegende Dissertationsschrift selbst verfasst und keine anderen als die angegebenen Quellen und Hilfsmittel benutzt habe.

I hereby declare, on oath, that I have written the present dissertation by my own and have not used other than the acknowledged resources and aids.

Hamburg, den ………………………

Unterschrift

UKE HAMBURG

Universitätsklinikum Hamburg-Eppendorf
Zentrum für Molekulare Neurobiologie Hamburg
Forschungsgruppe:
Neuronale Translationskontrolle

Dr. Kent Duncan
Forschungsgruppenleiter
Martinistraße 52
D-20246 Hamburg
Gebäude S50, Raum 3.23
Telefon: +49 (0) 40 7410-56274
Fax: +49 (0) 40 7410-53436
Kent.Duncan@zmnh.uni-hamburg.de
www.uke.de/zmnh
Hausanschrift:
Falkenried 94 / Martinistr. 85
D-20251 Hamburg

Universitätsklinikum Hamburg-Eppendorf | Martinistraße 52 | 20246 Hamburg
Zentrum für Molekulare Neurobiologie | Forschungsgruppe Dr. Kent Duncan

English Language Thesis Certification: Aida Cardona Alberich

Hamburg, 20.05.2018

To whom it may concern:

Aida Cardona Alberich, who was born on 27th of December 1989 and has matriculation number 6749694, is submitting her doctoral dissertation in English. The title of her thesis is: **'*In vivo* genome-wide analysis reveals that eIF2D coordinates motor neuronal synaptic function and locomotion behavior by regulating translation of specific mRNAs'.**

I hereby certify as a native speaker and molecular biologist that the English language used in this thesis is sufficiently correct for submission.

Yours truly,

Universität Hamburg
Universitätsklinikum Hamburg-Eppendorf
Zentrum für Molekulare Neurobiologie
AG Duncan
Falkenried 94 · D-20251 Hamburg

Kent Duncan, Ph.D.